공학박사 학위논문

Low-temperature grafting of carbon nanotubes on carbon fibers and their composites

탄소나노튜브 그라프트 탄소섬유의
저온제조공정과 이를 이용한 복합재료

2017년 8월

서울대학교 대학원

재료공학부

이 근 성

Low-temperature grafting of carbon nanotubes on carbon fibers and their composites

저온공정을 이용한 탄소나노튜브 그라프트 탄소섬유의 제조 및 이를 이용한 복합재료

지도교수 유 웅 열

이 논문을 공학박사 학위논문으로 제출함

2017년 8월

서울대학교 대학원

재료공학부

이 근 성

이근성의 공학박사 학위논문을 인준함

2017년 8월

위 원 장 윤 재 륜 (인)

부위원장 유 웅 열 (인)

위 원 박 종 래 (인)

위 원 이 진 용 (인)

위 원 육 지 호 (인)

Low-temperature grafting of carbon nanotubes on carbon fibers and their composites

Advisor: Woong-Ryeol Yu

by

Geunsung Lee

2017

Department of Materials Science and Engineering
Graduated School
Seoul National University

Abstract

The hybridization of carbon nanotubes (CNTs) and carbon fibers (CFs), which called as CNT-grafted CF has emerged as such an advanced and hierarchical material that can improve the reinforcing effect of CFs in composites and solve the dispersion problems of CNTs. Hierarchical structuring of the reinforcement is an effective method for improving the mechanical, electrical and thermal properties of the composites. Radially grown CNTs on CFs improve the radial stiffness and axial tensile strength of CF-reinforced composites, the interfacial shear strength (IFSS) of polymer composites, and the electrochemical performance as CF electrodes.

Even CNT-grafted CF has these merits, many researches for CNT-grafted CF as reinforcement of composites could not show good mechanical properties because of the degradation of mechanical properties of the CFs while chemical vapor deposition (CVD) process which is for grafting of CNTs on CF. Some of researchers succeed to prevent degradation by using buffer layer coated on CF or control of catalysts layer deposited on CF but these methods are not suitable for macroscale process. Because of these limits, previous researchers could not show the mechanical performance of CNT-grafted CF reinforced composites in macroscale. Through our previous research, we succeed to grow CNTs on CF without degradation of the mechanical properties of CFs by using low-temperature process with Ni-Fe bimetallic catalyst. We lowered growth temperature of CNTs to below 500^{o}C and succeed to inhibit the inter-diffusion between carbon and catalyst particles while CVD process.

By using CNT-grafted CF manufactured by low-temperature process, we studied about the thermal/electrical/mechanical properties of CNT-grafted CF reinforced

plastic composites. Tensile strength of CNT-grafted CFRP was increased 17% in unidirectional composites and 32% in woven composites compared to as-received CFRP. Increased interfacial shear strength (IFSS) was critically contributed to the strength of CFRP and we identified their failure mechanism by observation of fractured surface of CFRP. In addition, we manufactured CNT-grafted carbon fiber/carbon composites and characterized their thermal/electrical/mechanical properties. CNT-grafted CFs have excellent wettability to the liquid pitch which forms matrix of the C/C composites. Thus, CNT-grafted CF/carbon composites have much better mechanical/thermal properties especially through-the-thickness direction.

Lastly, we developed continuous manufacturing process of CNT-grafted CF for mass production. Water vapor-assisted CVD was adopted to accelerate CVD process and T-zone furnace was designed to minimize shade effect. We optimized lab-scale continuous process for CNT-grafted CF with detailed parameters.

Keywords: carbon fiber composite, interfacial shear strength, carbon nanotube, chemical vapor deposition, low-temperature process

Student number: 2014-30234

Contents

Abstract ..... **i**

List of figures ..... **vi**

List of tables ..... **xi**

1. Introduction **1**

1.1. Carbon nanotubes (CNTs) 1

1.2. Carbon fibers (CFs) 2

1.3. CNT-grafted CFs 6

1.3.1 Structure and properties of the CNT-grafted CFs 7

1.3.2 Grafting process of CNTs on CFs 7

1.3.3 Critical issues on the grafting of CNTs on CFs 6

1.3.4 CNT-grafted carbon fibers composites 8

1.4. Research objectives 12

2. Low temperature grafting of carbon nanotubes on carbon fibers using a bimetallic floating catalyst **14**

2.1. Introduction 14

2.2. Experimental 16

2.2.1 Preparation of CNT-grafted CFs by FCVD 16

2.2.2 Characterization of CNT-grafted CF 19

2.3. Results and discussion 21
2.3.1 Surface morphology of the CFs after FCVD process 21
2.3.2 Mechanical properties and microstructure of the CNT-grafted CFs ... 26
2.4. Summary 44

3. CNT-grafted carbon fibers reinforced composites 45
3.1. CNT-grafted carbon fibers reinforced plastics 45
3.1.1 Introduction 45
3.1.2 Experimental 47
3.1.2.1 Preparation of CNT-grafted CFs 47
3.1.2.2 Fabrication of CNT-grafted CFRP 49
3.1.2.3 Characterization 49
3.1.3 Results and discussion 52
3.1.3.1 Morphologies and properties of the CNT-grafted CFs 52
3.1.3.2 Properties of the CNT-grafted CF reinforced composites 57
3.1.3.3 The reinforce mechanism of the CNT-grafted CF 63
3.2. CNT-grafted carbon fiber reinforced carbon composites 71
3.2.1 Introduction 71
3.2.2 Experimental 71
3.2.2.1 Fabrication of the CNT-grafted CF 71
3.2.2.2 Fabrication of the C/C composites 72
3.2.2.3 Characterization 74
3.2.3 Results and discussion 74
3.2.3.1 Properties of the C/C composites 74
3.2.3.2 Effect of the hierarchical structure of the CNT-grafted CFs 78

3.3. Summary 84

4. Continuous process for carbon nanotube-grafted carbon fibers 85

4.1. Introduction 85

4.2. Experimental 89

4.3. Results and discussion 90

4.4. Summary 105

5. Concluding remarks 106

References 108

Korean abstract 117

List of figures

Figure 1.1. Typical micro-damage modes in single-fiber composite test with different IFSS showing different fracture mode. (a) Water-sized; (b) g-GPS-treated; (c) g-MPS-treated; (d)g-APS/urethane/paraffin-treated; and (e) urethane-sized [30].

Figure 1.2. The three representative modes of fracture in a single-fiber composite (a) strong interface (high IFSS): a disk-shaped matrix crack; (b) intermediate interface (strong interface but with a matrix that has relatively lower shear than tensile strength capability): a double cone matrix crack; and (c) weak interface (low IFSS): interfacial debonding [28].

Figure 2.1. (a) Schematic diagram of FCVD and (b) the two-zone furnace used in this research

Figure 1.2. Schemes of sample preparation with FIB for internal structure observation of CNT-grafted CF in TEM

Figure 2.2. Morphologies of CNT-grafted CFs prepared from different substrate CFs, catalysts, and CVD temperatures. (a) As-received CFs, bimetallic catalyst, 500°C; (b) oxidized CFs, bimetallic catalyst, 500°C; (c) as-received CFs, Fe-only catalyst, 750°C; (d) oxidized CFs, Fe-only catalyst, 750°C.

Figure 2.4. The effect of temperature on CNT growth on CFs during FCVD with the bimetallic catalyst. CNT growth was hindered with increasing temperature. (a) 500°C, (b) 600°C, (c) 750°C

Figure 2.5. Tensile strength and modulus of CNT-grafted CFs prepared using different FCVD conditions. The x-axis labels correspond to the as-received CFs, CFs CNT-grafted CFs prepared using the bimetallic catalysts (Bi-CNT) and Fe-only catalysts (Fe-CNT).

Figure 2.6. 1-D wide angle X-ray scattering patterns of CFs after heat treatment.
Figure 2.7. Debye diffractograms of CF surface; (a) as-received CF (b) as-received CF after heat treatment at 750^{o}C (c) surface of bimetallic catalyst-only deposited CF after heat treatment at 500^{o}C for 1 hr (Bi-500) (d) surface of Fe catalyst-only deposited CF after heat treatment at 750^{o}C for 1 hr. (Fe-750)
Figure 2.8. The strength distribution curve of Debye loop on the equator line for CFs; (a) as-received CF (b) as-received CF after heat treatment at 750^{o}C (c) surface of bimetallic catalyst-only deposited CF after heat treatment at 500^{o}C for 1 hr (Bi-500) (d) surface of Fe catalyst-only deposited CF after heat treatment at 750^{o}C for 1 hr (Fe-750).
Figure 2.9. Raman spectra of (a) CNTs grafted on CF by bimetallic catalyst FCVD at 500^{o}C (b) CNTs grafted on CF by Fe-only catalyst FCVD at 750^{o}C (c) surface of as-received CF (d) surface of Ni-Fe bimetallic catalyst-only deposited CF after heat treatment at 500^{o}C for 1 hr (Bi-500) (e) surface of Fe catalyst-only deposited CF after heat treatment at 750^{o}C for 1 hr (Fe-750)
Figure 2.10. Small angle X-ray scattering (SAXS) patterns of CFs; (a) as-received CF (b) Ni-Fe bimetallic catalyst-only deposited CF after heat treatment at 500^{o}C for 1 hr (Bi-500) (c) Fe catalyst-only deposited CF after heat treatment at 750^{o}C for 1 hr (Fe-750); and slice of scattering intensity at center of 2D SAXS pattern along meridian direction (d).
Figure 2.11. The internal structure of CNT-grafted CFs prepared from different FCVD processes. (a) FCVD using the Fe-only catalysts at 750°C, (b) FCVD with the bimetallic catalyst at 500°C, (c) FCVD with the bimetallic catalyst at 750°C.
Figure 3.1.1 Schemes for CVD procedure to fabricate CNT-grafted CF fabric
Figure 3.1.2 Formed micro-droplet of epoxy on the carbon fiber surface

Figure 3.1.3 Schematic diagram of micro-droplet test for IFSS measurement (a) apparatus consists of two blade collars (b)

Figure 3.1.4. Morphologies of the fabricated CNT-grafted CF fabrics and the CNT grafted on CF; CNT-grafted CF

Figure 3.1.5 Mechanical properties of the (a) as-receive CF and (b) CNT-grafted CF

Figure 3.1.6. Thermogravimetric profiles of the (a) CFs, (b) Epoxy resin and (c) composites

Figure 3.1.7 Representative stress-strain curve for (a) woven and (b) unidirectional CFRP

Figure 3.1.8. Morphology of the fractured surface of unidirectional composites after tensile test (a) and (b) as-received CFRP; (c) and (d) CNT-grafted CFRP

Figure 3.1.9. Stress-strain curve and in-situ microscope observation for surface crack of woven CFRP while tensile test; (a) as-received CF and thick-CNT-grafted CF (b) thin-CNT-grafted CF

Figure 3.1.10. Morphologies of the woven CFRP after in-situ microscope observation for surface crack; (a) as-received CF (b) thick-CNT-grafted CF

Figure 3.1.11. Stress intensity factor (K_σ^f) for the unidirectional CFRP

Figure 3.2.1. Temperature profile for pyrolysis of carbon-carbon composites

Figure 3.2.2 Mechanical properties of carbon-carbon composites (a) stress-strain curve; (b) experimental flexural strength over theoretical strength calculated by rule of mixture

Figure 3.2.3 Coefficient of thermal expansion of the C/C composites; (a) in-plane direction (b) through-the-thickness direction

Figure 3.2.4. Microscopic morphology of carbon-carbon composties; fiber bundle

section for (a) as-received CF carbon-carbon composites and (b) CNT-grafted CF carbon-carbon composites; interlaminar section for (c) as-received CF carbon-carbon composites and (d) CNT-grafted CF carbon-carbon composites
Figure 3.2.5. Internal morphology of carbon-carbon composties (a) as-received CF carbon-carbon composites and (b) CNT-grafted CF carbon-carbon composites
Figure 3.2.6. Wettability of the liquid pitch on the surface of; (a) as-received CF and (b) CNT-grafted CF and contact angle of liquid pitch droplet on the fiber surface (c)
Figure 4.1. (a) Schemes of the continuous process for the CNT-grafted CFs and (b) T-shaped two-zone furnace used for the research
Figure 4.2 The morphology of the CF substrates following FCVD growth. (a) Without grounding and with (b) copper, (c) steel, and (d) aluminium wire and (e) CF and (f) GF bundle grounding
Figure 4.3 The morphology of the surface of the ground wires following FCVD growth. (a) Copper, (b) steel, (c) and aluminium wires and the (d) CF and (e) GF bundles
Figure 4.4 Raman spectra of the CF substrates after the FCVD growth process. (a) The CF substrates without grounding (bottom) and with non-metal (CF: middle GF: top) grounding, (b) the as-received CF and CF substrates with metal ground wires
Figure 4.5 The electric potential distribution in the furnace with grounding wires with various relative permittivities, εr. (a) The geometry and location of the ground wires. (b) Without ground wires and with (c) silicon dioxide (εr = 3.9), (d) graphite (εr = 15), and (e) metal (εr = 100,000) ground wires
Figure 4.6 Variation of the morphology of the CNT-grafted CF on the condition of

the continuous process

Figure 4. 7 Mechanical properties of the CNT-grafted CF with various condition

List of tables

Table 2.1. Orientation index and crystallinity of CF surface crystalline

Table 3.1.1 Properties of the CFRP

1. Introduction

1.1. Carbon nanotubes (CNTs)

Carbon structures can exhibit multiple allotropic forms with very disparate properties from soft and conductive graphite to the hard and insulating diamond. Fullerenes, also called buckyballs named after Richard Buckminster Fuller [1], are molecules composed entirely of carbon arranged like the classic soccer balls, and can assume the form of a hollow sphere. CNTs are another allotrope of carbon and, when they synthesized, are often closed by a half of fullerene [2]. CNTs have exceptional and anisotropic properties[1]. Thus, they have been widely investigated for electrical, thermal and mechanical applications such as microelectronic interconnects[3,4], structural composites[5-10] and heat sinks[11-13].

Because of their particularly strong bonding between the carbons (sp^2 hybridization of the athomic orbitals) of the curved graphene sheet [14,15], CNTs have extreme stability against deformations. The tensile strength of single walled carbon nanotubes (SWCNTs) can be 20 times that of steel and has actually been measured as about of 45 GPa [16]. Very high tensile strength values are also expected for ideal multi-walled carbon nanotubes (MWCNTs), since combining perfect tubes concentrically is not supposed to be detrimental to the overall tube strength, provided the tube ends are well capped (otherwise, concentric tubes could glide relative to each other, inducing high strain). Tensile strength value as high as 150 GPa have actually been measured for perfect MWNTs from an electric arc method [17], although the reason for such a high value compared to that measured for SWCNTs is not clear. It probably reveals the difficulties involved in carrying out such measurements in reliable manner. The flexural modulus of perfect MWCNTs should

logically be higher than that for SWNTs, with a flexibility that decreases as the number of walls increases [18]. On the other hand, measurements performed on defective MWCNTs obtained from catalytic chemical vapor deposition (CVD) exhibit a range of 3-30GPA [19]. Values of tensile modulus are also the highest value known, 1TPa for MWCNTs, and possibly even higher for SWCNTs, up to 1.3TPa. [18]

In theory, metallic nanotubes can carry an electric current density of 4 x 10^9 A/cm^2, which is more than 1,000 times greater than those of metals such as copper[3,4]. Furthermore, all nanotubes are expected to be very good thermal conductors along the tube, exhibiting a property known as "ballistic conduction", but good insulators laterally to the tube axis [20,21]. Measurements show that a SWCNT has a room-temperature thermal conductivity along its axis of about 3500 $Wm^{-1}K^{-1}$; compare this to copper, a metal well known for its good thermal conductivity, which transmits $385Wm^{-1}K^{-1}$ [22]. A SWCNT has a room-temperature thermal conductivity across its axis (in the radial direction) of about $1.52Wm^{-1}K^{-1}$ which is about as thermally conductive as soil [22]. The temperature stability of carbon nanotubes is estimated to be up to 2800^{o}C in vacuum about 750^{o}C in air.

1.2. Carbon fibers (CFs)

Carbon fibers refers to fibers which are at least 92 wt.% carbon in composition[23]. Types of carbon fibers are separated by their precursors; Rayon, polyacrylonitrile (PAN) and pitch [24]. Among them, PAN precursors are the basis for the majority of CFs commercially available today because of their cost and performance [25]. They provide a CF conversion yield that is 50 to 55%. These precursors can be thermally rearranged before the CF conversion process, while maintaining the same the same filamentary configuration. The chemical composition of

PAN precursors defines the thermal characteristics that the material displays throughout the oxidation/stabilization portion of the conversion process [26, 27]. These thermal characteristics influence the processing sequences that are used to convert PAN precursors to carbon fiber. CF based on a PAN precursor generally has a higher tensile strength than a fiber based on any other precursor [25]. This is due to a lack of surface defects, which act as stress concentrators and, hence, reduce tensile strength

For the fiber structure and the degree of crystallite orientation, the CFs can be classified as three types. Type 1 CFs are highly graphitized and are characterized by a high modulus (HM). When incorporated into structures, they give the highst stiffness per unit weight. Type 2 CFs, which are heat-treated to a lower temperature, have a low modulus but a very high strength (HS). Type 3 CFs have random orientation of the crystallites. Thus, they have low modulus and strength. Their main advantage is their low cost [28].

The structure of CF can be crystalline, amorphous, or partly crystalline. The crystalline form has the crystal structure of graphite, which consists of sp^2 hybridized carbon atoms arranged tow-dimensionally in the x-y plane. There is general agreement that CFs are composed of two-dimensional turbostratic graphite crystallites, oriented preferentially parallel to the fiber axis [29].

The cross-sectional texture of a CF can be different between the core and the skin of the fiber, wheter the cross-sectional shape of the fiber is round, dog-bone, or others. For PAN-based carbon fibers, the skin tends to have the carbon layers lined up parallel to the perimeter of the fiber, whereas the core tends to have the carbon layers exhibiting a random cross-sectional texture (also called a turbostratic texture) This duplex structure (skin-core heterogeneity) is characteristic of HM

Pan-based CF [28]. The formation of a skin is probably the result of layer-plane ordering, which occurs as the heat treatment temperature is increased. The skin-core heterogeneity can also be due to the higher temperature at the skin than the core during carbonization, and the larger stretching force experienced by the skin than the core. For HS type PAN-based fibers, there is no skin and the crystallites are smaller than those of Type 1. The smaller crystallites of HS type cause the strength to be higher for higher for HS type than HM type. In HS type, a high proportion of the carbon layers are not parallel to the fiber's cylindrical surface; instead they protrude. This edge exposure enhances the bonding of the fiber to the matrix when the fiber is used in composite. The stronger texture along the fiber axis gives HM type a higher modulus than HS type.

Carbon fibers are usually used with other materials as matrix. When combined with a plastic resin and molded it forms CF reinforced plastic (CFRP) which is a very high strength-to-weight, extremely rigid, although somewhat brittle material. However, the efficient translation of these outstanding mechanical properties into usable structural form such as composites has not been achieved. The composites obtained from them have poor interlaminar shear strength. This has been attributed to weak adhesion or poor bonding between the carbon fiber surface and the resin matrix, which is related to the inert graphitic structure at the CF surface.

The mechanisms of fiber-matrix bonding include chemical bonding, van der Waals bonding, and mechanical interlocking. Chemical bonding gives the largest bonding force, provided that the density of chemical bonding across the fiber-matrix interface is sufficiently high. This density can be increased by chemical treatments of the fibers of by sizings on the fibers. Mechanical interlocking between the fibers and the matrix is an important contribution to the bonding if the

fibers form a three-dimensional network. Otherwise, the fibers should have a rough surface in order for a small degree of mechanical interlocking to take place. Both chemical bonding and van der Waals bonding require the fibers to be in intimate contact with the matrix. The occurrence of a reaction between the fibers and the matrix helps the wetting and bonding between the fibers and the matrix. However, an excessive reaction degrades the fibers and the reaction products may be undesirable for the mechanical, thermal, or moisture resistance properties of the composite. Therefore, an optimum amount of reaction is preferred.

Many researches for surface treatments of CFs have been conducted to improve the bonding between the fibers and the polymer matrix. They involve oxidation treatments and the use of coupling agents, wetting agents, and/or sizings (coatings). Oxidation treatments can be applied by gaseous, solution, electrochemical, and plasma methods. They serve mainly to remove a weak surface layer from the fibers. More severe oxidation treatments also serve oxidation treatments also serve to roughen the fiber surface, thereby enhancing the mechanical interlocking between the fibers and the matrix. Chemical modification occurs, but contributes little to the fiber-matrix adhesion [30].

Effective reinforcement requires good bonding between the fibers and the matrix. Strong bonding between the fiber-matrix can reduces split, delamination of the composites while loading and helps load transfer to the broken fibers by the interfacial shear strength (IFSS). Therefore, an enough degree of fiber-matrix bonding is needed for the carbon fiber reinforced composites [31]

1.3. CNT-grafted CFs

1.3.1 Structure and properties of the CNT-grafted CFs

Due to their excellent mechanical, electrical and thermal properties, carbon fibers (CFs) have been used in nearly all-engineering fields, promoting vast research to improve their mechanical properties. However, the improvements of the mechanical properties of CFs are now saturated; thereby researchers pursue a new direction for improving the mechanical properties of the CF reinforced composites. On the other hand, carbon nanotubes (CNTs) have been emerged to a new generation reinforcement material and stimulated a considerable amount of research. [3-13] However, the application of CNTs as reinforcement has brought many problems related with aggregation of CNTs in matrix and low volume fraction of reinforcement. [32] To solve these problems and also improve the mechanical properties of CF reinforced composites, the hybridization of CNTs and CFs by grafting CNTs on the surface of CFs has been suggested. The main motivation for adding CNTs to conventional fiber composite is to alleviate the existing limitations associated with the matrix dominated properties such as the delamination resistance and through-thickness properties [33], without compromising in-plane performance. In addition, the CNTs may introduce additional damage preprocess that could enhance the local toughness of the matrix during fracture. Hybrid structure which called CNT-grafted CF has the nano-micro multiscale hierarchical structure with increased surface area and radial reinforcement. These grafted CNTs onto fiber surface can create mechanical interlocking, and/or local stiffening at the fiber/matrix interface, all of which may improve stress transfer and interfacial properties. Furthermore, the radially grown CNTs can influence the surrounding matrix, thus, are to stiffen the matrix and

provide increased lateral support for the load-bearing microscale fibers.

1.3.2 Grafting process of CNTs on CFs

Grafting CNTs onto conventional fiber surfaces could provide higher loadings of CNTs, potentially with a radial orientation, which is expected to be optimal for transverse reinforcement. This method also alleviates the problem of agglomeration, commonly observed when CNTs are freely dispersed in a matrix. On the other hand, grafting CNTs onto bulk quantities of primary fibers requires process development, both for the initial synthesis and the subsequent preparation of hierarchical composites. So far, most researchers have grafted CNTs onto individual fibers, an approach that might be extended to continuous processing of fiber tows; other have chosen to graft CNTs onto woven fiber preforms or felts. Four different techniques to graft or attach CNTs onto a variety of fiber materials have been reported so far: (1) direct growth of CNTs on fibers by CVD [34-36] (2) electrophoretic deposition of CNTs on fiber surfaces [37], (3) chemical reactions between functionalized CNTs and fibers and [38] (4) spraying or coating of fibers with CNT-containing sizes [39-40]. Catalytic CVD is typical method to graft CNTs on the CFs.

1.3.3 Critical issues on the grafting of CNTs on CFs

There have been several researches to graft CNTs on various substrates using catalytic CVD. When CFs are used as the substrate, the catalyst nanoparticles diffuse into the CFs and become poisoned and deactivated by carbon atoms separated from the CFs because the CFs are porous. Diffused catalysts destroy the internal structure of CFs, while the poisoning and deactivation of catalyst particles hinders CNT growth. Diffused catalysts depopulate the CF surfaces of active catalyst particles, also hampering CNT growth. To prevent the deactivation and diffusion of the catalysts, buffer layers have been coated on CF surfaces to inhibit

inter-diffusion between carbon and catalyst particles. [41] Buffer layers and coatings increase material and manufacturing costs. An alternative surface treatment technique was developed that improves the chemical affinity of CFs and enlarges their surface roughness [34]. Such surface-treated CFs have a greater affinity for catalyst nanoparticles and show improved CNT growth, but the CFs still degrade during the high-temperature CVD process.

In recent, various studies have been conducted to graft CNTs on CF without degradation and buffer layers. There were two kinds of methods for preventing degradation. Some of researches tried to graft CNTs on CF by spraying [39] or electrophoresis [37] which do not need high-temperature procedure such as CVD. These methods are easy and suitable to massive production but they needs additional process to stabilize bond between CNTs and CF [37]. On the other hand, trials with CVD headed to way to inhibit diffusion. In our previous research, we solved problems with mechanical degradation of CNT-grafted CF by control amount of catalysts introduced to CF [38]. But this method was not suitable to massive production because of high-cost, sensitive procedure to control amount of catalyst. Thus, we need the suitable grafting process which maintains mechanical properties of the carbon fibers with low cost and simple step.

1.3.4 CNT-grafted CF reinforced composites

As a reinforce material of composite, CNT-grafted CF has two obvious advantages. One is radial fracture toughness caused by radially grown CNTs and another one is increased interfacial shear strength. Kepple, K. L. and Godara [33] revealed increased radial directional toughness of CNT-grafted CF reinforced composites which comes from bridge effect of CNTs between carbon fiber laminar. Interfacial shear strength of CNT-grafted CF has been investigated by several

researches [42-49] and their interfacial shear strength is much higher than that of the as-received CFs.

The effect of IFSS on the tensile properties of composite have been reported by several researches[50-53]. The common report is that as the IFSS increases, the tensile strength increases also even though it doesn't increase linearly. In addition to that the fracture surface was also observed and reported in same trend. Typically is accepted that a brittle failure is done with treated (i.e., high IFSS) fiber composites, and a broom-like small-bundle failure is done with untreated (i.e., low IFSS) fiber composites. The fracture mechanism have been studied systematically and the interfacial adhesion and micro-damage was observed by single fiber fragmentation test [54,55]. The studies supplied the basic results for examination of the effect of IFSS on tensile property of UD composites. Especially the work by Drzal [56] has revealed that the improvement in tensile strength depends on the IFSS. The major conclusions from single fiber fragmentation test are following: the fracture modes are changed according to the IFSS. Thus, when the IFSS is low the interface is debonded only, and in opposite case the interfacial debonding is reduced. Furthermore in the high IFSS case the interfacial shear stress makes the matrix failure, inducing sharp disk-shaped failure. In the Fig. 1.1 [57] and 1.2 [55] the results are shown in microscopic image and schematic diagram

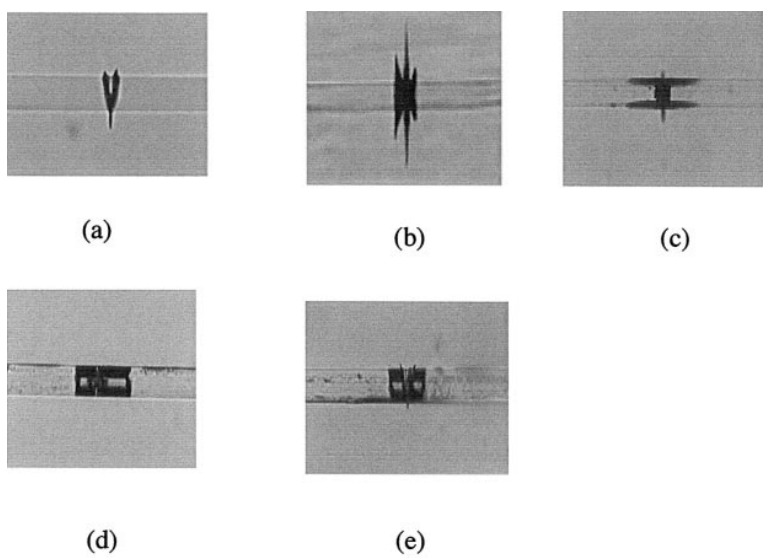

Figure 1.1. Typical micro-damage modes in single-fiber composite test with different IFSS showing different fracture mode. (a) Water-sized; (b) g-GPS-treated; (c) g-MPS-treated; (d)g-APS/urethane/paraffin-treated; and (e) urethane-sized [57].

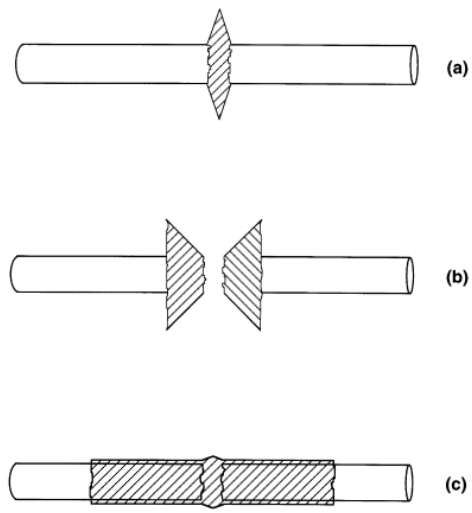

Figure. 1.2. The three representative modes of fracture in a single-fiber composite (a) strong interface (high IFSS): a disk-shaped matrix crack; (b) intermediate interface (strong interface but with a matrix that has relatively lower shear than tensile strength capability): a double cone matrix crack; and (c) weak interface (low IFSS): interfacial debonding [55].

However, in the previous researches with CNT-grafted CF reinforced composites, CNT-grafted CF reinforced composites could not show higher tensile or flexural strength than as-received CF reinforced composites because of the critical issues as we mentioned above. Degradation of the mechanical properties of the CFs were critical to the mechanical properties of the composites.

1.4. Research objectives

In the CF reinforced composites, the interfacial bonding between CF and matrix is important issue for the fibers to fully load the applied force transferred from the matrix. Grafting CNTs on CF surface can improve the interfacial shear strength and also the mechanical properties in transverse direction. In this thesis, the main objective is to fabricate CNT-grafted CFs and their composites.

In the chapter 2, it was aimed to fabricate CNT-grafted CF without any degradation on the tensile strength of CF. Since inter-diffusion of catalysts and CFs and the thermal degradation of CFs are high-temperature phenomena, lowering the CVD temperature may be the most effective means of solving the catalyst poisoning and diffusion issues. This hypothesis was investigated using thermal CVD with Ni-Fe bimetallic catalysts. Bimetallic catalysts are known to lower the activation energy for CNT growth and thus CVD temperature. In this chapter, we also investigated mechanisms for mechanical degradation of CFs by microstructural analysis from angstrom to over-nanometer scale. We considered many of factors in microstructural changes for mechanical degradation and found out the mechanisms and evidences for them.

In the chapter 3, it was aimed to fabricate and characterize CNT-grafted CF reinforced composites with a bimetallic catalyst CVD process which developed in the chapter 2. We fabricated and characterized CNT-grafted CF reinforced plastic (CFRP) and CNT-grafted CF/carbon composites. Mechanical/thermal/electrical properties of the composite was characterized and their reinforce mechanism was detailed with observation of fractured surface and additional experiments. For the CFRP, increased IFSS, inhibited split of fibers and delamination was critical factors

for the strength of the composites. For the C/C composites, increased wettability of CNT-grafted CF to the pitch which composing carbon matrix was main issue for the increased mechanical/thermal/electrical properties.

In the chapter 4, it was aimed to develop the continuous process for CNT-grafted CFs. . By using bimetallic catalysts and water-vapour, we could lower the manufacturing temperature and accelerate process speed. Decreased process time and lowered CVD temperature contributed to prevent inter-diffusion between catalyst particles and CFs which occurs mechanical degradation. In addition, we established compartment with slit at the jacket of the furnace to supply CF bundle from outside of the furnace. CFs were allowed to pass the slit but gas from side of the compartment prevented infiltration of outer atmosphere. We also investigated the effect of conducting pathways to the ground on the growth of CNTs on CF substrates during FCVD to establish electrostatic condition of CF substrates and take-up reel.

2. Low temperature grafting of carbon nanotubes on carbon fibers using a bimetallic floating catalyst

2.1. Introduction

The hybridization of carbon nanotubes (CNTs) and carbon fibers (CFs) has been considered as a versatile method to develop new advanced materials by hierarchically combining their excellent thermal, electrical, and mechanical properties in nano and micro scales [32]. CNT-grafted CF made via direct growth has emerged as such an advanced and hierarchical material that can improve the reinforcing effect of CFs in composites and solve the dispersion problems of CNTs [58]. Radially grown CNTs on CFs improve the radial stiffness [33] and axial tensile strength [39, 40] of CF-reinforced composites, the interfacial shear strength (IFSS) of polymer composites[42-49], and the electrochemical performance as CF electrodes [5,6]. Several issues must be resolved, however, for successful dissemination of CNT-grafted CFs. These issues include the manufacturing method, which degrades the mechanical properties of the resulting CFs and the high cost of the batch process used for their manufacture, i.e., the pre-process for introducing catalyst nanoparticles on the CF surface [40] and the main process for growing CNTs via chemical vapor deposition (CVD)[37]. Herein, we demonstrate that a bimetallic catalyst and floating catalyst chemical vapor deposition (FCVD) can solve these problems.

As one of the simplest methods to graft CNTs on CFs, FCVD provides

carbon sources and catalysts concurrently, inducing the deposition and growth of CNTs on substrates. There have been several researches to graft CNTs on various substrates using FCVD [39,60-62]. When CFs are used as the substrate, the catalyst nanoparticles diffuse into the CFs and become poisoned and deactivated by carbon atoms separated from the CFs because the CFs are porous [63]. Diffused catalysts destroy the internal structure of CFs, while the poisoning and deactivation of catalyst particles hinders CNT growth [64]. Diffused catalysts depopulate the CF surfaces of active catalyst particles, also hampering CNT growth[65]. To prevent the deactivation and diffusion of the catalysts, buffer layers have been coated on CF surfaces to inhibit inter-diffusion between carbon and catalyst particles[66]. Buffer layers and coatings increase material and manufacturing costs. An alternative surface treatment technique was developed that improves the chemical affinity of CFs and enlarges their surface roughness [67.68]. Such surface-treated CFs have a greater affinity for catalyst nanoparticles and show improved CNT growth, but the CFs still degrade during the high-temperature CVD process.

In recent, various studies have been conducted to graft CNTs on CF without degradation and buffer layers. There were two kinds of methods for preventing degradation. Some of researches tried to graft CNTs on CF by spraying [69] or electrophoresis [37] which do not need high-temperature procedure such as CVD. These methods are easy and suitable to massive production but they needs additional process to stabilize bond between CNTs and CF. On the other hand, trials with CVD headed to way to inhibit diffusion. In our previous research, we solved problems with mechanical degradation of CNT-grafted CF by control amount of catalysts introduced to CF [39]. But this method was not suitable to massive production because of high-cost, sensitive procedure to control amount of

catalyst

In this chapter, we will demonstrate low-temperature CVD process for CNT-grafted CF using a bimetallic floating catalyst. Since inter-diffusion of catalysts and CFs and the thermal degradation of CFs are high-temperature phenomena, lowering the CVD temperature may be the most effective means of solving the catalyst poisoning and diffusion issues. This hypothesis was investigated using FCVD with Ni-Fe bimetallic catalysts. Bimetallic catalysts are known to lower the activation energy for CNT growth and thus CVD temperature. In this research, we also investigated mechanisms for mechanical degradation of CFs by microstructural analysis from angstrom to over-nanometer scale. We considered many of factors in microstructural changes for mechanical degradation and found out the mechanisms and evidences for them.

2.2. Experimental

2.2.1 Preparation of CNT-grafted CFs by FCVD

FCVD using a two-zone furnace offers a simplified and continuous process to manufacture CNT-grafted CFs (Figure 2.1). A mixture of catalyst precursors and a carbon source are injected into the first zone, where the precursors are sublimated or vaporized. CFs are placed in the second zone in batch or continuous processes. The sublimated catalysts and vaporized carbon sources are decomposed in the second zone into catalysts and carbon atoms, resulting in CNT growth on the CF substrates. CF (T700SC, Toray) were spread and used as a substrate to minimize shade effect. For comparison purpose, oxidized CFs were also prepared by heating as-received CFs at 500°C for 1 h to vary chemical affinity of CF surface to catalyst particles. A bimetallic catalyst system was prepared using ferocene (Fe(η5–C5H5)2, Sigma–Aldrich) and nickelocene (Ni(η5-C5H5)2, Sigma–Aldrich). Ferrocene and

nickelocene have the same structure and differ only in their metallic element. Their 1:1 mixture in toluene (99.5%, Sigma–Aldrich) was introduced into the first FCVD zone as precursors of the catalysts and as a carbon source. FCVD was conducted at 500^{o}C, 600^{o}C, 750^{o}C to investigate their temperature dependency. To investigate the effect of heat on the diffusion of catalysts into CF, heat treatment was applied to CFs without catalysts at the same temperature of FCVD process

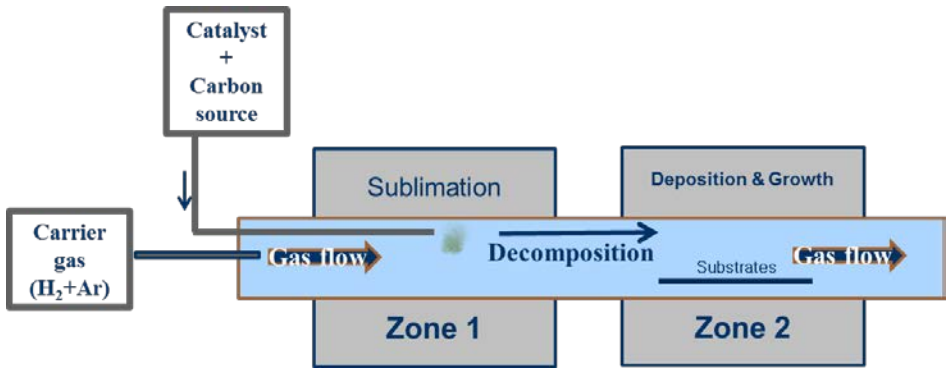

(a)

(b)

Figure 2.1. (a) Schematic diagram of FCVD and (b) the two-zone furnace used in this research

2.2.2 Characterization of CNT-grafted CFs by FCVD

Morphologies of CFs after FCVD process were observed by field emission scanning electron microscopy (FE-SEM, JEOL, JSM 7600F). To investigate effect of diffusion of catalysts into the CF, internal microstructure of the CNT-grafted CFs was investigated using a high-resolution transmission electron microscope (HR-TEM, JEM-3000F, JEOL Ltd). The specimens were prepared using a focused ion beam (FIB, SMI3050SE, SII Nanotechnology Inc) of Ga+ ions. The CNT-grafted CF was attached to a silicon wafer. Amorphous carbon was then deposited on the surface of the CNT-grafted CF to prevent damage during the focused ion beam process. Schemes for sample preparation are detailed in Figure 2. 2.

The mechanical properties of CNT-grafted CFs were measured using a single-fiber tensile test with 20mm of gage length and 2mm/min of strain ratio by lab-made universal test machine.

Wide angle and small angle X-ray scattering analysis (WAXS and SAXS) with Debye images (WAXS: RIGAKU, D/MAX-2500, SAXS: Techvalley, TVXA-ENIF1) were carried out to investigate the orientation of carbon crystals and microvoids in the CF after CVD process. Raman spectroscopy (T64000, Ar laser, 514nm, HORIBA) was conducted to evaluate the quality of CNTs grafted on CFs and the carbon structure of substrate CFs

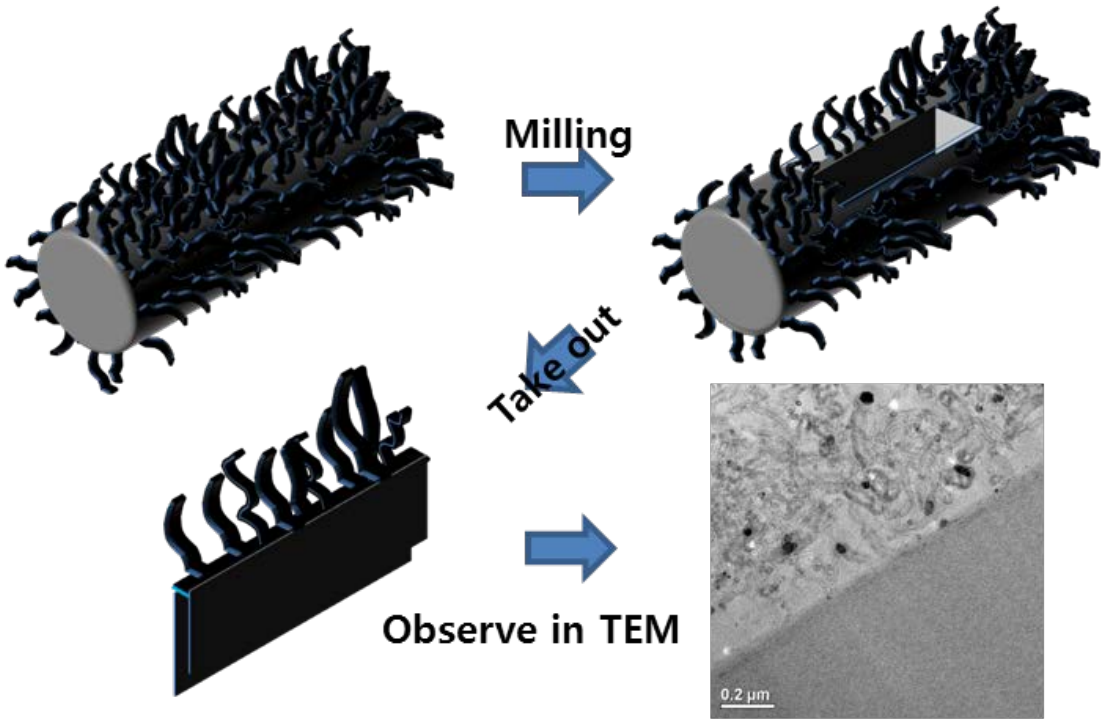

Figure 3.2. Schemes of sample preparation with FIB for internal structure observation of CNT-grafted CF in TEM

2.3. Results and discussion

2.3.1 Surface morphology of the CFs after FCVD process

The effect of temperature and catalyst (bimetallic or Fe-only catalysts) on CNT growth on CF surfaces was investigated by observing the morphologies of the CFs after the FCVD process. Figure 2. 3 (a) and (b) show the morphologies of the as-received and oxidized CFs, respectively, demonstrating that CNTs grew at low temperature (500°C) in the presence of the bimetallic catalyst. The chemical affinity and roughness of the substrate CFs had little effect on the bimetallic catalyst. Note that CNT growth was not observed at such a low temperature with the single metallic catalyst (Fe-only) (e.g., see Figure 2. 3 (c)). In the Fe-only catalyst cases, CNT growth was highly dependent on the surface condition (Figure 2. 3 (c) and (d))): at 750°C, CNTs grew only on oxidized CFs. At the moment, we deduce that chemical affinity introduced in oxidized CFs is helpful to prevent the diffusion of catalysts into CF, which will be further investigated later. Note that catalyst nanoparticles at high temperatures are prone to diffusing into the substrate CFs or becoming poisoned and deactivated [63]. The behavior of the bimetallic catalyst as a function of temperature was also investigated. Figure 2. 4 shows that CNTs grew uniformly on the surface of CFs during FCVD at 500 °C, however as temperature increased, CNT growth was hindered. It is known that the growth speed of CNTs increases as CVD temperature increases [70]. As such, the tendency observed in CFs above implies that the hindrance of CNT growth was caused not by a kinetic process but deterioration of catalysts, e.g., resulting from inter-diffusion between carbon and catalysts.

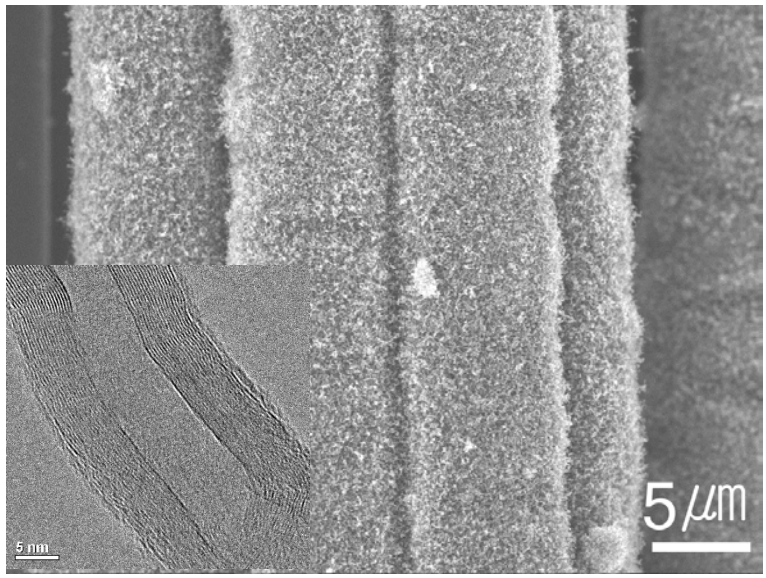

(a)

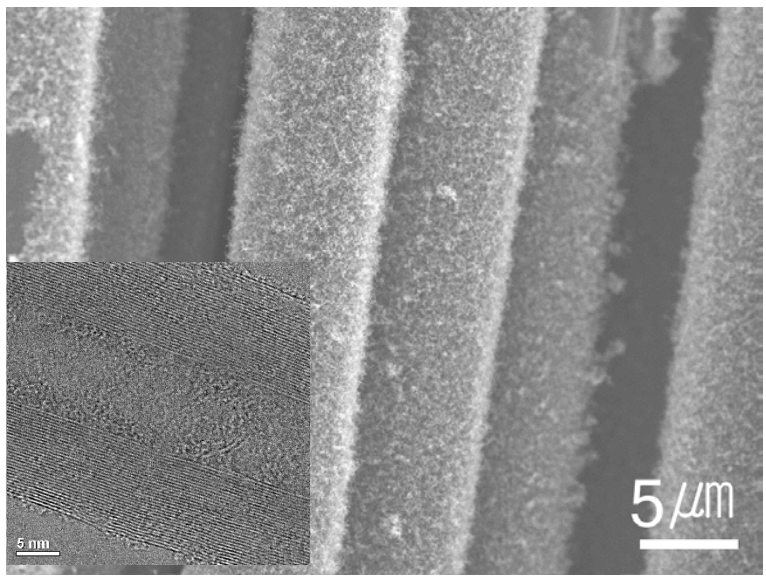

(b)

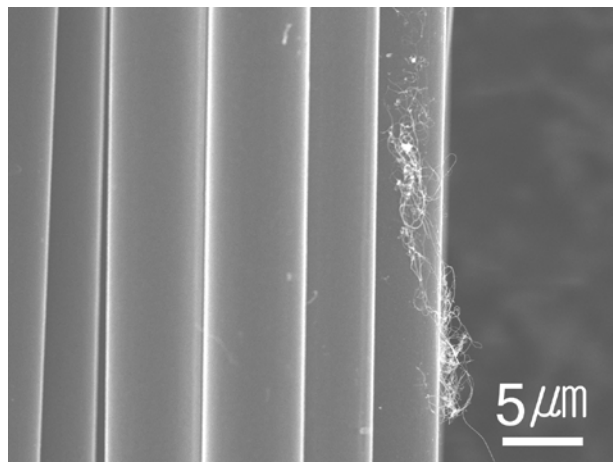

(c)

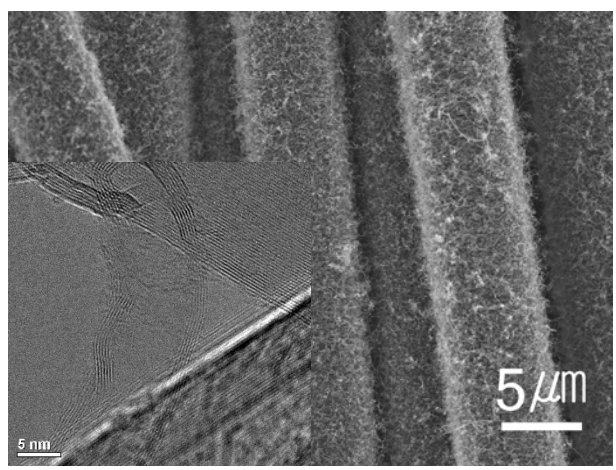

(d)

Figure 2.4. Morphologies of CNT-grafted CFs prepared from different substrate CFs, catalysts, and CVD temperatures. (a) As-received CFs, bimetallic catalyst, 500°C; (b) oxidized CFs, bimetallic catalyst, 500°C; (c) as-received CFs, Fe-only catalyst, 750°C; (d) oxidized CFs, Fe-only catalyst, 750°C.

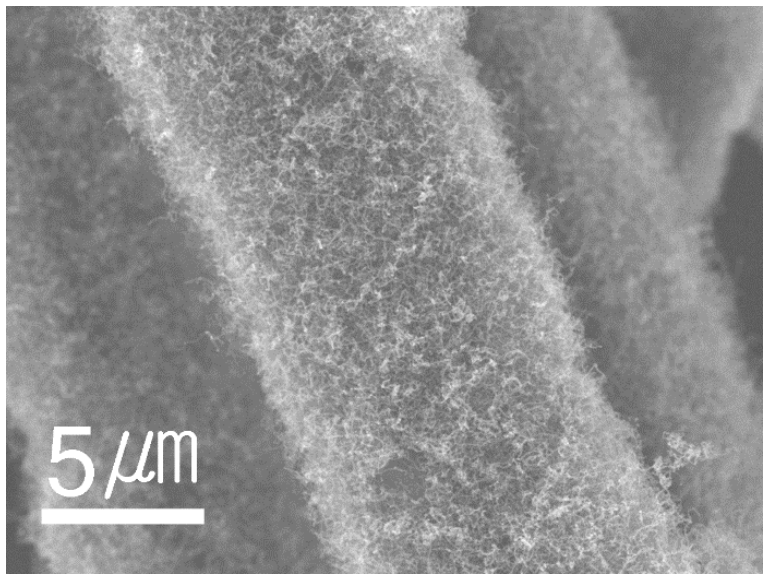

(a)

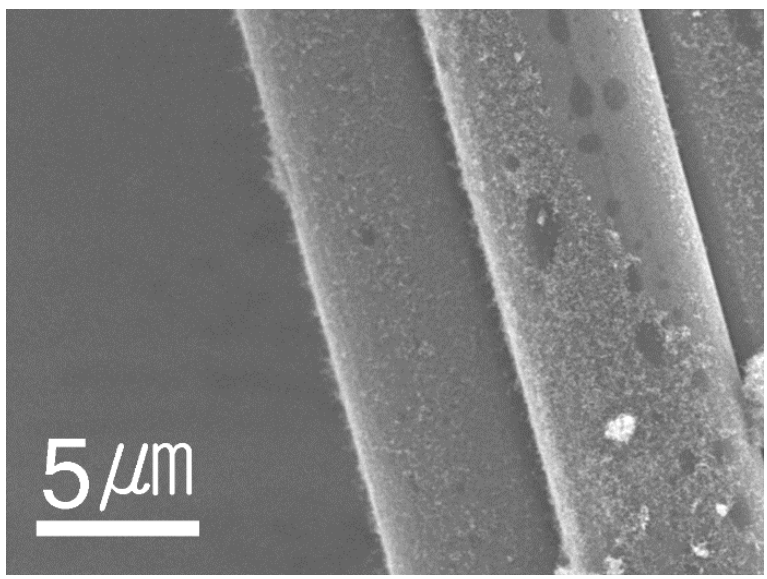

(b)

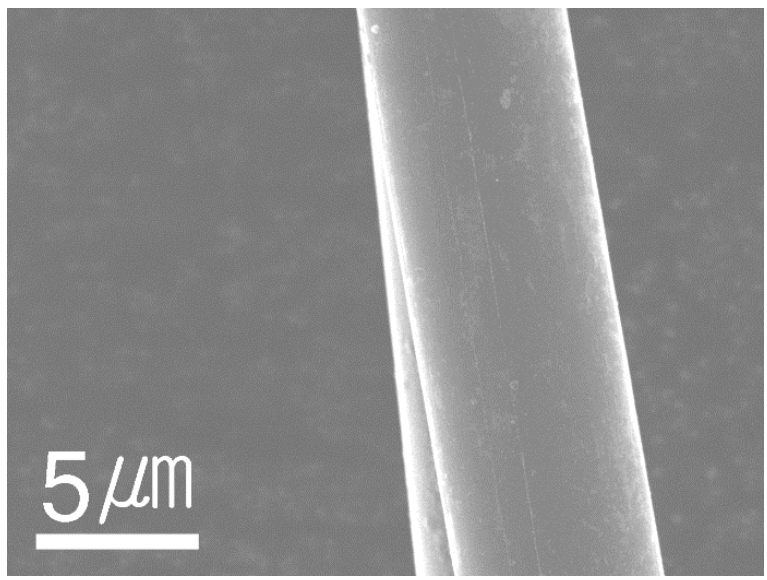

(c)

Figure 2.4. The effect of temperature on CNT growth on CFs during FCVD with the bimetallic catalyst. CNT growth was hindered with increasing temperature. (a) 500°C, (b) 600°C, (c) 750°C.

2.3.2 Mechanical properties and microstructure of the CNT-grafted CFs

The effect of CVD process on the mechanical properties of CNT-grafted CFs was investigated (Figure 2.5). For the comparison, as-received CF and heat-treated CFs at 750 °C without CVD process were also characterized. Note that CVD temperature for preparing CNT-grafted CFs using the Fe-only and the bimetallic catalysts were 750 and 500 °C, respectively. Two noticeable features can be identified. The elastic moduli of all samples were similar regardless of the treatment conditions, whereas the tensile strength of CNT-grafted CFs prepared using Fe-only catalyst was severely degraded. Since the tensile strength of materials is governed by material defects or imperfections [71], it can be deduced that some defects were generated during Fe-only CVD process. The microstructure of CFs was then examined to reveal the cause of such degradation and to explain similar elastic modulus of all samples.

For the first, wide angle X-ray diffraction analysis was carried out and Debye images were obtained for the CFs. To subtract effect of CNTs on WAXS data, catalyst-only deposited CFs were used as sample (Ni-Fe bimetallic catalyst-only deposited CF after heat treatment at 500^{o}C for 1 hr (Bi-500) and Fe catalyst-only deposited CF after heat treatment at 750^{o}C for 1 hr (Fe-750)). We compared crystallinity of CFs by Full width at half maximum (FWHM) of each peaks in 1-D WAXS data (Figure 2.6). And since the crystalline orientation of materials has an important influence on their mechanical properties, Debye ring images were investigated in Figure 2.7. The crystal orientation of CFs seems similar for four samples. For further investigation, the strength distribution curve of Debye loop on the equator line were obtained as shown in Figure 2.8, from which both full width at half maximum (FWHM) and peak integration (Int.W) were obtained [72]. As shown in

Table 1, the crystallinity and orientation index of CFs is not very different, suggesting that the crystal structure and orientation of CFs were not degraded after high-temperature CVD process. As such, X-ray diffraction analysis also cannot explain such a huge difference in the tensile strength of CFs observed in Figure 2.5.

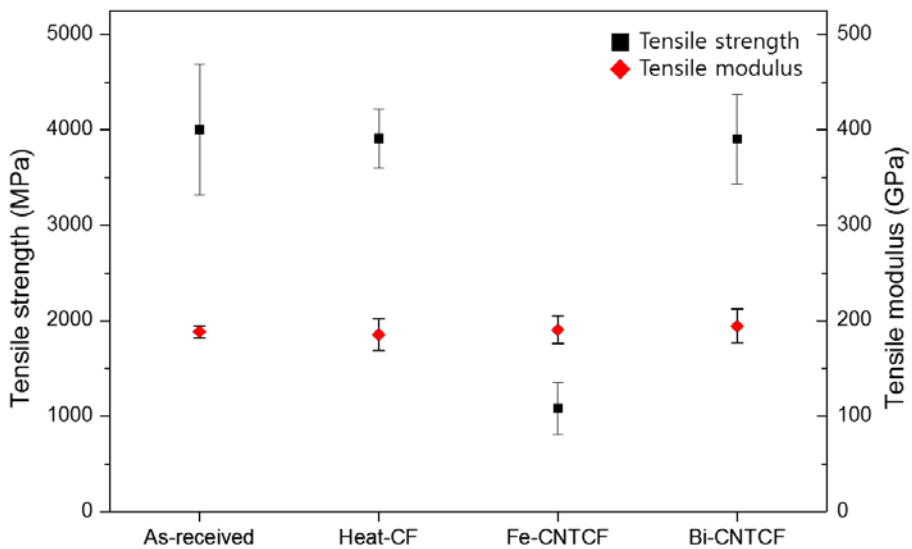

Figure 2.5. Tensile strength and modulus of CNT-grafted CFs prepared using different FCVD conditions. The *x*-axis labels correspond to the as-received CFs, CFs CNT-grafted CFs prepared using the bimetallic catalysts (Bi-CNT) and Fe-only catalysts (Fe-CNT).

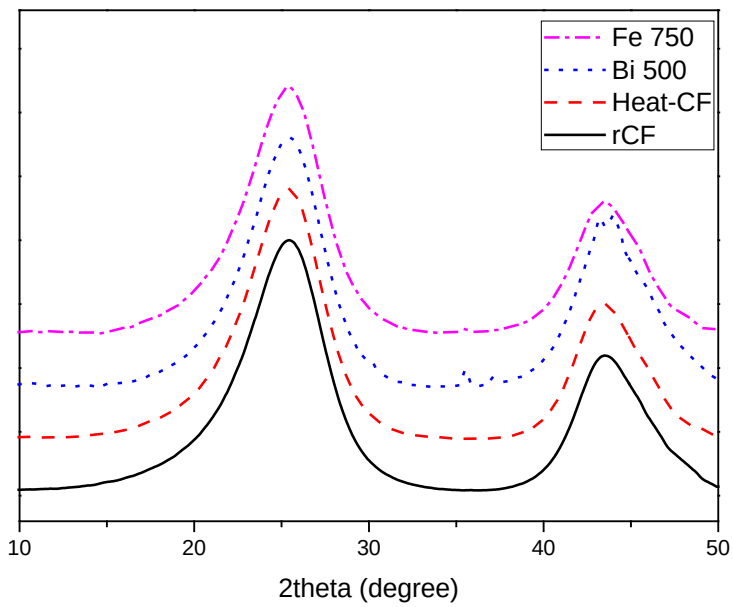

Figure 2.6. 1-D wide angle X-ray scattering patterns of CFs after heat treatment.

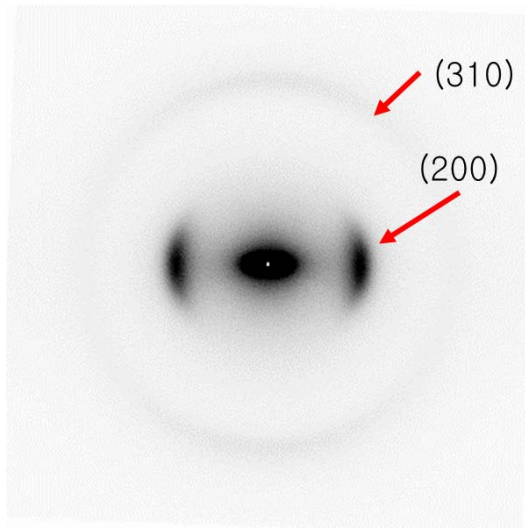

(a)

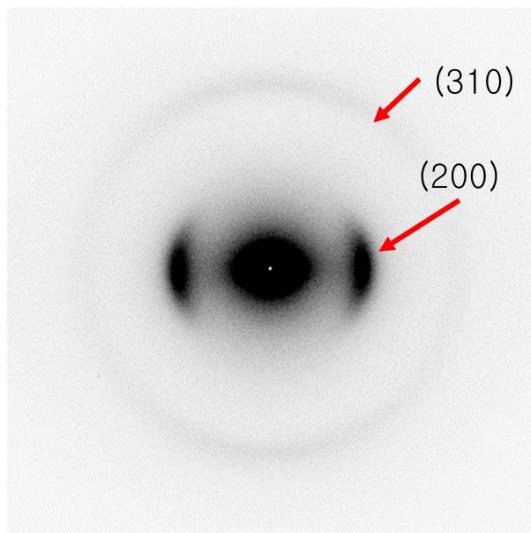

(b)

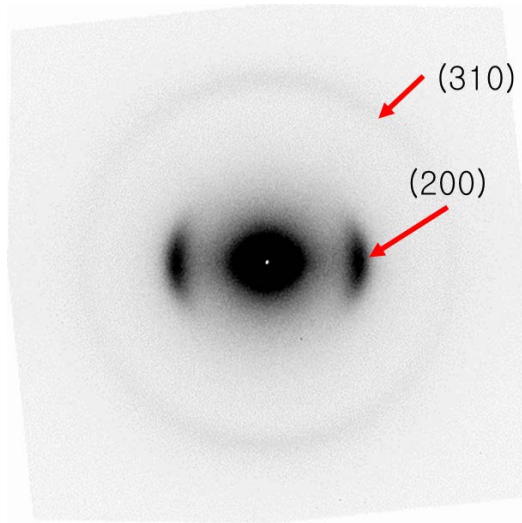

(c)

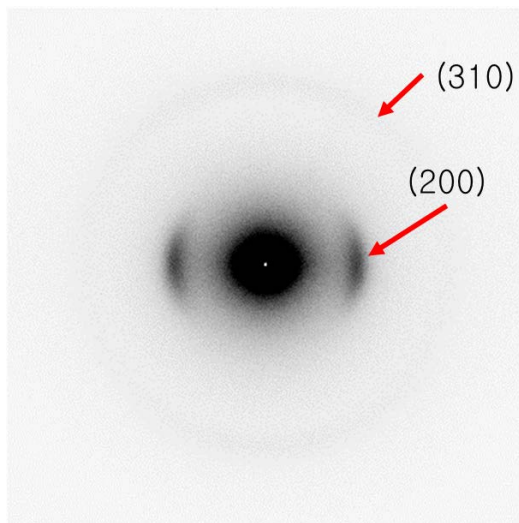

(d)

Figure 2.7. Debye diffractograms of CF surface; (a) as-received CF (b) as-received CF after heat treatment at 750°C (c) surface of bimetallic catalyst-only deposited CF after heat treatment at 500°C for 1 hr (Bi-500) (d) surface of Fe catalyst-only deposited CF after heat treatment at 750°C for 1 hr. (Fe-750)

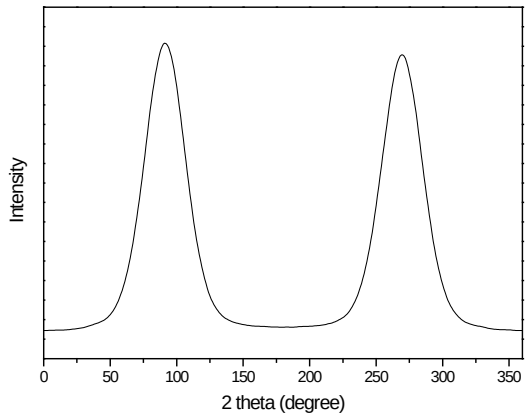
Intensity
0
50
100
150
200
250
300
350
2 theta (degree)

(a)

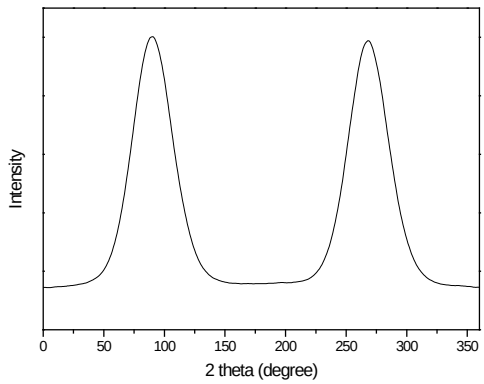
Intensity
0
50
100
150
200
250
300
350
2 theta (degree)

(b)

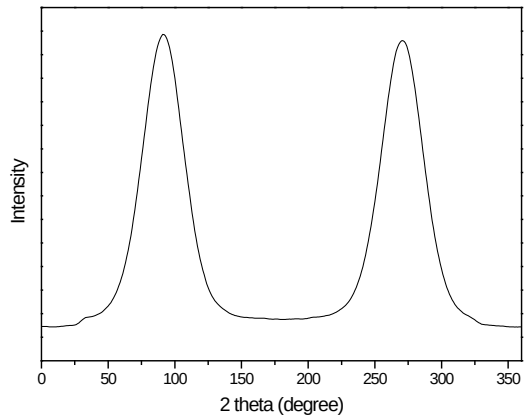

(c)

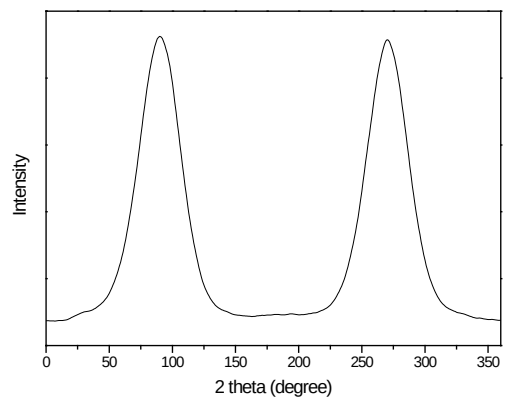

(d)

Figure 2.8. The strength distribution curve of Debye loop on the equator line for CFs; (a) as-received CF (b) as-received CF after heat treatment at 750°C (c) surface of bimetallic catalyst-only deposited CF after heat treatment at 500°C for 1 hr (Bi-500) (d) surface of Fe catalyst-only deposited CF after heat treatment at 750°C for 1 hr (Fe-750).

Table 2.1. Orientation index and crystallinity of CF surface crystalline

Sample	*Preferred orientation*		*Crystallinity*	*Tensile strength*
	FWHM (%)	Int.W (%)	FWHM (°)	*(MPa)*
As-received	89.8	77.2	5.25	4002 (683)
Heat-CF	89.1	75.7	5.1	3608 (306)
Bi-500	89.7	76.4	5.1	3944 (508)
Fe-750	89.1	75.5	5.2	1082 (74)

Because we could not find out any significant differences in WAXS analysis, we considered about microstructural analysis over-nanometer scale. The size of nanoparticles was 10 to 20 nm and structural difference with these scale such as lamellar structure and voids cannot be seen in WAXS. So we conducted Raman spectroscopy and SAXS analysis which can see those over-nanometer scale difference in microstructure.

Raman spectra were obtained for both CNTs grown on CF and CFs without CNTs. Figure 2.9 (a) and (b) shows Raman spectra of CNTs grown on CF by FCVD process with different temperature and catalysts. CNTs grafted on CF from high-temperature FCVD process shows much lower ID/IG ratio (0.43) than that of CNTs grafted on CF from low temperature FCVD process (1.28). As reported in [73], the annealing effect in high-temperature causes higher quality of CNTs. But in case of substrate CFs, CFs after high-temperature heat treatment with Fe catalysts (Fe-750) showed higher IG/ID ratio (Figure 2.9 (e), 0.91) than as received CFs (rCF) (Figure 2.9 (c), 0.75) and CFs after low temperature heat treatment with bimetallic catalysts (Bi-500) (Figure 2.9 (d), 0.76) which means smaller crystallite size on the surface [74]. From Raman spectra, we concluded that the quality of CNTs grafted on CF was varied according to catalysts and CVD temperature, however the carbon structures of CFs showed opposed behavior, inferring that the mechanical properties observed in Figure 2.5 can be affected by microstructural difference.

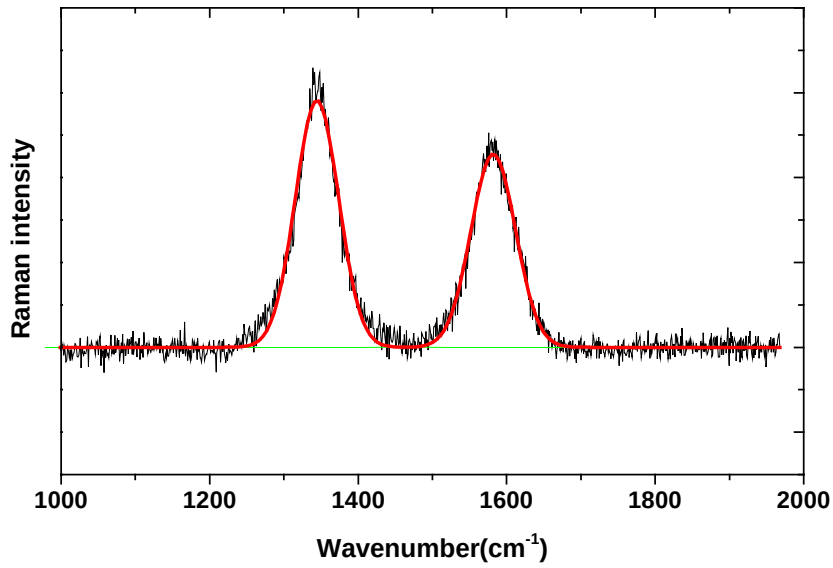
Raman intensity
1000
1200
1400
1600
1800
2000
Wavenumber(cm-1)

(a)

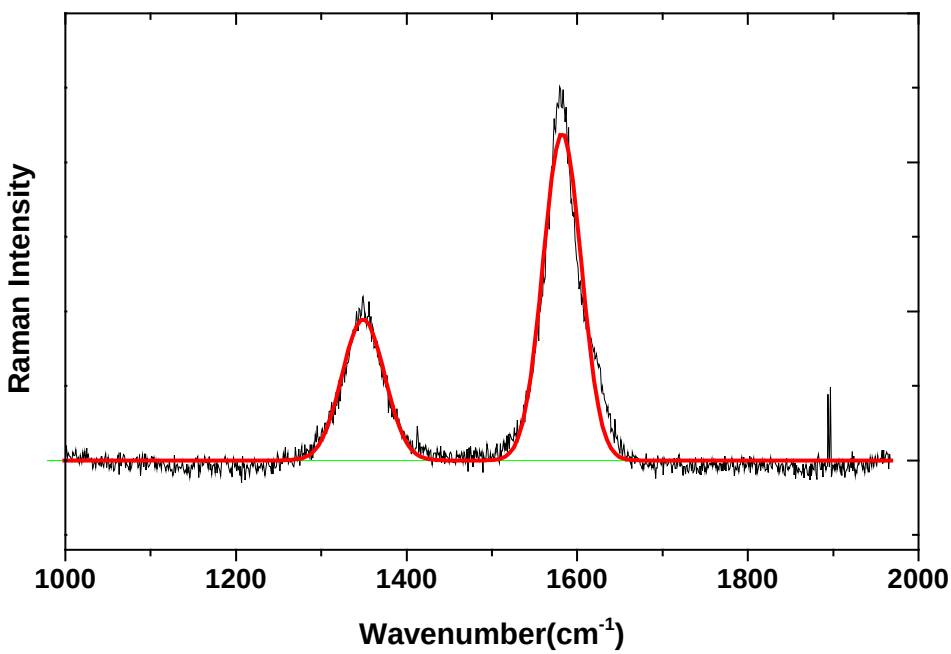
Raman Intensity
1000
1200
1400
1600
1800
2000
Wavenumber(cm-1)

(b)

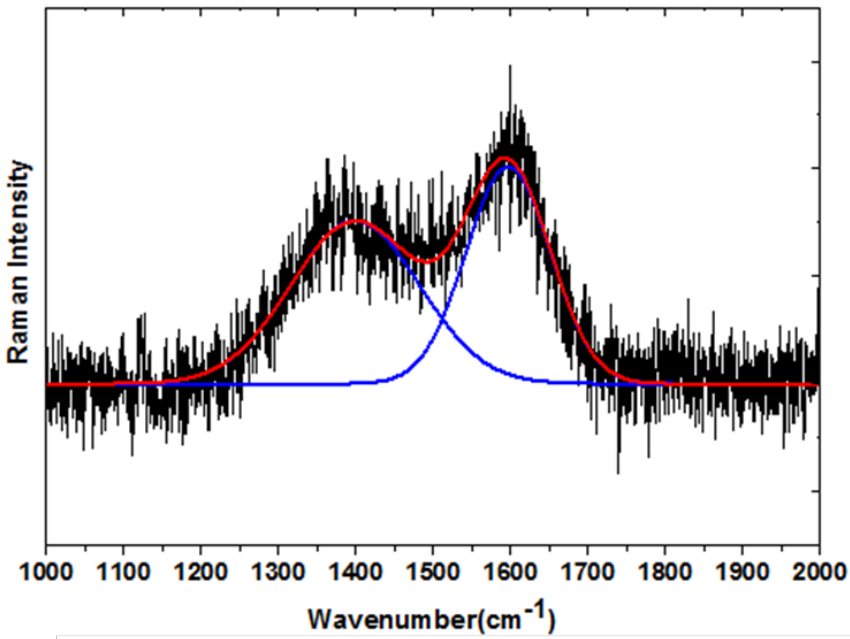
Raman Intensity
1000 1100 1200 1300 1400 1500 1600 1700 1800 1900 2000
Wavenumber(cm-1)

(c)

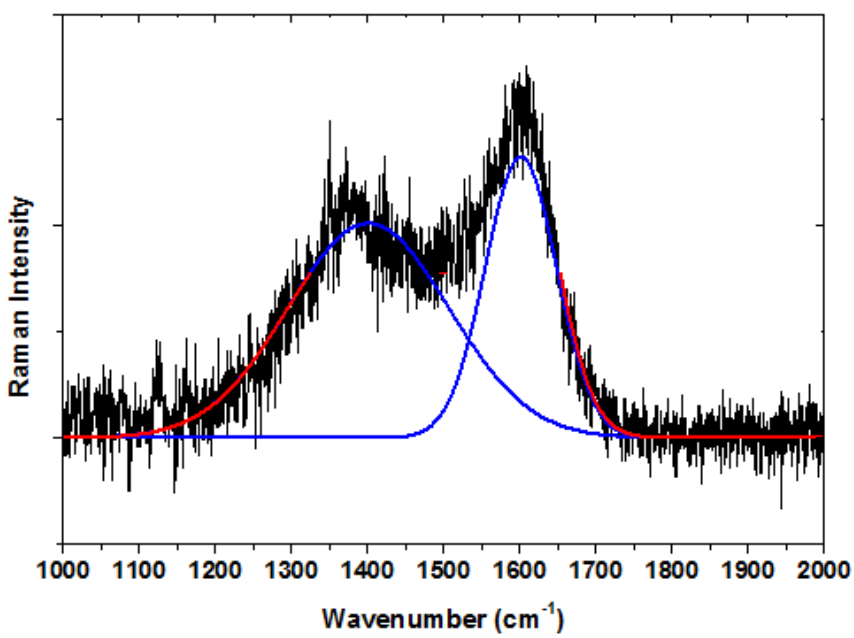
Raman Intensity
1000 1100 1200 1300 1400 1500 1600 1700 1800 1900 2000
Wavenumber (cm-1)

(d)

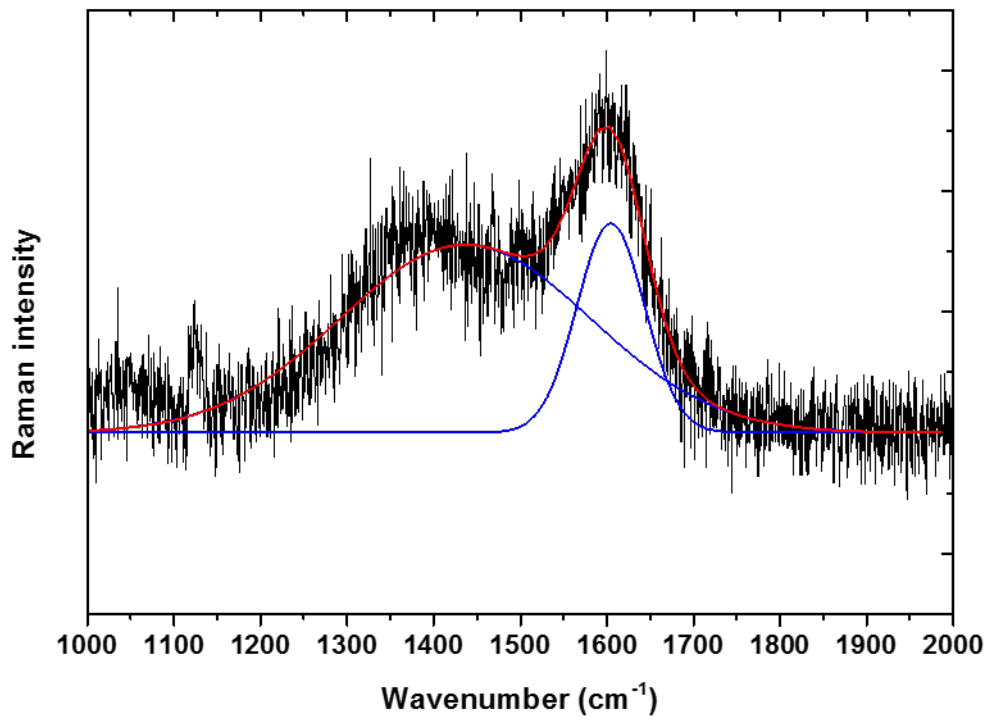

(e)

Figure 2.9. Raman spectra of (a) CNTs grafted on CF by bimetallic catalyst FCVD at 500 (b) CNTs grafted on CF by Fe-only catalyst FCVD at 750°C (c) surface of as-received CF (d) surface of Ni-Fe bimetallic catalyst-only deposited CF after heat treatment at 500°C for 1 hr (Bi-500) (e) surface of Fe catalyst-only deposited CF after heat treatment at 750°C for 1 hr (Fe-750)

SAXS analysis is a useful method to characterize microstructure [75, 76] and microvoids [77, 78] in fiber due to X-ray's penetration and its statistical results. Especially, the microvoids in CFs have great influence on its mechanical properties [79]. Through SAXS analysis for the CFs (Figure 10), we found that scattering intensity of Fe-750 sample after same time exposure to the X-ray is way higher than that of the other samples which means larger relative volume of microvoids [80] between lamellar which can be act as defect and reason of mechanical degradation.

Lastly, the internal structure of CFs was directly observed using FIB and TEM, from which significantly different morphologies were observed. Figures 2.11 (a) clearly showed that catalyst nanoparticles had diffused into CFs undergoing Fe-only catalyst FCVD at 750 °C. We believe that this diffusion prevented CNTs from being grown on CFs (Figure 2.3 (c)). In contrast, no catalyst nanoparticles were observed in CNT-grafted CFs prepared using bimetallic catalyst FCVD (Figure 2.11 (b)), explaining well growth of CNTs on CFs observed in Figure 2.3 (a). Elevated temperature in bimetallic FCVD process, e.g., to 750 °C, resulted in again some catalysts nanoparticles diffused into CFs (Figure 2.11 (c)). This diffusion can explain no growth of CNTs from the bimetallic FCVD at elevated temperature (Figure 2.4 (c)). It can be claimed that regardless of catalyst type, high-temperature CVD caused catalyst nanoparticles to be diffused into the CFs. Furthermore, we believe that the diffusion of catalyst particles into CFs brought about lowered tensile strength by introducing some defects near surface of CFs.

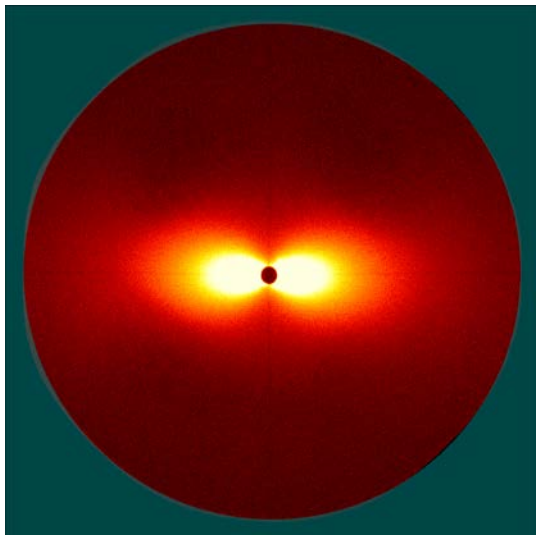

(a)

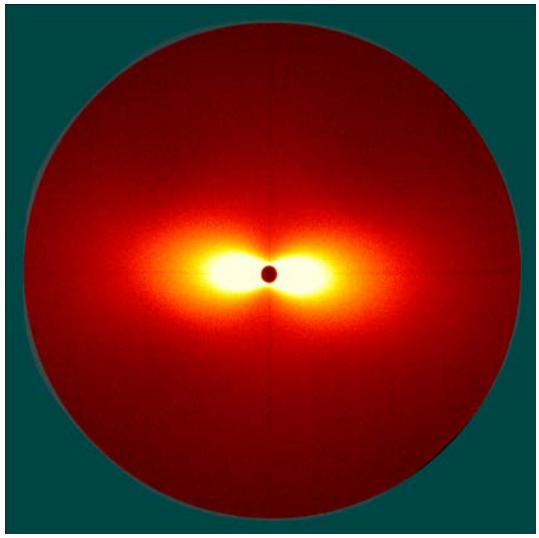

(b)

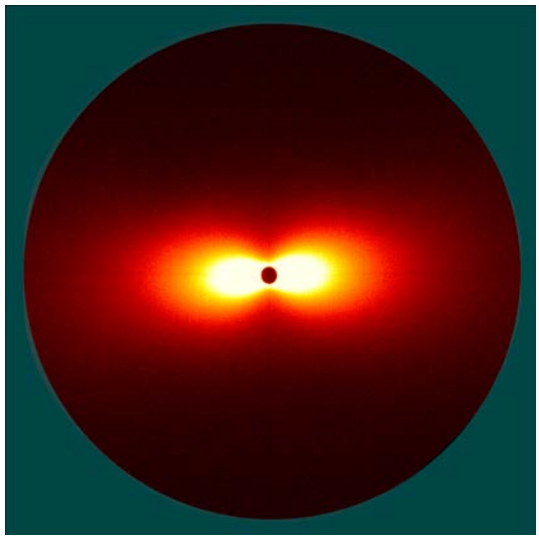

(c)

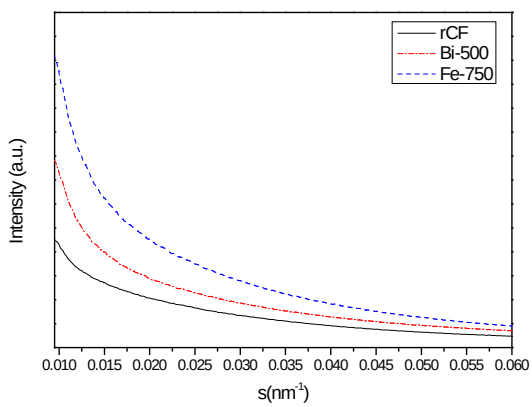

(d)

Figure 2.10. Small angle X-ray scattering (SAXS) patterns of CFs; (a) as-received CF (b) Ni-Fe bimetallic catalyst-only deposited CF after heat treatment at 500°C for 1 hr (Bi-500) (c) Fe catalyst-only deposited CF after heat treatment at 750°C for 1 hr (Fe-750); and slice of scattering intensity at center of 2D SAXS pattern along meridian direction (d).

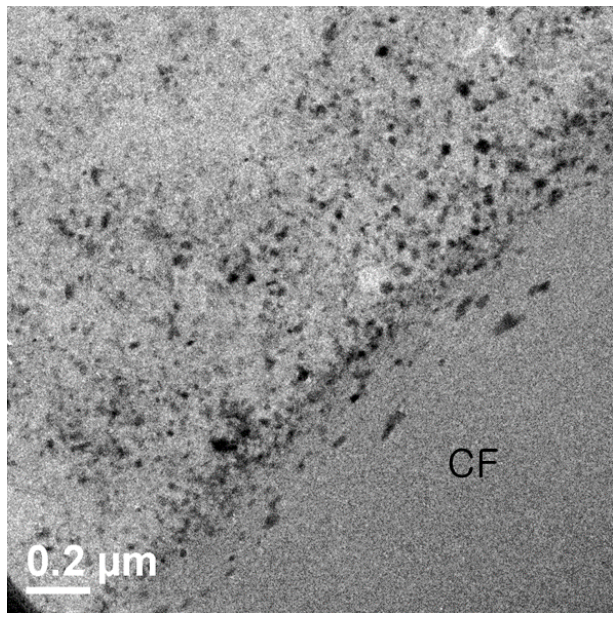

(a)

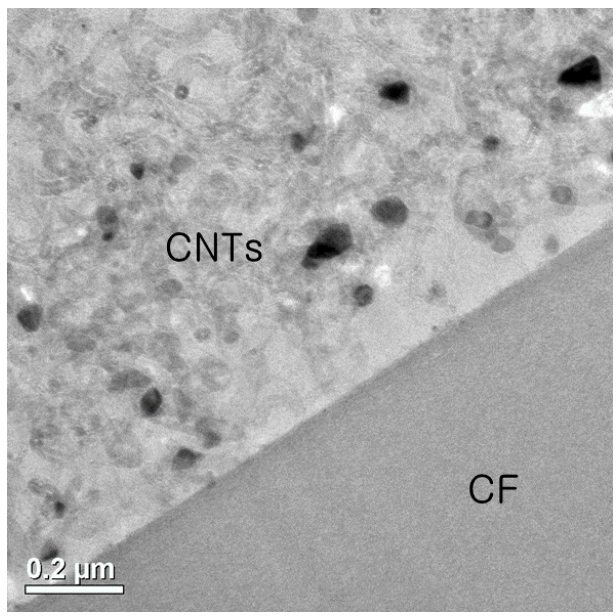

(b)

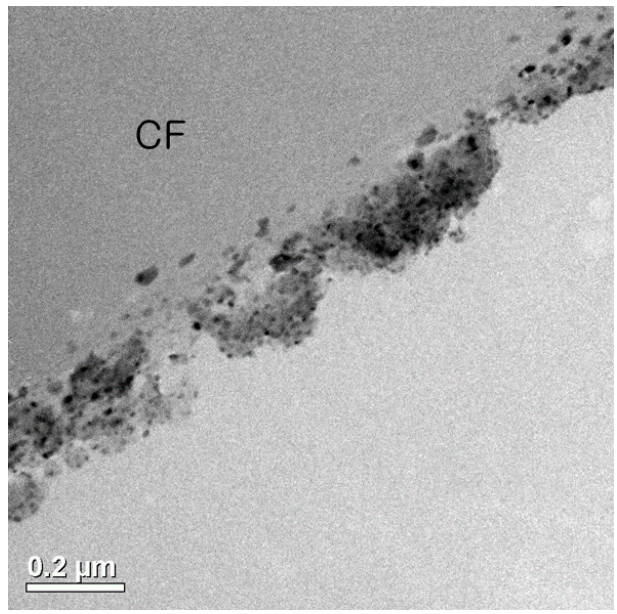

(c)

Figure 2.11. The internal structure of CNT-grafted CFs prepared from different FCVD processes. (a) FCVD using the Fe-only catalysts at 750°C, (b) FCVD with the bimetallic catalyst at 500°C, (c) FCVD with the bimetallic catalyst at 750°C.

2.4. Summary

We demonstrated that CNT-grafted CFs can be manufactured without mechanical degradation of the CFs. This was achieved using a bimetallic catalyst, which lowered the activation energy for CNT growth, thereby enabling a lower CVD temperature to be used. Inter-diffusion of CFs and catalysts, which is the main source of mechanical degradation and reduced CNT growth, was successfully avoided with the low-temperature CVD process.

3. CNT-grafted carbon fibers reinforced composites

3.1. CNT-grafted carbon fibers reinforced plastics

3.1.1 Introduction

Due to their excellent mechanical, electrical and thermal properties, CFs and their composites have been used in nearly all-engineering fields, promoting vast research to improve their mechanical properties. However, the improvements of the mechanical properties of CFs are now saturated; thereby researchers pursue a new direction for improving the mechanical properties of the CF reinforced composites. On the other hand, CNTs have been emerged to a new generation reinforcement material and stimulated a considerable amount of research. However, the application of CNTs as reinforcement has brought many problems related with aggregation of CNTs in polymeric matrix and low volume fraction of reinforcement. Thus, the hybridization of CNTs and carbon fibers CFs, which called as CNT-grafted CF has emerged as such an advanced and hierarchical material that can improve the reinforcing effect of CFs in composites and solve the dispersion problems of CNTs1. Radially grown CNTs on CFs improve the radial stiffness and axial tensile strength of CF-reinforced composites, IFSS of polymer composites, and the electrochemical performance as CF electrodes.

CNTs have been directly grown on the CF surface using CVD. Early research into this method was focused on uniform CNT growth, by investigating the effect of process conditions, such as CVD temperature, various carbon sources and their flow rates, and the type and concentration of catalyst, on CNT growth, and also by

investigating the growth mechanism, the morphology of the resulting CNTs or carbon nanofibers and the anchorage of CNTs on CFs

Beside these fabrication process, the mechanical properties of CNT-grafted CFs and their composites have been scrutinized by focusing on the tensile properties of CFs undergoing CNT grafting process and the interfacial properties of CNT-grafted, CF-reinforced composites. The interfacial properties of the composites were improved but the CF tensile properties may have been degraded during grafting process, although the potential to increase the CF mechanical properties has been reported.

Through the chapter 2, we succeed to grow CNTs on CF without degradation of the mechanical properties of CFs by using low-temperature process with Ni-Fe bimetallic catalyst. We lowered growth temperature of CNTs to below 500^{o}C and succeed to inhibit the inter-diffusion between carbon and catalyst particles while CVD process.

Many researches for CNT-grafted CF as reinforcement of composites could not show good mechanical properties because of the degradation of mechanical properties of the CFs while chemical vapor deposition (CVD) process which is for grafting of CNTs on CF. Some of researchers succeed to prevent degradation by using buffer layer coated on CF or control of catalysts layer deposited on CF8 but these methods are not suitable for macroscale process. Because of these limits, previous researchers could not show the mechanical performance of CNT-grafted CF reinforced composites in macroscale

In this study, we report about the manufacturing process for CNT-grafted CF reinforced composites without degradation of mechanical properties of CFs and their thermal/electrical/mechanical properties. Tensile strength of CNT-grafted CFRP

was increased 19% in unidirectional composites and 32% in woven composites compared to as-received CFRP. Increased interfacial shear strength (IFSS) was critically contributed to the strength of CFRP and we identified their failure mechanism by observation of fractured surface of CFRP.

3.1.2 Experimental

3.1.2.1 Preparation of CNT-grafted CFs

We chose soaking method to introduce catalysts on the CF woven and unidirectional fabric (T-300 grade, Entra-Korea) since its simplicity and low cost for mass production. Especially, we used Ni-Fe bi-metallic catalysts and lowered CVD temperature to maintain mechanical properties of the CF. As a catalyst precursors, we used FeCl3·(H2O)6 and Ni(NO3)2·(H2O)6 and ethanol as a solvent. CFs were soaked in solution of catalysts precursors for 30 minutes and dried at 70℃ for 4 hours. We varied H2 ratio in CVD atmosphere to make CNT-grafted CF with different CNT diameter8 but we did not varied H2 ratio for unidirectional CNT-grafted CF to avoid needless efforts. We also prepared CNT-grafted CF fabrics with Fe-only catalysts at the high temperature (750^{o}C) to show effect of bimetallic catalysts on the mechanical property of CNT-grafted CFs. Catalyst precursor-introduced CF fabrics were batched in the furnace and CVD process was conducted. Details for CVD process are shown in the Figure 3.1.1

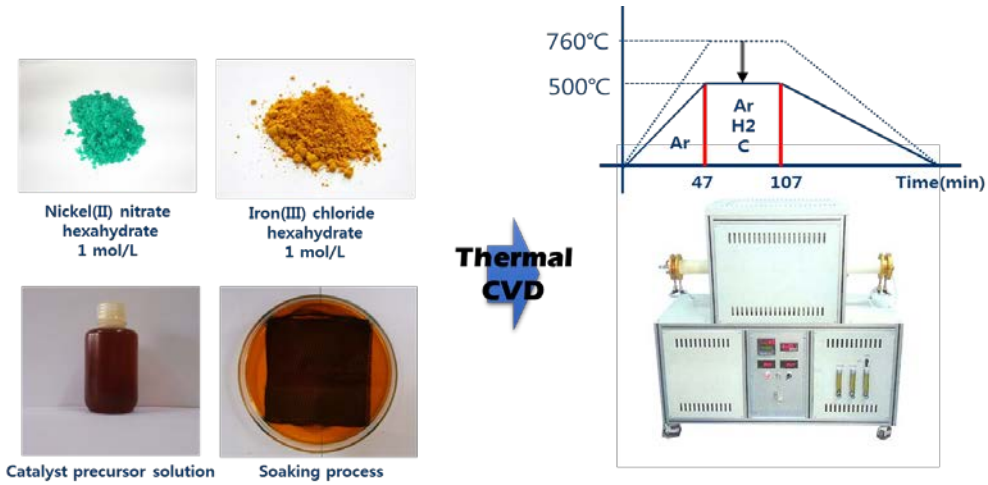

Figure 3.1.1 Schemes for CVD procedure to fabricate CNT-grafted CF fabric

3.1.2.2 Fabrication of CNT-grafted CFRP

We prepared woven and unidirectional, composites to examine the effects of CNT-grafted CFs on the mechanical properties of composites. We prepared 4 layers of As-received/CNT-grafted CF woven/unidirectional fabrics in the mold and infused epoxy resin (Epofix, Struers) by vacuum assisted resin transfer molding (VARTM) process. After infusion of epoxy resin, composites were pressed on the hot press with stopper to make composites with same volume fraction. Height of the stopper was 1mm and composite was molded with 100kgf/cm^2 of pressure at 60^{o}C. Intended volume fractions of composites were 47.4% for woven (23.7% for tensile direction) and 46% for unidirectional composites.

3.1.2.3 Characterizations

The mechanical properties and Weibull properties of CNT-grafted CFs were measured using a single-fiber tensile test with 20mm and 30mm of gage length and 2mm/min of strain ratio by lab-made universal test machine. IFSS of CFs for epoxy resin was measured by micro-droplet debonding test by lab-made tester. We measured tensile properties of composites by universal testing machine (INSTRON 5569). Specimens for each sample were tested and the specimen size was 150 x 15 x 1 mm^3 (gage length = 100 mm).

Morphologies of CFs after FCVD process were observed by field emission scanning electron microscopy (FE-SEM, JEOL, JSM 7600F) and wall structure of CNTs on CF was observed by high-resolution transmission electron microscopy (HR-TEM, JEOL 3000F). We observed fractured surface of samples after tensile test by FE-SEM to identify failure mechanism of composite material and reinforcement effects of CNT grafting process. In-situ microscope observation of surface crack while tensile test was conducted to investigate the reason for varied in-

crements of tensile strength in unidirectional and woven composites.

To measure the stress intensity needs for the splitting crack initiation, 4-point bending test with notched UD specimen has been conducted by following reference[83].

Electrical conductivity of CFRP was measured by electrometer (KEITELEY 6517A) with several voltages (1, 10 and 100V) and thermal conductivity of CFRP was measured by laser flash analysis (LFA 457).

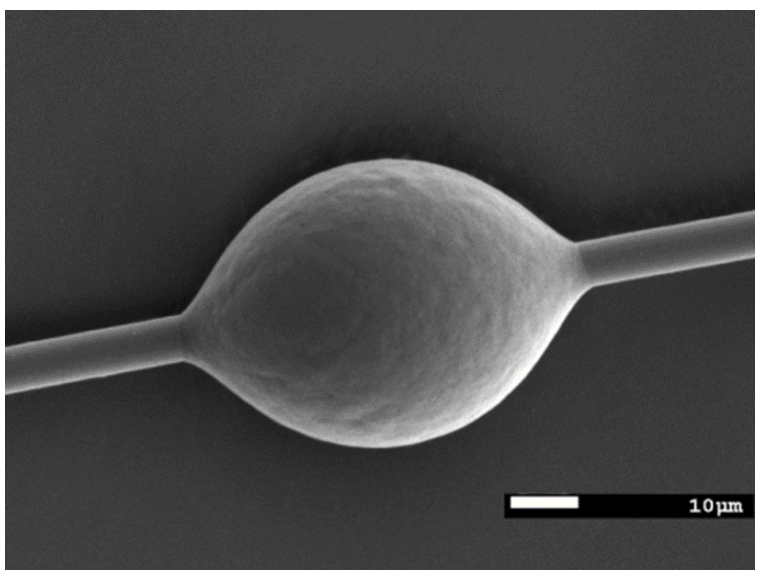

Figure 3.1.2 Formed micro-droplet of epoxy on the carbon fiber surface

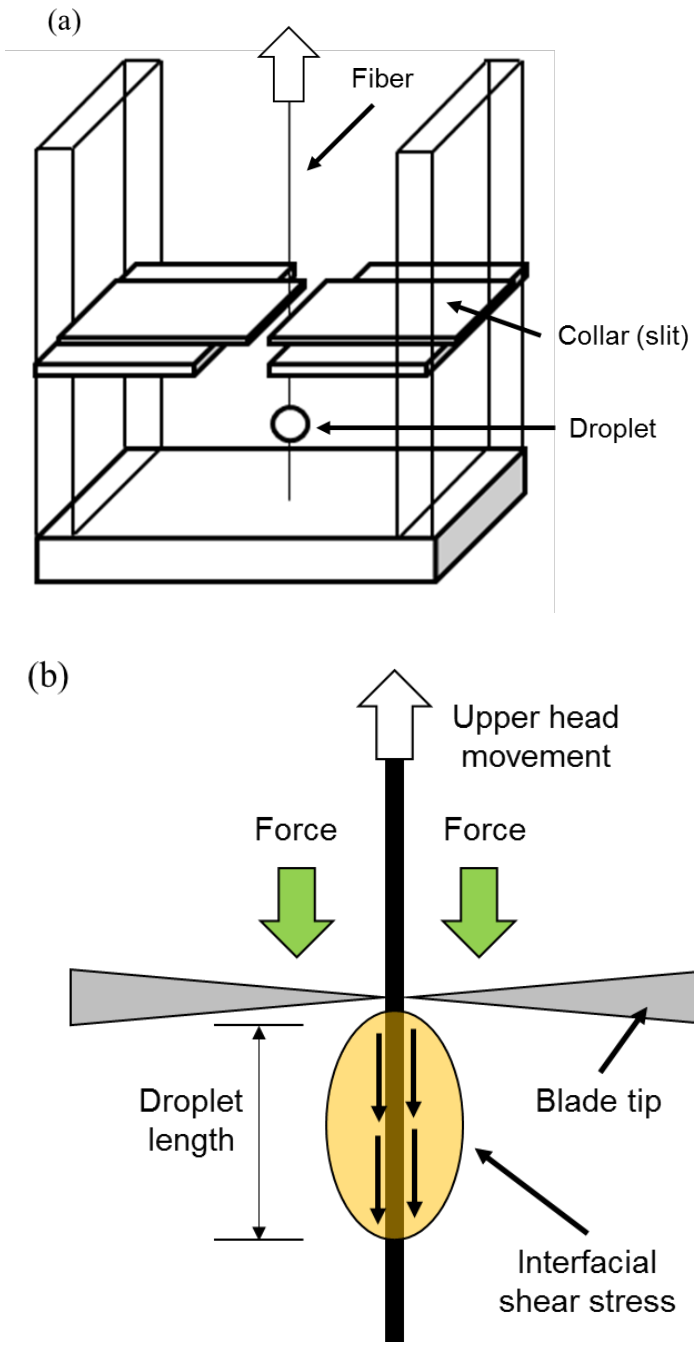

Figure 3.1.3 Schematic diagram of micro-droplet test for IFSS measurement (a) apparatus consists of two blade collars (b)

3.1.3 Results and discussion

3.1.3.1 Morphologies and properties of the CNT-grafted CFs

The morphology of CNT-grafted CF fabrics, prepared by thermal CVD process with Ni/Fe bimetallic catalysts, was observed by FE-SEM. As shown in Figure 3.1.4, CNTs are uniformly grown on CF fabric surface and diameter of CNTs was varied by the H_2 ratio in the CVD atmosphere. Average diameter of the CNTs grown in the atmosphere with low H_2 ratio (H_2:Ar = 1:9) was 22.1nm and that of the CNTs grown in the atmosphere with high H_2 ratio (H_2:Ar = 1:3) was 49.2nm. The wall structure of CNTs was well developed as you can see in Figure 3.1.4 (c) and (f)

We measured the amount of CNTs on CF by weighing the weight of CF fabric before CV process and after CVD process. The weight of CF woven fabric with 15cm x 15cm of area. The amount of CNTs on CF was about 0.3 wt% of CF fabric. Figure 3.1.5 shows the tensile properties of CNT-grafted CFs measured by single fiber tensile test. Weibull modulus of CNT-grafted CF was 12.62 and that of as-received CF was 11.74 and their characteristic stress from Weibull distribution were 4.11 3GPa and 4.077 GPa. Actually, tensile strength of CNT-grafted CF and as-received CF were almost same but IFSS of CNT-grafted CF (58MPa) was 58% higher than that of as-received CF (37MPa). By using bimetallic catalysts, we could prepare CNT-grafted CF woven without degradation of mechanical properties of CFs but with higher IFSS.

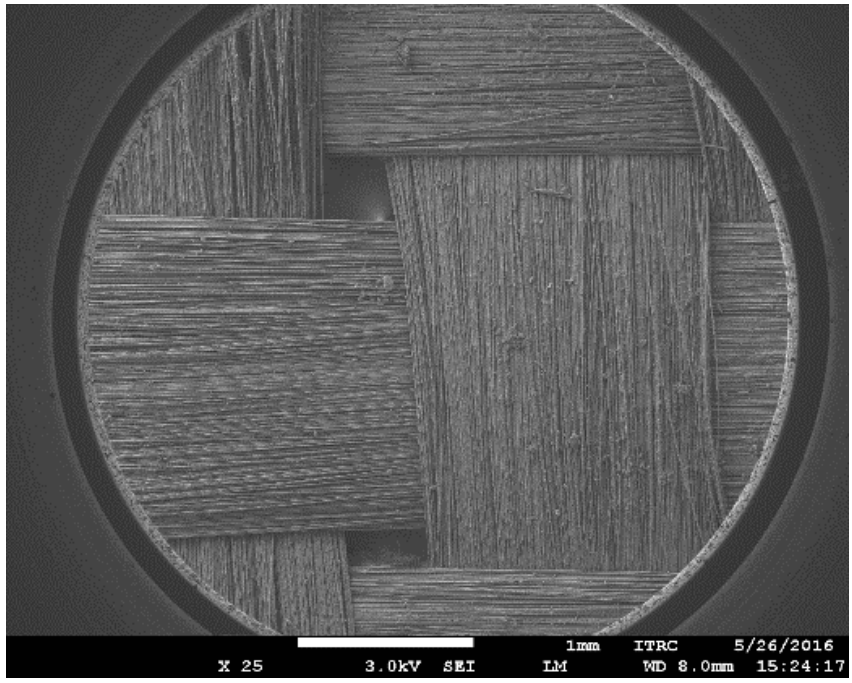
1mm ITRC 5/26/2016
X 25 3.0kV SEI LM WD 8.0mm 15:24:17

(a)

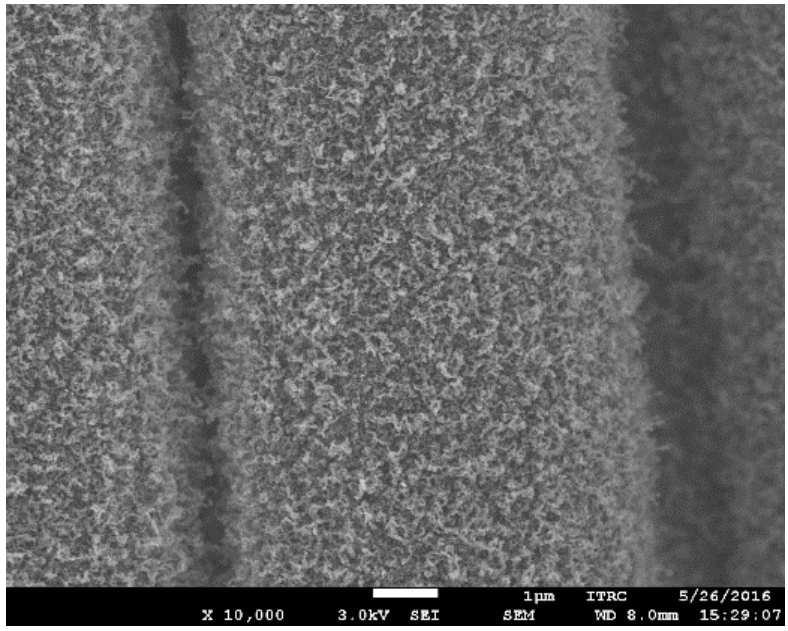
1μm ITRC 5/26/2016
X 10,000 3.0kV SEI SEM WD 8.0mm 15:29:07

(b)

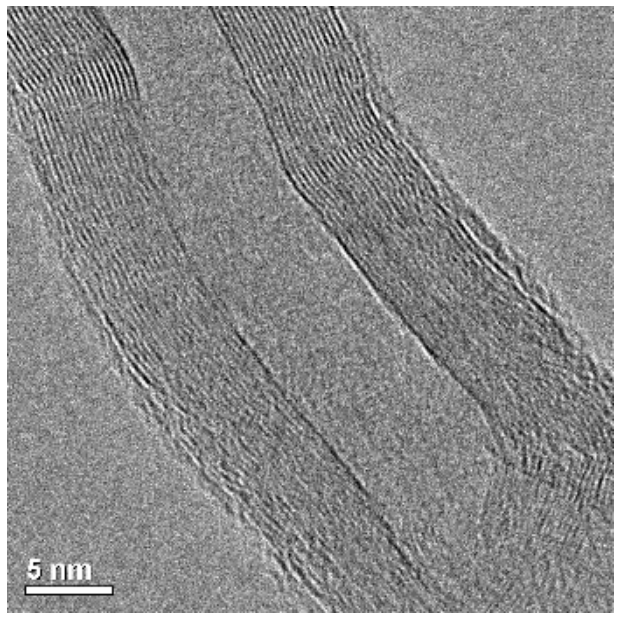

(c)

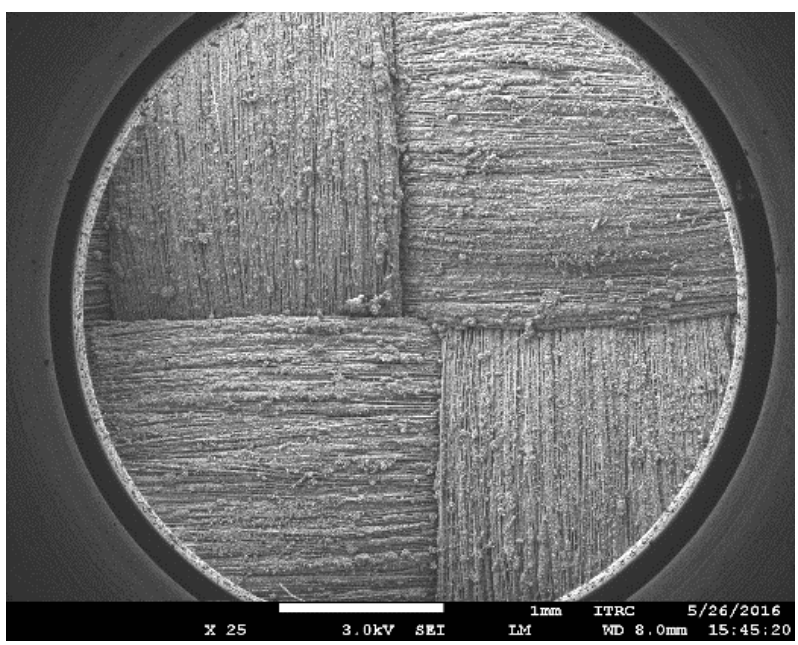

(d)

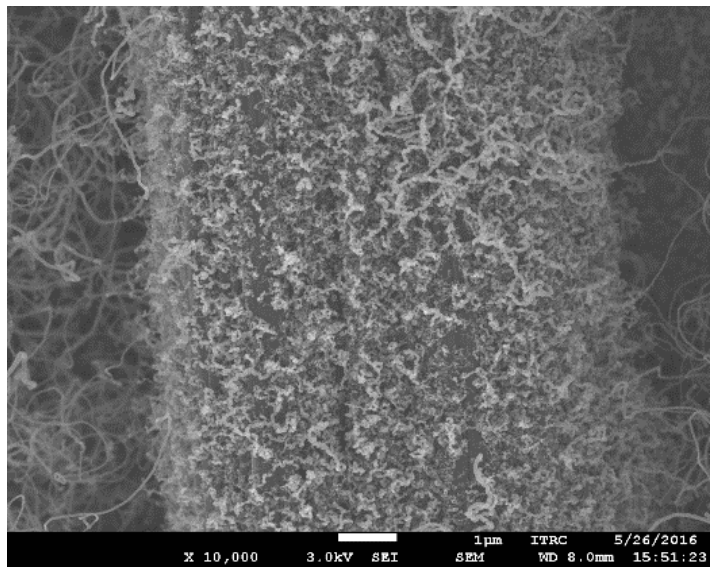

(e)

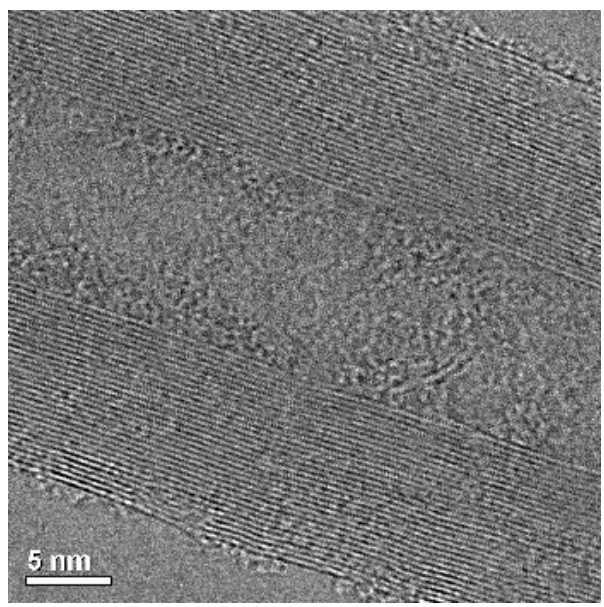

(f)

Figure 3.1.4. Morphologies of the fabricated CNT-grafted CF fabrics and the CNT grafted on CF; CNT-grafted CF

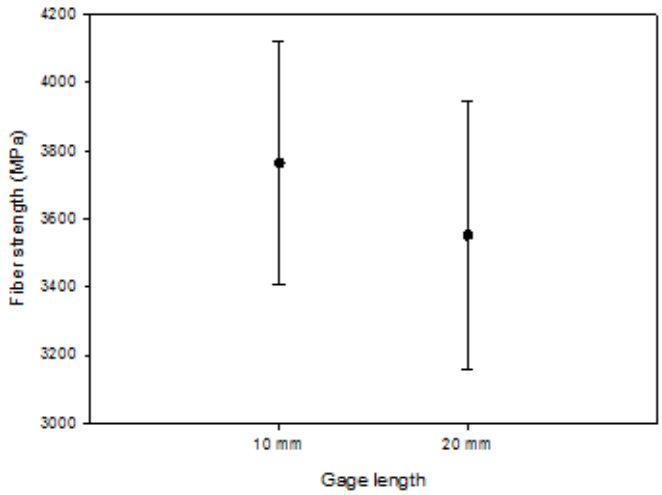

(a)

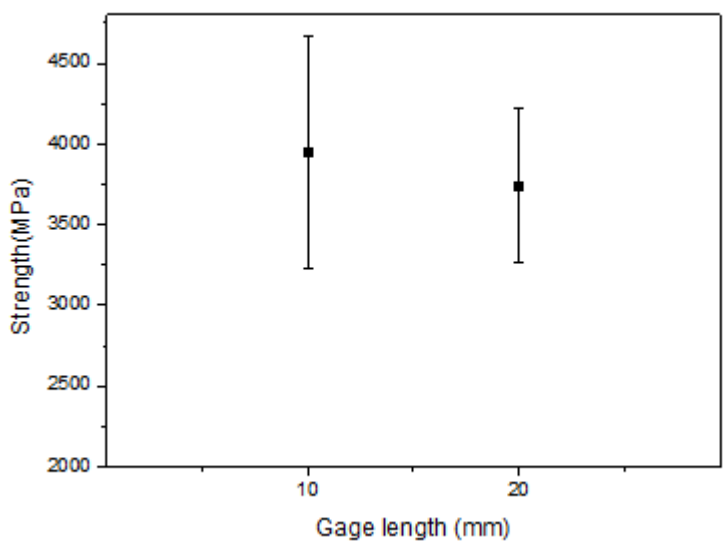

(b)

Figure 3.1.5 Mechanical properties of the (a) as-receive CF and (b) CNT-grafted CF

3.1.3.2 Properties of the CNT-grafted CF reinforced composites

For the first, we measured volume fraction of composites by TGA. As-received CF, CNT-grafted CF, epoxy which we used as matrix, CNT-grafted CF and As-received CF composites were analyzed by TGA and we obtained their thermogravimetric profile (Figure 3.1.6) and calculated their volume fraction with their weight loss at 700°C. Results were almost same with intended volume fraction.

Mechanical properties of composites were measured by tensile test. Commonly, composites made by CNT-grafted CF showed higher tensile strength than composites made by as-received CF composites while modulus of composites was almost same and the increment effect of tensile strength was slightly higher in case of woven composites. Figure 3.1.7 is representative stress-strain curve for tensile test of composites. CNT-grafted CF woven composites which have CNTs with large diameter showed relatively higher increment (32%) than that of composites which have CNTs with small diameter (9%). Especially, maximum strain of composites were dramatically increased. For a while, unidirectional composites showed relatively lower increment than woven composites even though we grafted CNTs with large diameter (17%). We considered that these different increments in strain and strength come from the increased interfacial properties and interlaminar properties. We tried to investigate the reason why CNT-grafted CF composites have better mechanical properties.

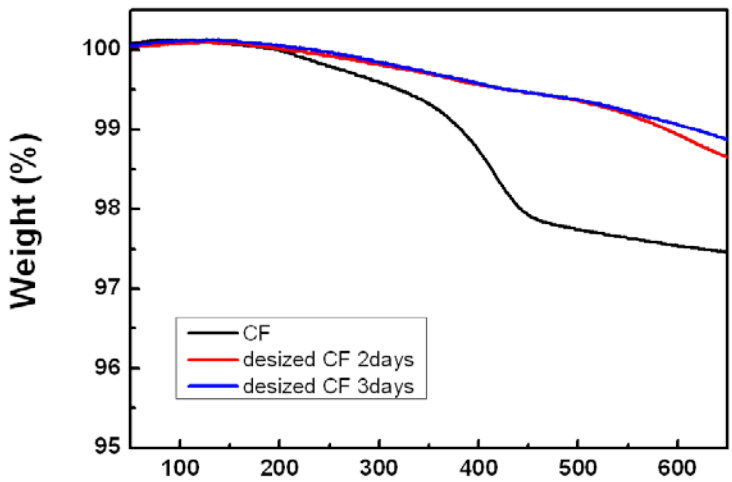
Weight (%)
100
99
98
97
96
95
100
200
300
400
500
600
CF
desized CF 2days
desized CF 3days

(a)

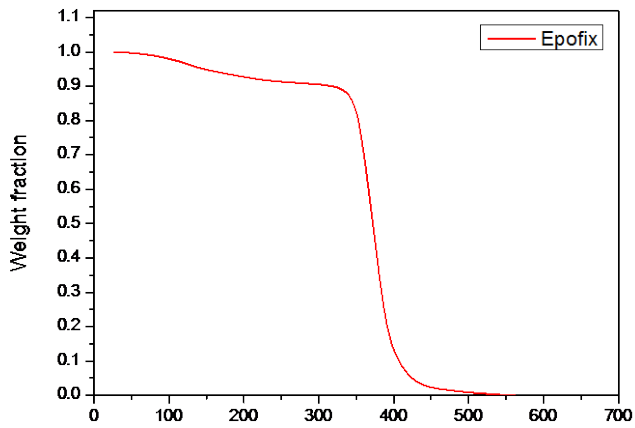
Weight fraction
1.1
1.0
0.9
0.8
0.7
0.6
0.5
0.4
0.3
0.2
0.1
0.0
0
100
200
300
400
500
600
700
Epofix

(b)

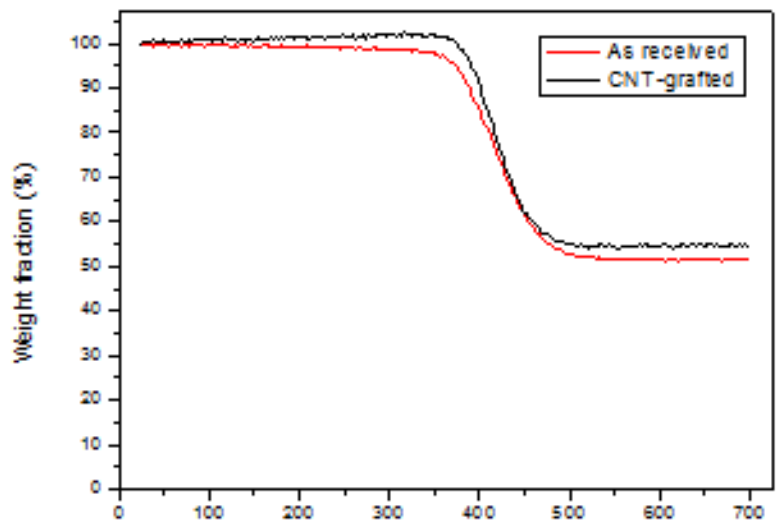

(c)

Figure 3.1.6. Thermogravimetric profiles of the (a) CFs, (b) Epoxy resin and (c) composites

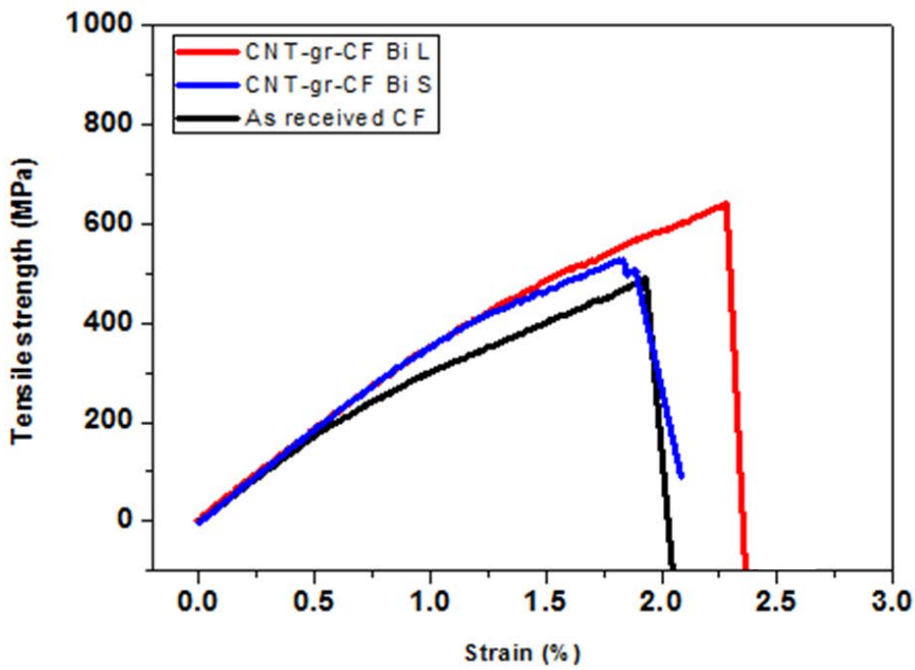
CNT-gr-CF Bi L
CNT-gr-CF Bi S
As received CF
Tensile strength (MPa)
Strain (%)
1000
800
600
400
200
0
0.0
0.5
1.0
1.5
2.0
2.5
3.0

(a)

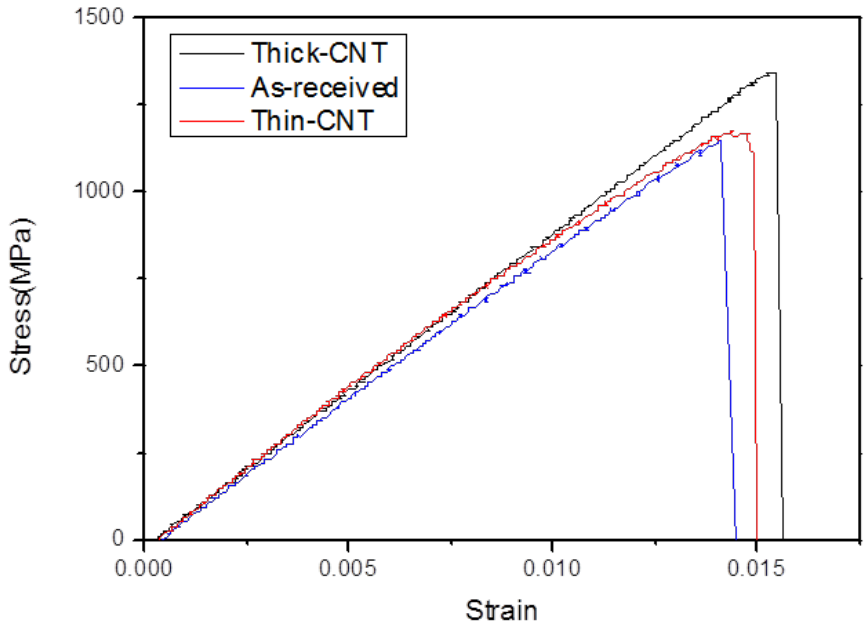

(b)

Figure 3.1.7 Representative stress-strain curve for (a) woven and (b) unidirectional CFRP

We also measured electrical/thermal conductivity of woven CFRP. CNT-grafted CFRP and as-received CFRP showed almost same electrical conductivity in-plane direction but electrical conductivity through the thickness of the CNT-grafted CFRP was 62% higher than that of as-received CFRP. Similarly, thermal conductivity of the CNT-grafted CFRP was 51% higher than that of as-received CFRP but their thermal conductivity in-plane direction was almost same. We considered that these phenomena occurred by bridge effect of CNTs between CF and CF fabric. CNT networks constructed between CF and CF laminar contributed to conduction but in-plane direction, effect of CNT was negligible because the conductivity of fibers was dominant.

Table 3.1.1 Properties of the CFRP

	As-received CFRP		CNT-grafted CFRP	
	Unidirectional	Woven	Unidirectional	woven
Elastic modulus (GPa)	90.02 (1.98)	35.3 (0.72)	91.22 (1.79)	38.0 (0.91)
Tensile strength (MPa)	1210 (103.6)	473.2 (20.5)	1373 (97.5)	627.8 (28.3)
Maximum strain (%)	1.44 (0.02)	2.07 (0.05)	1.66 (0.03)	2.32 (0.04)
Electrical conductivity in-plane direction (S/m)	138.2 (7.2)		148.8 (9.1)	
Electrical conductivity through-the-thickness direction (S/m)	23.7 (3.1)		38.4 (2.7)	
Thermal conductivity in-plane direction (W/mK)	2.72 (0.13)		2.78 (0.16)	
Thermal conductivity through-the-thickness direction (W/mK)	0.607 (0.06)		0.945 (0.09)	

3.1.3.3 Investigation of the reinforce mechanism of the CNT-grafted CF

To understand the role of CNTs grafted on the CF surface in failure mechanisms of composite material, their fractured surfaces were observed in FE-SEM (Figure 6). As-received CF composite showed some of CFs pulled-out from the matrix (Figure 3.1.8 (a)) while CNT-grafted CF composites showed failure in stair-like fractured surface (Figure 3.1.8 (c)) which means higher IFSS[12]. The amount of pulled-out CFs was lower in the CNT-grafted CF composites due to the increased IFSS which helps effective load transfer[13]. Hence, the CFs fragmented into shorter fibers and could show higher tensile strength because of their stochastic properties. Furthermore, we could observe that surface of broken CFs were clear in case of as-received CF composites (Figure 3.1.8 (b)) but that of CNT-grafted CF shows complicated cracks because of CNTs (Figure 3.1.8 (d)). We considered that CNTs grafted on CFs inhibited crack propagation through CF surface and caused longer crack path .Thus, strength and toughness of CNT-grafted CF composites were increased.

In-situ microscope observation for surface crack of woven composites were conducted to investigate different increment of tensile strength. As you can see in Figure 3.1.9, cracks were developed at inter-laminar region in case of as-received CFRP and entire laminar was pulled-out. But in case of CNT-grafted CFRP, transverse cracks in the fiber tow showed first and composites were suddenly broken. This phenomenon could be seen in ex-situ observation with FE-SEM (figure 3.1.10).

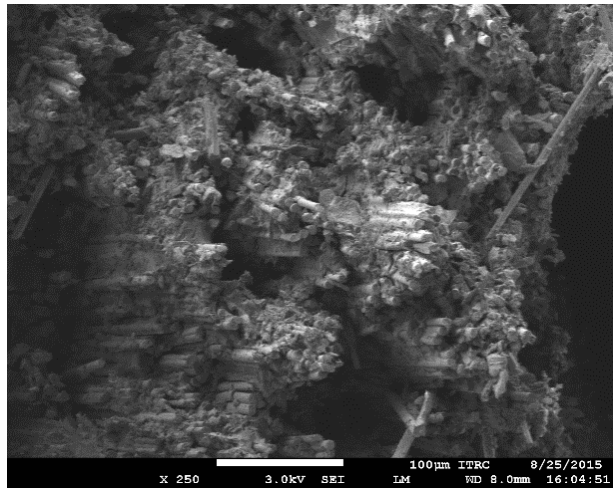
100µm ITRC 8/25/2015
X 250 3.0kV SEI LM WD 8.0mm 16:04:51

(a)

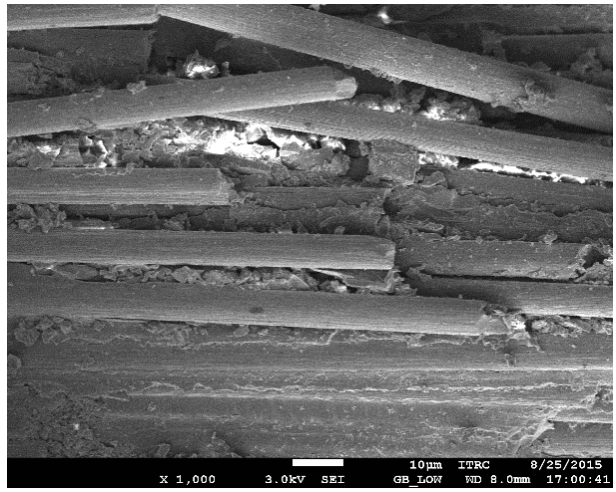
10µm ITRC 8/25/2015
X 1,000 3.0kV SEI GB_LOW WD 8.0mm 17:00:41

(b)

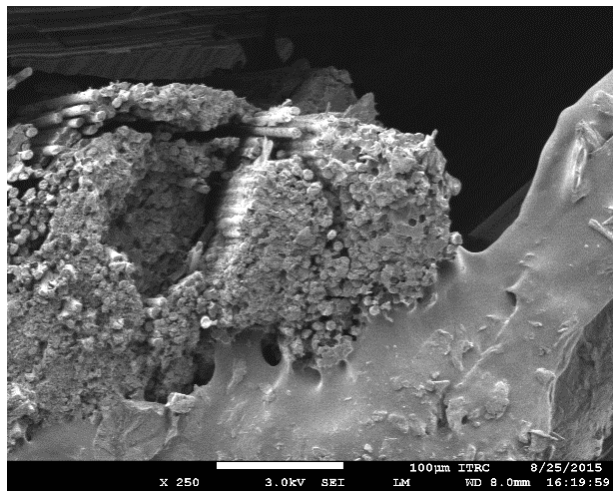

(c)

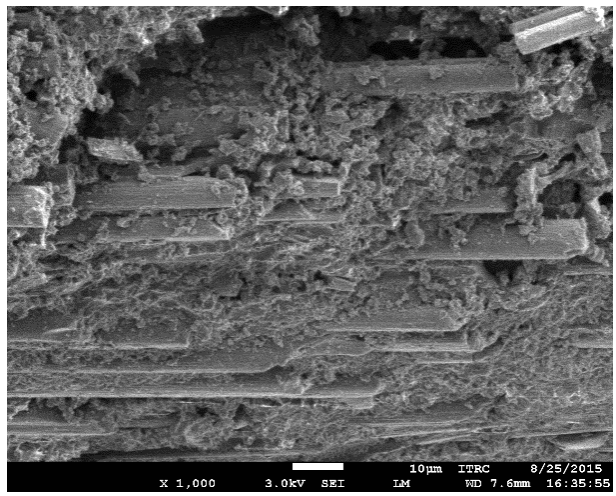

(d)

Figure 3.1.8. Morphology of the fractured surface of unidirectional composites after tensile test (a) and (b) as-received CFRP; (c) and (d) CNT-grafted CFRP

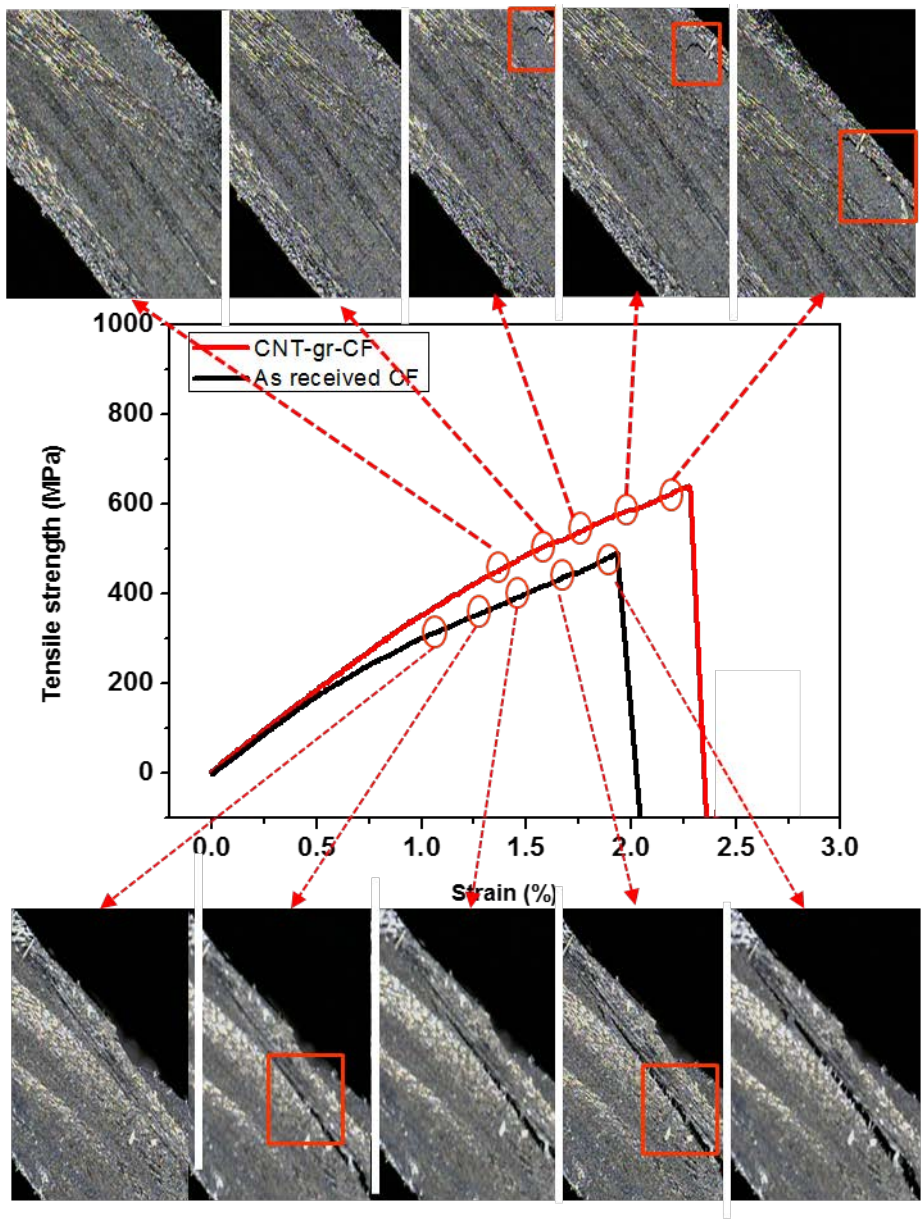
CNT-gr-CF
As received CF
Tensile strength (MPa)
Strain (%)
0
200
400
600
800
1000
0.0
0.5
1.0
1.5
2.0
2.5
3.0

(a)

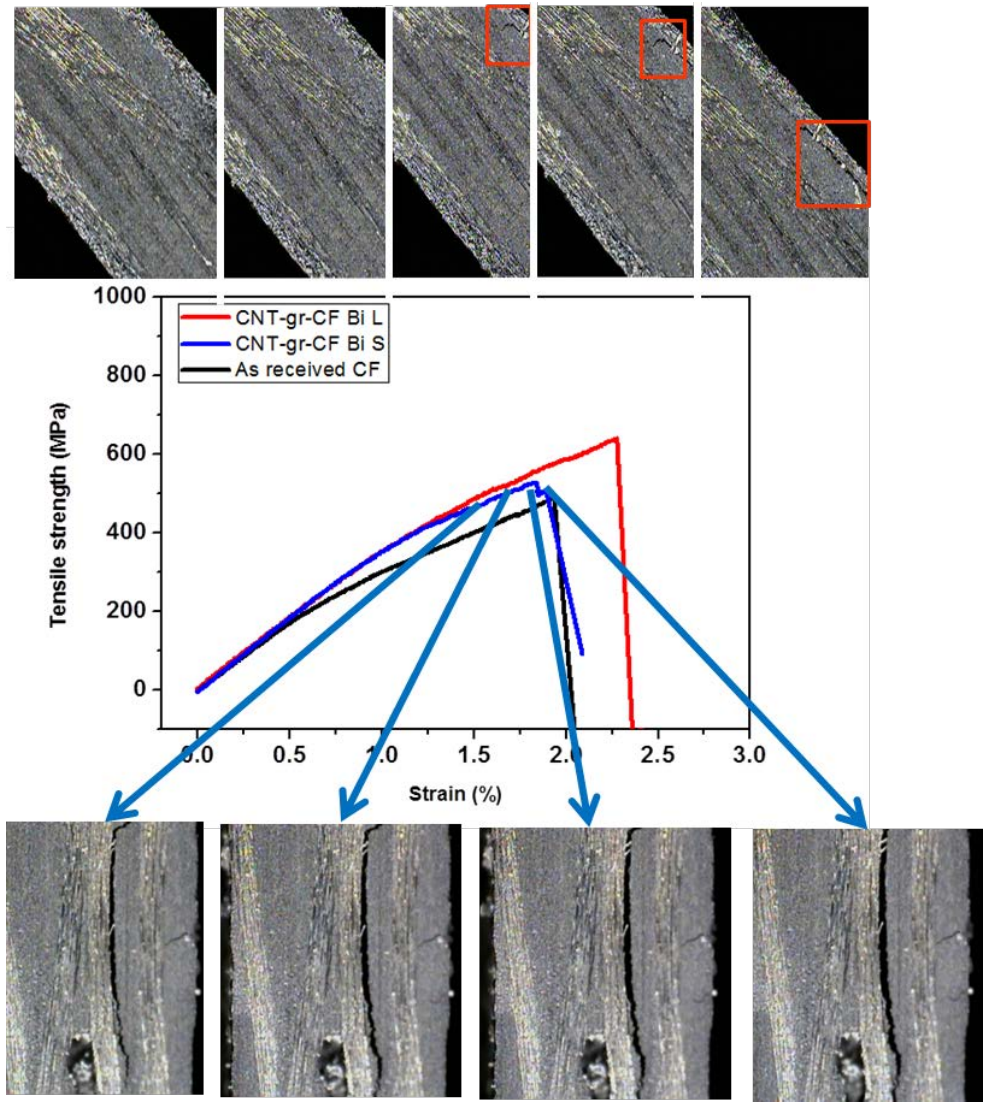

(b)

Figure 3.1.9. Stress-strain curve and in-situ microscope observation for surface crack of woven CFRP while tensile test; (a) as-received CF and thick-CNT-grafted CF (b) thin-CNT-grafted CF

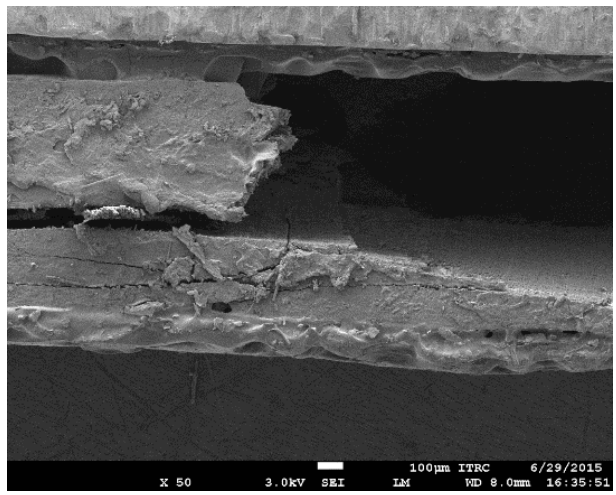

(a)

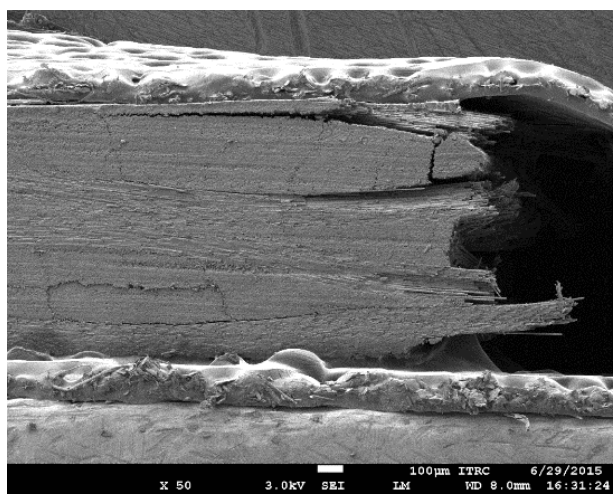

(b)

Figure 3.1.10. Morphologies of the woven CFRP after in-situ microscope observation for surface crack; (a) as-received CF (b) thick-CNT-grafted CF

As it well known, in unidirectional composites, crack initiation occurs along the fiber direction from pre-existing defects because of the anisotropy in its strength. Thus, splitting of the fibers is important factor for the mechanical properties of the unidirectional fiber reinforced composites. CNT-grafted CFs have their advantages to inhibit splitting of the fibers through the bridge effect of CNTs which interconnect fibers. We investigated their bridge effect by evaluate their stress intensity for initiation of the splitting crack with experiments following reference. Figure 3.1.11 shows the stress intensity needs to initiation of the splitting crack for each sample. As you can see in figure 3.1.11, splitting of fibers were suppressed in case of thick-CNT-grafted CF composites but thin-CNT-grafted CFRP showed similar properties with as-received CFRP. Because short and thin CNTs cannot make bridge between CF, thin-CNT-grafted CFs were not effective to suppress splitting of the fibers. Thus, tensile strength of the thick-CNT-grafted CFRP is higher than that of thin-CNT-grafted CFRP.

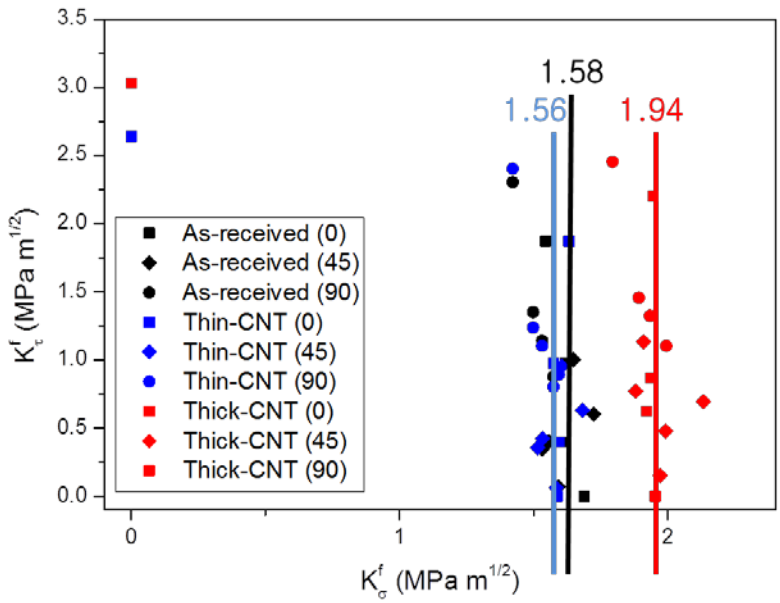

Figure 3.1.11. Stress intensity factor (K_σ^f) for the unidirectional CFRP

In conclusion, grafted CNTs on CF caused large surface area and increased interfacial/interlaminar properties. These increment helped effective load transfer between fiber and prevented delamination and mechanical strength and strain of composites increased finally.

3.2. CNT-grafted carbon fiber reinforced carbon composites

3.2.1 Introduction

Carbon-carbon (C/C) composites are well-suited materials to structural applications at high temperature and where needs high thermal shock resistance. Furthermore, they have more impact resistance than usual ceramic materials. But the manufacturing process of C/C composites is too complicate, expansive and routine because of the high-temperature pyrolysis process and the densification process which reduces defects generated through the pyrolysis process. In this section, we tried to fabricate C/C composites with CNT-grafted CF to use their own advantages as reinforcement of composites and better wettability comes from hierarchical structure.

3.2.2 Experimental

3.2.2.1 Fabrication of CNT-grafted CF

We chose soaking method to introduce catalysts on the CF fabric (T-300 grade, Entra-Korea) since its simplicity and low cost for mass production. Especially, we used Ni-Fe bi-metallic catalysts and lowered CVD temperature to maintain mechanical properties of the CF. As a catalyst precursors, we used $FeCl_3 \cdot (H_2O)_6$ and $Ni(NO_3)_2 \cdot (H_2O)_6$ and ethanol as a solvent. CFs were soaked in solution of catalysts

precursors for 30 minutes and dried at 70℃ for 4 hours. For woven fabric, we varied H_2 ratio in CVD atmosphere to make CNT-grafted CF with different CNT diameter but we did not varied H_2 ratio for unidirectional CNT-grafted CF to avoid needless efforts. We also prepared CNT-grafted CF fabrics with Fe-only catalysts at the high temperature (750^{o}C) to show effect of bimetallic catalysts on the mechanical property of CNT-grafted CFs. Catalyst precursor-introduced CF fabrics were batched in the furnace and CVD process was conducted.

3.2.2.2 Fabrication of C/C composites

Carbon-carbon composites were fabricated through 3-step process. For the first, we fabricated green body composites using vacuum assisted resin transfer molding (VARTM) of phenol-resol resin (KC-4354,Kangnam corporation) and their curing process. After than, green body composites were pyrolized in the furnace with Ar atmosphere. The temperature profile for pyrolysis is detailed at figure 3.2.1. Finally, densification process with liquid pitch was conducted at 700 and 1000 bar.

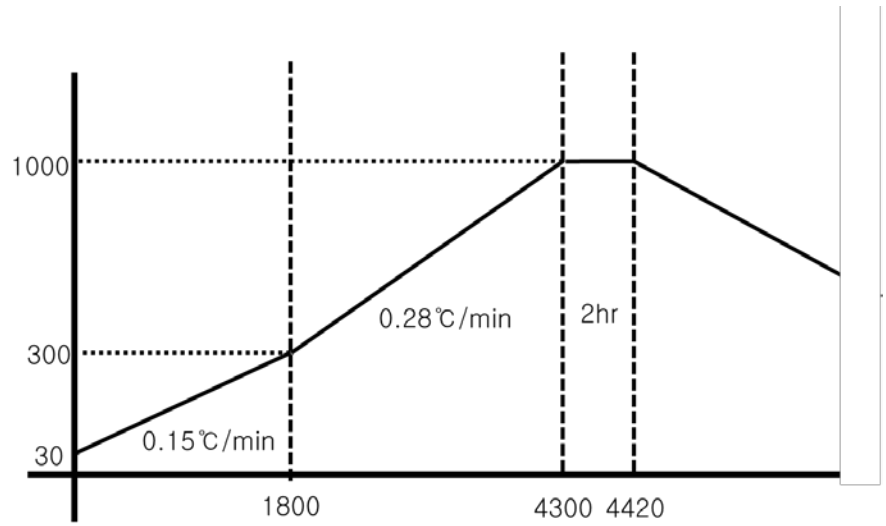

Figure 3.2.1. Temperature profile for pyrolysis of carbon-carbon composites

3.2.2.3 Characterization of C/C composites

Morphology of CNT-grafted CFs was characterized by field emission scanning electron microscope (FE-SEM, JEOL-7100) and high-resolution transmission electron microscope (HR-TEM, JSM-3000). We characterized mechanical properties of CNT-grafted CF by single fiber tensile test with lab-made universal test machine (R&B). Gage length was 20mm and more than 20 specimens were tested for each sample. Density of green body composites, skeletal carbon-carbon composites, densified carbon-carbon composites are measured by Archimedes method. Mechanical properties of carbon-carbon composites were characterized by 3-point bending test followed by ASTM D790-10. After test, fractured surface of carbon-carbon composites were observed by FE-SEM to observe fracture behavior of composites.

We also measured the thermal properties of the C/C composites. Thermal conductivity of the C/C composites was measured by the laser flash analysis and their coefficients of the thermal expansion were measured by thermomechanical analyzer (TMA). Finally, their thermal shock robustness which indicates thermal stability was calculated by following equation.

3.2.3 Results and discussion

3.2.3.1 Properties of the C/C composites

Density of composites was varied through fabrication process and fabricated carbon-carbon composites showed different volume fraction because of different thickness. As-received CF composites had 31.3% of fiber volume fraction to axial direction and CNT-grafted CF had 23.5% of fiber volume fraction. Their density was similar to each other (as-received CF: 1.357, CNT-grafted CF: 1.382). Figure 3.2.2 (a) is stress-strain curve for 3-point bending test of carbon-carbon composites.

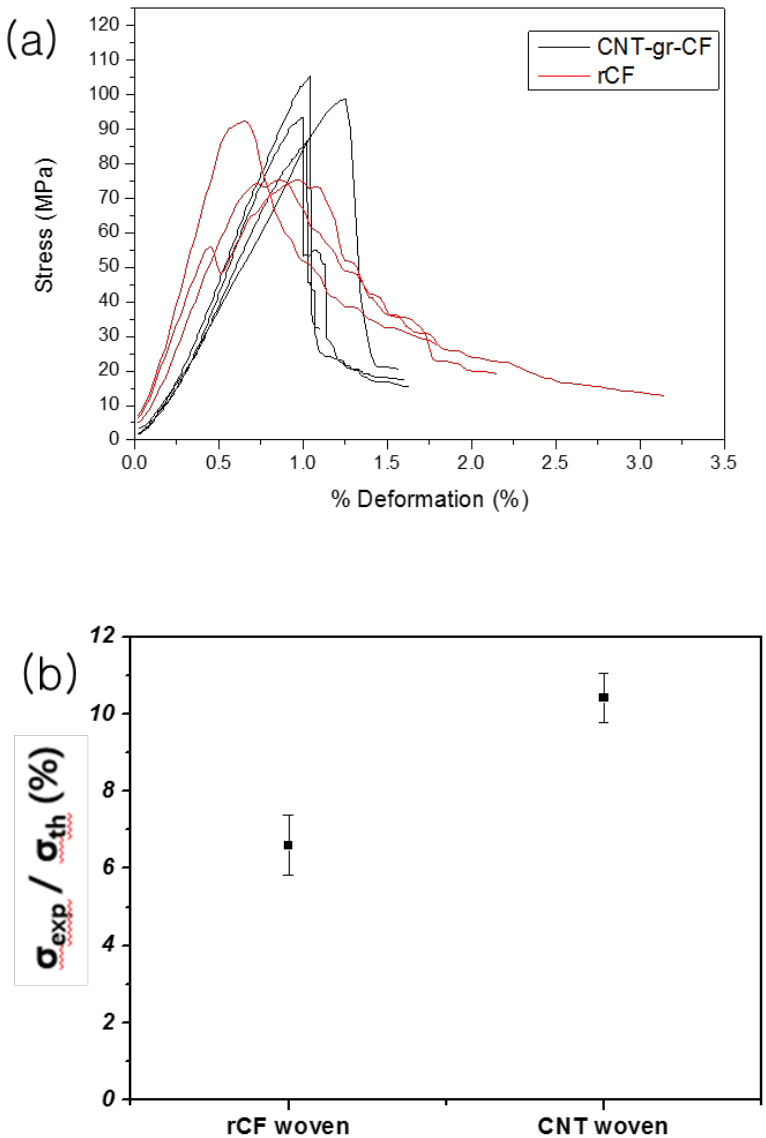

Figure 3.2.2 Mechanical properties of carbon-carbon composites (a) stress-strain curve; (b) experimental flexural strength over theoretical strength calculated by rule of mixture.

Even as-received CF (rCF) carbon-carbon composites have higher volume fraction, CNT-grafted CF (CNT-gr-CF) carbon-carbon composites showed better mechanical properties. CNT-grafted CF showed 58% higher performance than as-received CF when they compared to mechanical strength calculated by rule of mixture (Figure 3.2.2 (b)). To examine the reason for different mechanical strength, we observed fractured surface of carbon-carbon composites. In microscopic observation, CNT-grafted CF carbon-carbon composites showed perfect interface between laminar (Figure 3.2.4 (b)) and fiber bundles but as-received CF had closed pores between laminar and bundles (Figure 3.2.4 (a)). And furthermore, CNT-grafted CF carbon-carbon composites showed larger blocks made by multiple fracture which means higher interfacial shear strength (Figure 3.2.4 (c), (d)).

Thermal properties of C/C composites were measured by LFA and TMA. CNT-grafted C/C composites had 72% higher through the thickness direction thermal conductivity and 17% higher in-plane direction thermal conductivity than that of as-received C/C composites. According to TMA results, two samples have similar coefficients of thermal expansion.

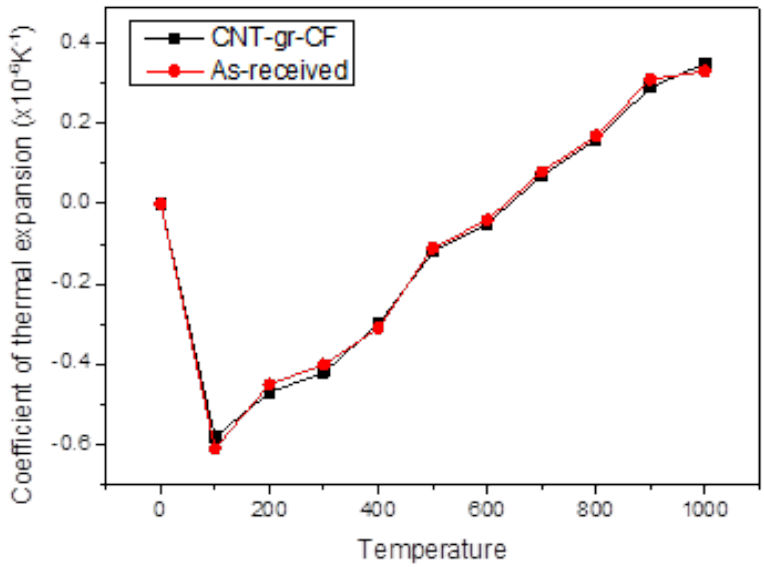

(a)

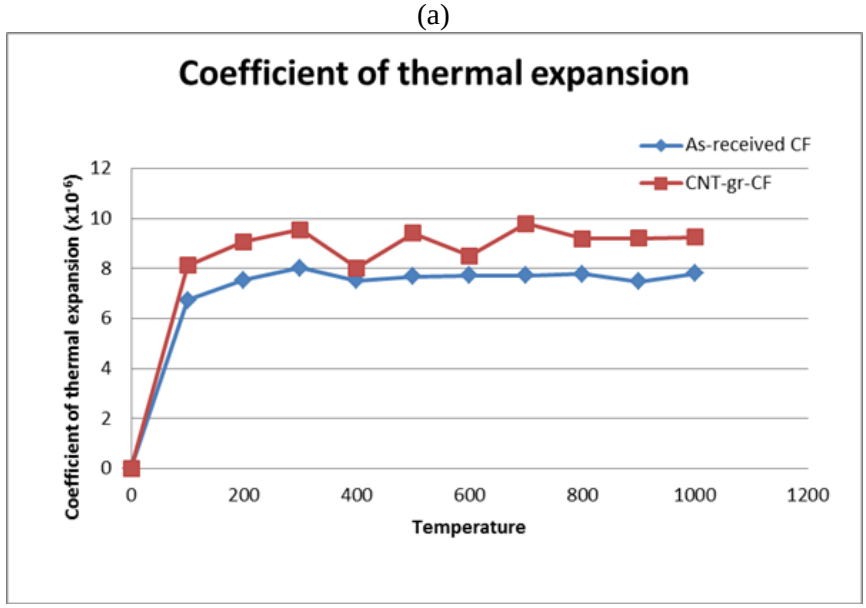

(b)

Figure 3.2.3 Coefficient of thermal expansion of the C/C composites; (a) in-plane direction (b) through-the-thickness direction

3.2.3.2 Effect of the hierarchical structure of the CNT-grafted CF

The main difference between CNT-grafted C/C composite and as-received C/C composite was internal porosity. In micro CT observation, CNT-grafted C/C composite had lower porosity than that of as-received CF and cracks in CNT-grafted C/C composites are showed closed loop while as-received CF C/C composites have continuous crack through interlaminar region. The reason for these differences in internal structure was wettability of the fibers to the liquid pitch. Developed hierarchical structure through grafting of CNTs caused better wettability to the matrix. Hierarchical structure improves their tendency of the wetting. Hydrophobic materials become more hydrophobic, Oleophilic materials become more oleophillic. Liquid pitch, which is matrix material in densifying process of C/C composites, has low interfacial energy with CF because of their similar molecular structure. We expected that hierarchical structure of CNT-grafted CF can improve the wetting between matrix and fibers. As you can see in figure 3.2.6, CNT-grafted CF showed perfect wet to the liquid pitch or lower contact angle of droplet than that of as-received CF. Good wettability to the liquid pitch caused more perfect internal structure and thermal/mechanical properties of the composite could be improved.

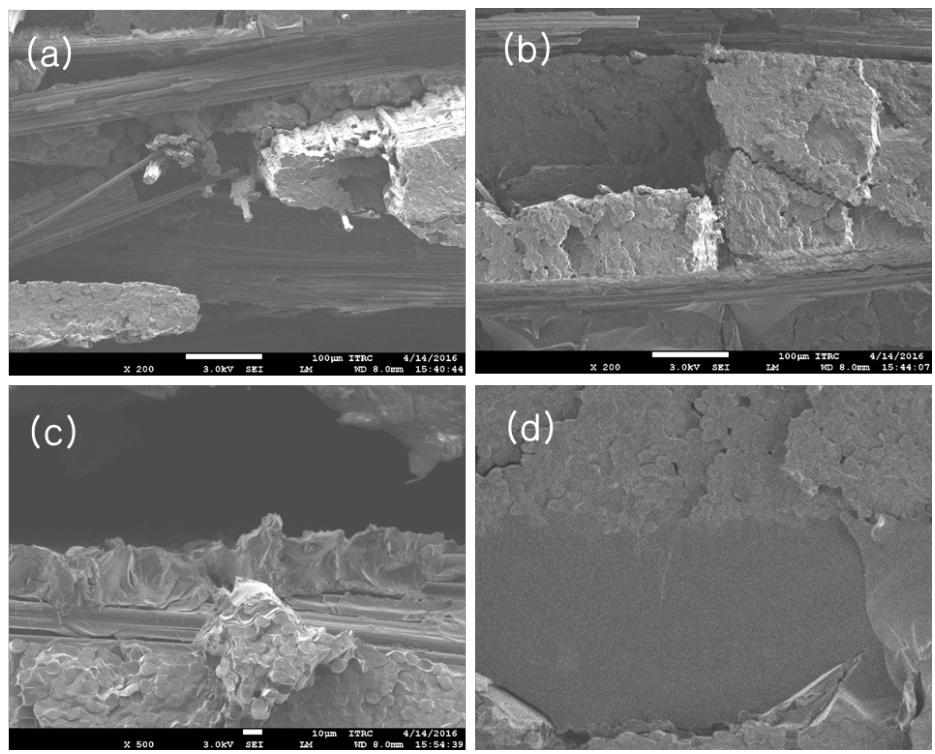

Figure 3.2.4**.** Microscopic morphology of carbon-carbon composties; fiber bundle section for (a) as-received CF carbon-carbon composites and (b) CNT-grafted CF carbon-carbon composites; interlaminar section for (c) as-received CF carbon-carbon composites and (d) CNT-grafted CF carbon-carbon composites

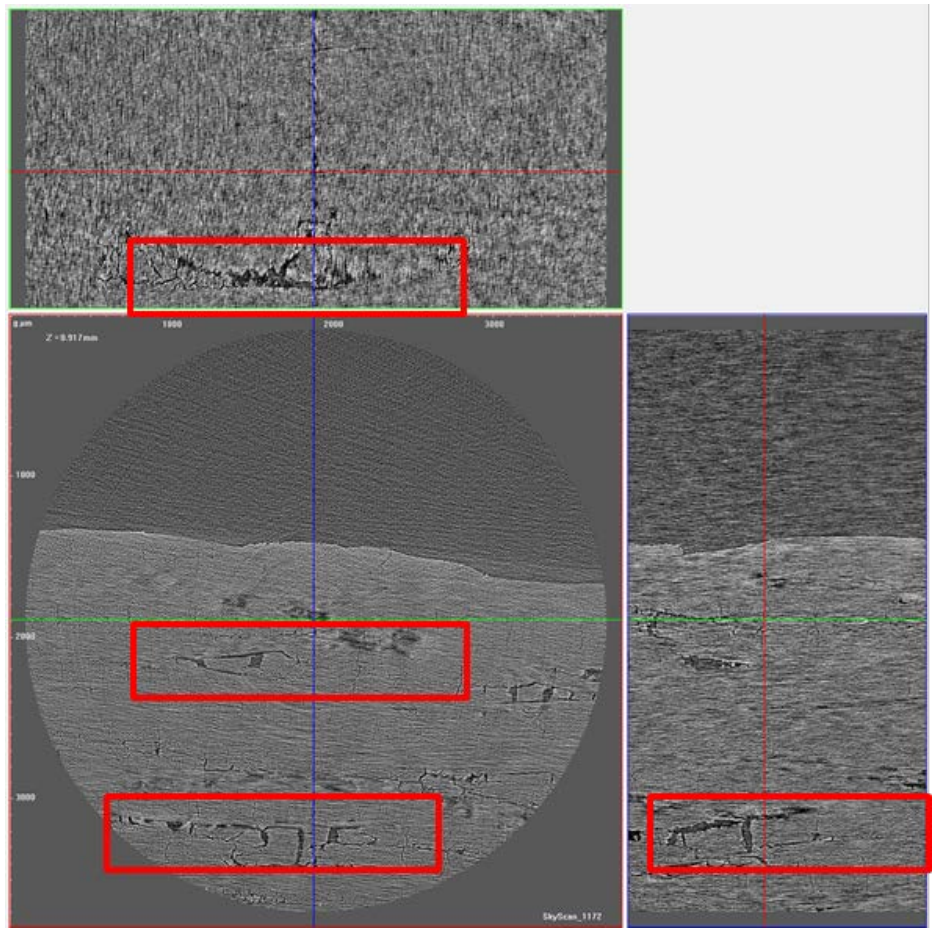

(a)

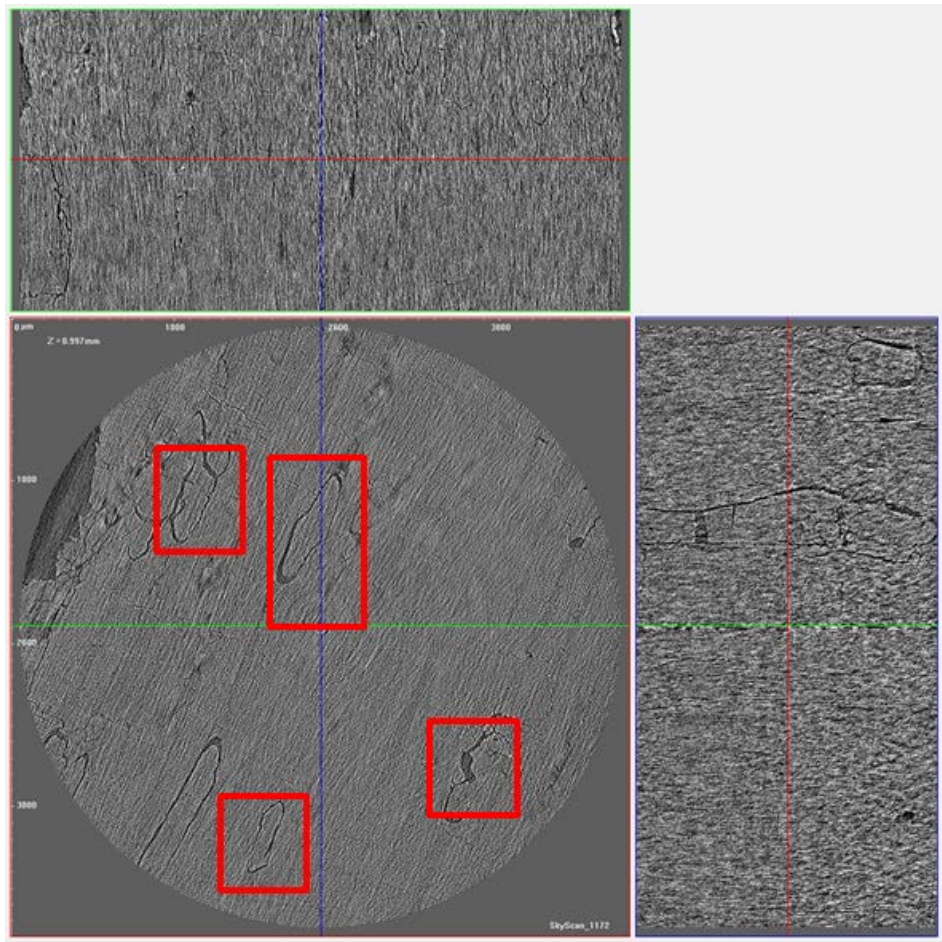

(b)

Figure 3.2.5**.** Internal morphology of carbon-carbon composties (a) as-received CF carbon-carbon composites and (b) CNT-grafted CF carbon-carbon composites

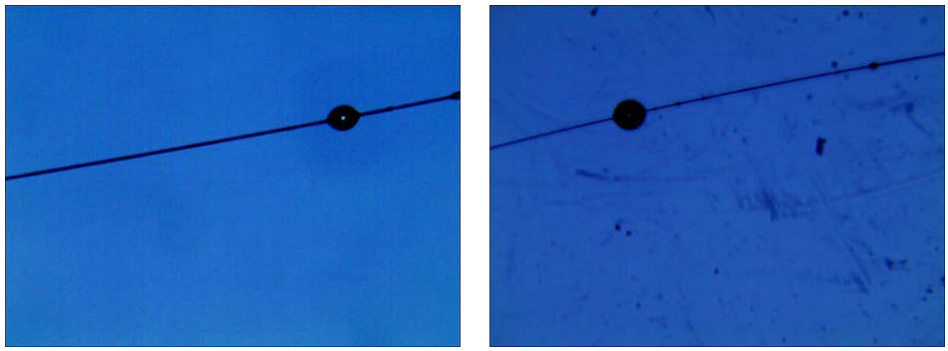

(a)

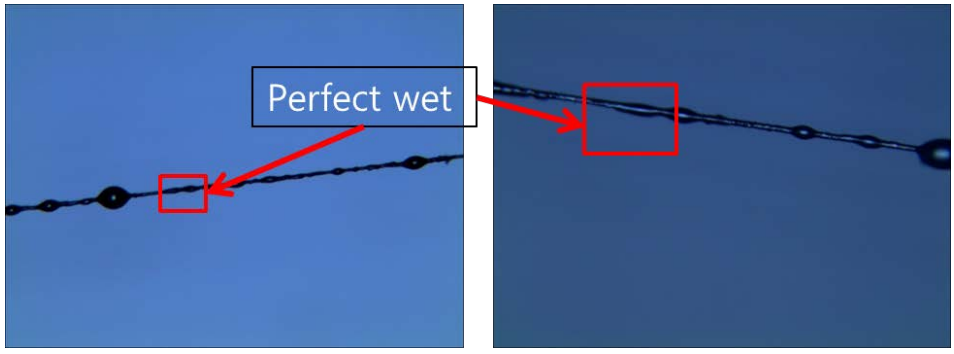

(b)

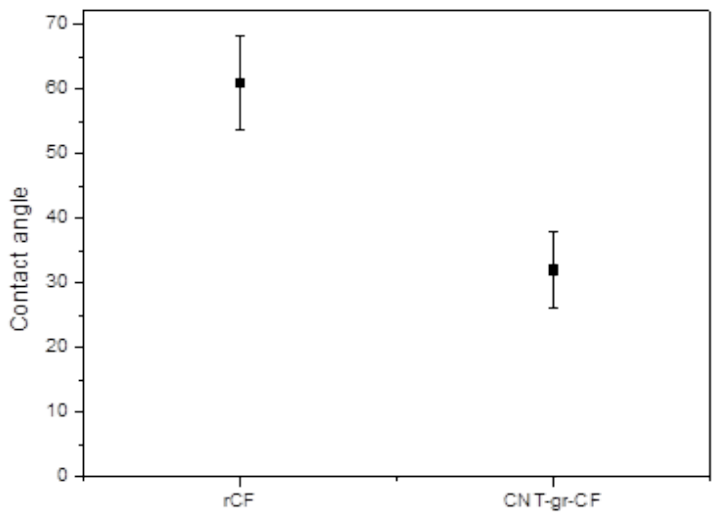

(c)

Figure 3.2.6**.** Wettability of the liquid pitch on the surface of; (a) as-received CF and (b) CNT-grafted CF and contact angle of liquid pitch droplet on the fiber surface (c)

3.3. Summary

In this chapter, we fabricated CNT-grafted CFRP and CNT-grafted C/C composites without degradation of the mechanical properties of CFs by low temperature CVD process using Ni-Fe bimetallic catalysts. Unidirectional CNT-grafted CFRP showed 17% higher tensile strength and woven CNT-grafted CFRP showed 32% higher tensile strength. These improvements were come from increased interlaminar properrties and interfacial shear strength which helps load transfer in composites. In case of C/C composites, hierarchical structure of the CNT-grafted CF caused better wettability to the matrix material, liquid pitch. Thus, defects of the composites were decreased and thermal/mechanical properties of the composite were increased

4. Continuous process for carbon nanotube-grafted carbon fibers

4.1. Introduction

In the chapter 4, we demonstrate lab-scale continuous process for carbon nanotube-grafted carbon fibers. For the massive production which can be applied in the industrial area, continuous process is necessary. There are four essential elements for continuous process; growth speed of CNTs, uniform growth of CNTs, preservation of mechanical properties of carbon fibers and continuous supplement of CFs. But in the previous researches, too long growth time to extend to continuous process was needed like an hour. And for uniform growth of CFs, shade effect caused by placement of substrates and CFs themselves were obstacles to the uniform growth. And mechanical degradation caused by interdiffusion between CF and catalysts through high-temperature CVD process was occurred. And for semi-permanent continuous process, CFs should be supplied and taken up from outside of chamber. There is problem with preservation of CVD atmosphere which have passages to the outside of chamber.

4.2. Experimental

4.2.1 Continuous process using T-shaped two zone furnace

We used T-shaped two zone furnace to maximize the contact area between CFs and chemical vapour and to minimize shade effect. To prevent inter-diffusion between CF and catalyst particles which causes degradation of mechanical properties of CFs, we lowered CVD temperature from 750℃ to 500℃ by introducing Ni-Fe

bi-metallic catalysts. Nickelocene (Ni(η5-C5H5)2, Sigma-Aldrich) and ferrocene (Fe(η5–C5H5)2, Sigma-Aldrich) were used as catalysts precursors and toluene was used as carbon source. The first zone of the furnace was preheated to 200ºC to vaporize/sublimate the catalyst precursor–toluene solution. Then, CNTs were grown on the CF substrate in the second zone at 500ºC In addition, we applied water-vapor assisted CVD to boost manufacturing speed of CNT-grafted CFs. We injected water to the first zone and vaporized water vapour was carried to second zone which CNT growth occurs. We adopted compartment with slit on the jacket of the furnace to supply bundle of CFs from outside of furnace without disturbance in the CVD atmosphere. Spread CFs (Toray T700SC, 12K) were continuously supplied from reel and collected by lab-made take up reel.

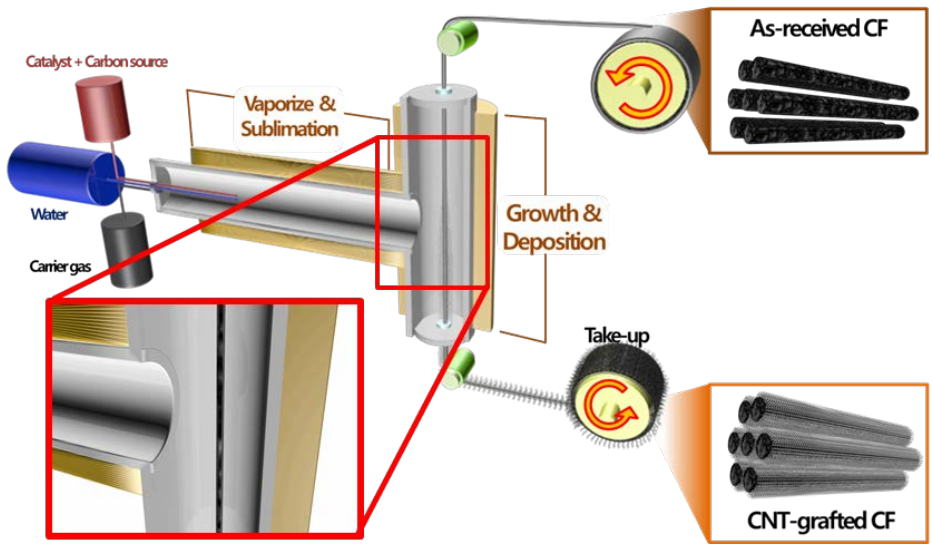
Catalyst + Carbon source
Vaporize &
Sublimation
Water
Carrier gas
Growth &
Deposition
As-received CF
Take-up
CNT-grafted CF

(a)

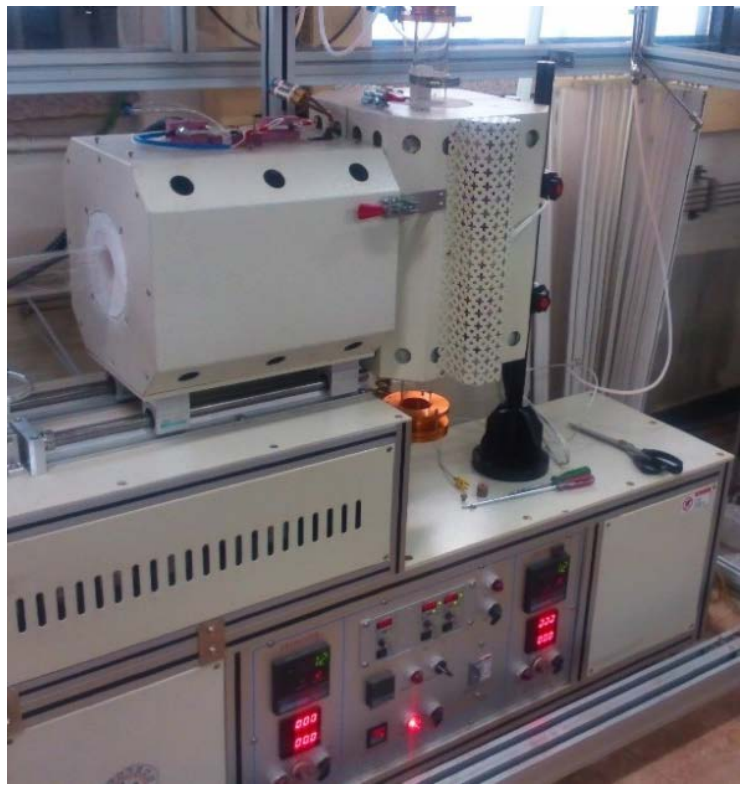

(b)

Figure 4.1. (a) Schemes of the continuous process for the CNT-grafted CFs and (b) T-shaped two-zone furnace used for the research

4.2.2 The effects of conducting pathways to ground on the growth of CNTs

CNTs were grown on CF substrates using FCVD. A T-shaped two-zone furnace was used to allow the catalytic precursors and carbon sources to permeate into the CF bundles, as shown in Figure 4.1. The furnace operates on principles similar to the two-zone furnace described in Ref. [1]. A mixture of catalyst precursor and carbon source was injected into the first zone, where the precursors were sublimated or vaporised. The CFs were located in the second zone and were aligned vertically. To form the conductive pathways, steel, copper, or aluminium wires were connected between the CFs and ground; alternatively, weakly conducting CF or GF bundles were used to connect the CFs to ground. The sublimated catalyst precursors and vaporised carbon sources were decomposed in the second zone into the catalysts and carbon atoms, resulting in CNT growth on the CF substrates. A bimetallic catalyst system was prepared using ferrocene (Fe(η5–C5H5)2) (Sigma–Aldrich) and nickelocene (Ni(η5-C5H5)2) (Sigma–Aldrich). These precursors have identical chemical structures, with only the metallic element differing between them. A mixture of ferrocene and nickelocene in a 2:1 molar ratio was dissolved in toluene at a concentration of 2 wt.%, and ultrasonicated for 30 min. Then, the solution was injected into the first zone at a feed rate of 6.0 mL/h using a syringe pump. A mixture of argon and hydrogen (in a 9:1 volume ratio) was used as the carrier gas. The first zone of the furnace was preheated to 200ºC to vaporise/sublimate the catalyst precursor–toluene solution. Then, CNTs were grown on the CF substrate in the second zone at 500ºC for 30 min. Spread CF (T700SC, Toray) tows were used as the substrate.

4.3. Results and discussion

4.3.1 Boosting of the manufacturing speed of the CNT-grafted CFs by water-vapor assisted CVD

The CNTs were grown on CF substrates using FCVD. A T-shaped two-zone furnace was used to allow the catalytic precursors and carbon sources to permeate into the We tried to boost the speed of the growth of CNTs by assisting water vapour in the CVD atmosphere. By adopting water vapor in the CVD atmosphere, we could accelerate manufacturing speed of CNT-grafted CFs by 4 times (6mm/min to 24mm/min) without mechanical degradation of CFs and by adopting water vapor-assisted CVD, tensile strength of CF were slightly increased because of their less time of exposure to the harsh environment and healing effect from CNT growth.

4.3.2 The effects of conducting pathways to ground on the growth of CNTs on CF substrates

The effects of conducting pathways formed by the metal wires, as well as the GF and CF bundles, on CNT growth were investigated by observing the morphology of the CFs following the FCVD growth process. With no conducting pathway, the CNTs formed a dense coating on the CF substrates, with a tangled morphology, as shown in Figure 4.2(a), which is consistent with reports [39,40]. Interestingly, with the conductive pathways consisting of copper, steel, or aluminium wires, CNTs did not form on the CF substrates, and only catalyst particles were observed on the surfaces of the CFs, as shown in Figure 4.2(b-d). When the CF substrates were grounded using weakly conducting CF or GF bundles, the CNTs also formed a dense covering, as shown in Figures 4.2(e) and 4.2(f). The HR-TEM images shown in the insets of Figures 4.2(e) and 4.2(f) reveal that the nanofibers were CNTs, with hollow centres and wall structures. Figure 4.3 shows the surface morphology of the

connecting wires following FCVD growth, which differed significantly depending on the electrical conductivity. With copper wire, crystalline nanoparticles were densely deposited on the surface, as shown in Figure 4.3(a). Interestingly, carbon nanofibres with a cup–stack structure were observed on the surface of the steel wire, as shown in Figure 4.3(b), which suggests that the iron in the wire acted as a catalyst for vapour-phase growth of carbon nanofibres. With the aluminium wire, CNTs were sparsely distributed on the surface, as shown in Figure 4.3(c). With the CF and GF bundles, CNTs were densely distributed across the surfaces, as shown in Figures 4.3(d) and 4.3(e). The surface potential of the quartz furnace tube at the upper section of the T-shape was 3.0 kV during FCVD with no conducting pathways. With conducting pathways formed from metal wires, the surface potential of the quartz tube was almost zero. With pathways to ground formed using the GF and CF bundles, the surface potential of the quartz tube was similar to that of the electrically insulated case. Using the measured surface potential, the distribution of the electrical potential within the furnace tube was calculated using COMSOL Multiphysics. Figure 4.5(a) shows the geometry of the model and grounding conditions. With the insulated case, a uniform potential was maintained in the second zone, where the CNT grew, as shown in Figure 4.5 (b). With the GF and CF bundles, which had dielectric constants of 10–15 and 3.9, respectively, the electric potential did not change significantly compared with the insulated case. Where conducting pathways were formed by metal wires, the potential distribution differed considerably compared with the insulated case. The electric potential in the furnace decreased to approximately zero, particularly near the grounding wire and substrate. These changes in the electric potential are believed to have inhibited growth of the CNTs on the substrate. The conducting pathways connected to the CF substrates

appear to have halted the growth of the CNTs by changing the potential distribution in the furnace, due to the involvement of charged nanoparticles in the growth process [23], because changes in the electrical potential that result from the conducting pathways alter the motion of the charged nanoparticles, as well as their generation inside the furnace. Further study is necessary to gain greater insight into the effects of the conducting pathways on the growth of CNTs.

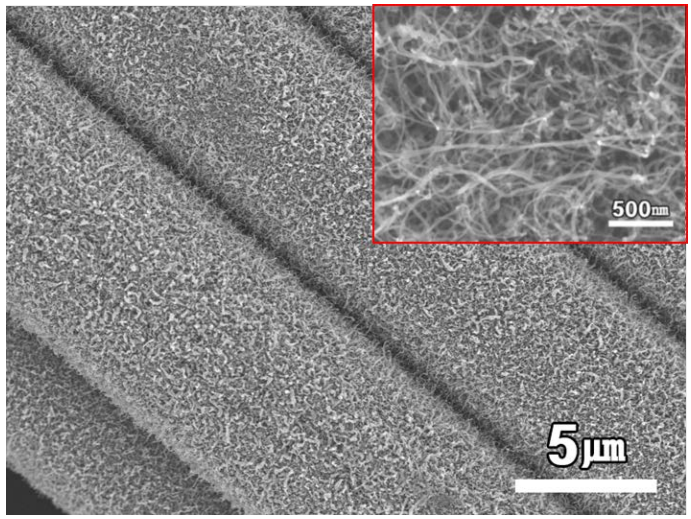

(a)

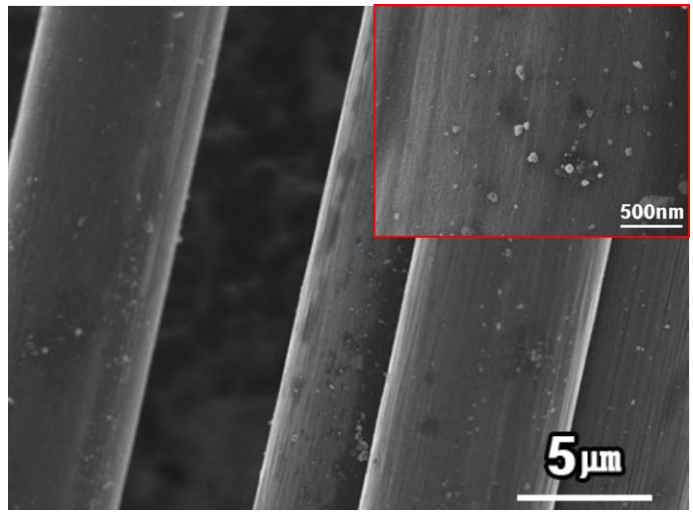

(b)

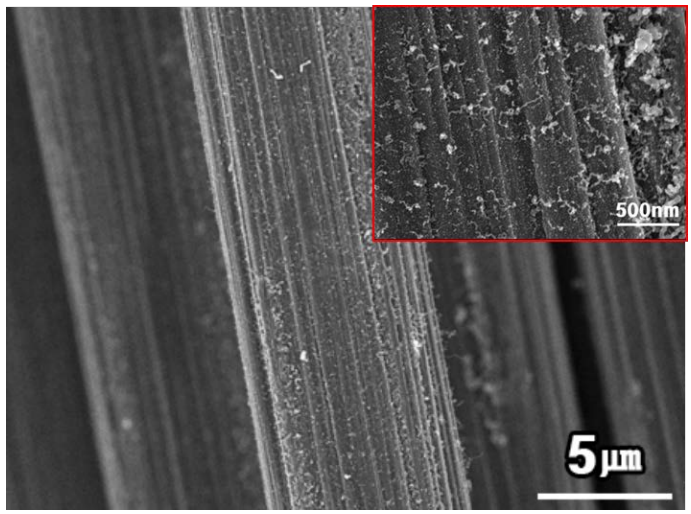

(c)

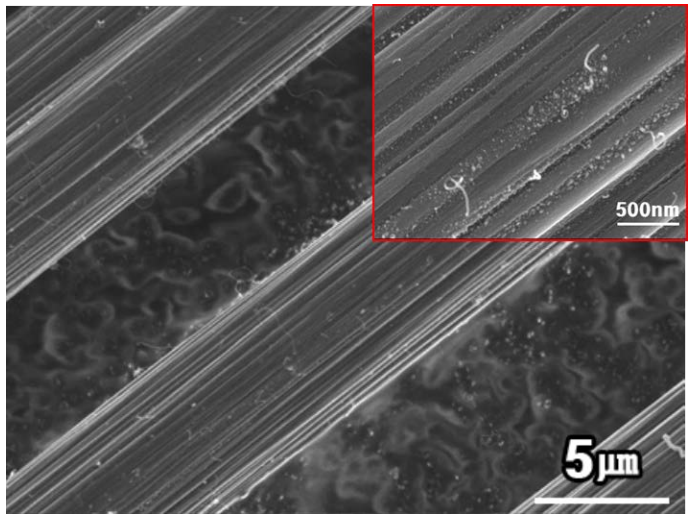

(d)

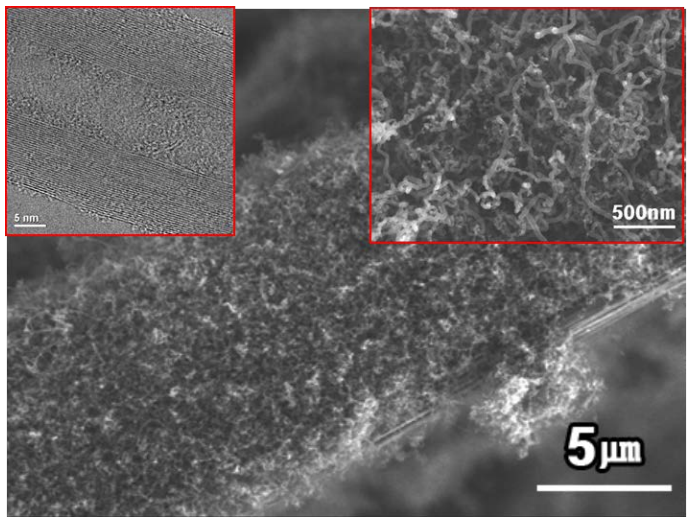

(e)

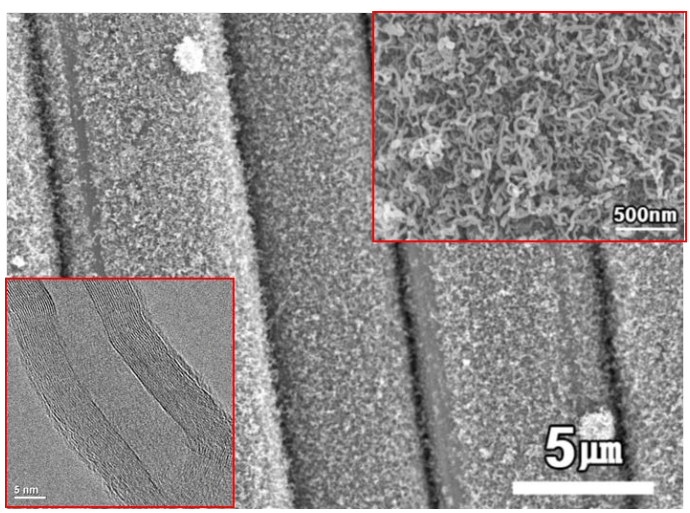

(f)

Figure 4. 2 The morphology of the CF substrates following FCVD growth. (a) Without grounding and with (b) copper, (c) steel, and (d) aluminium wire and (e) CF and (f) GF bundle grounding

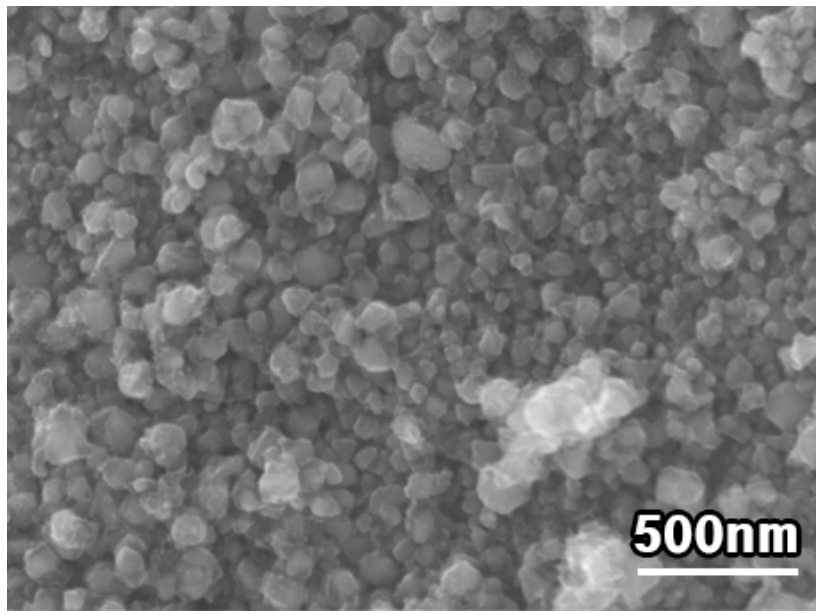

(a)

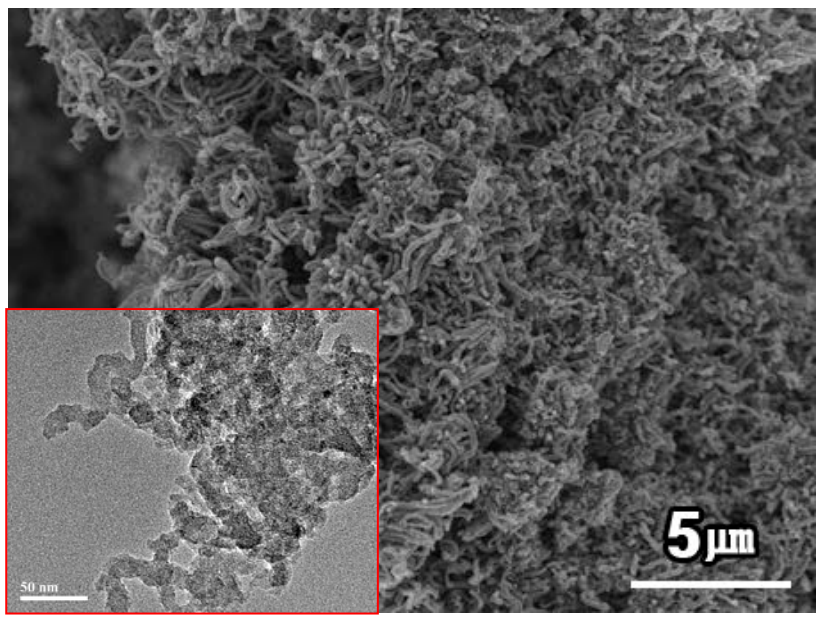

(b)

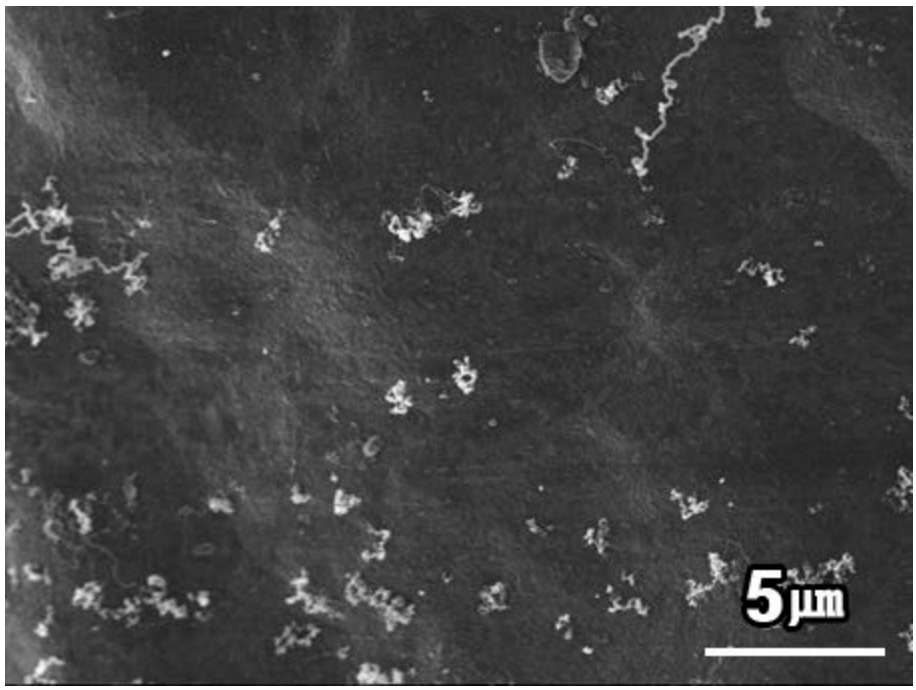

(c)

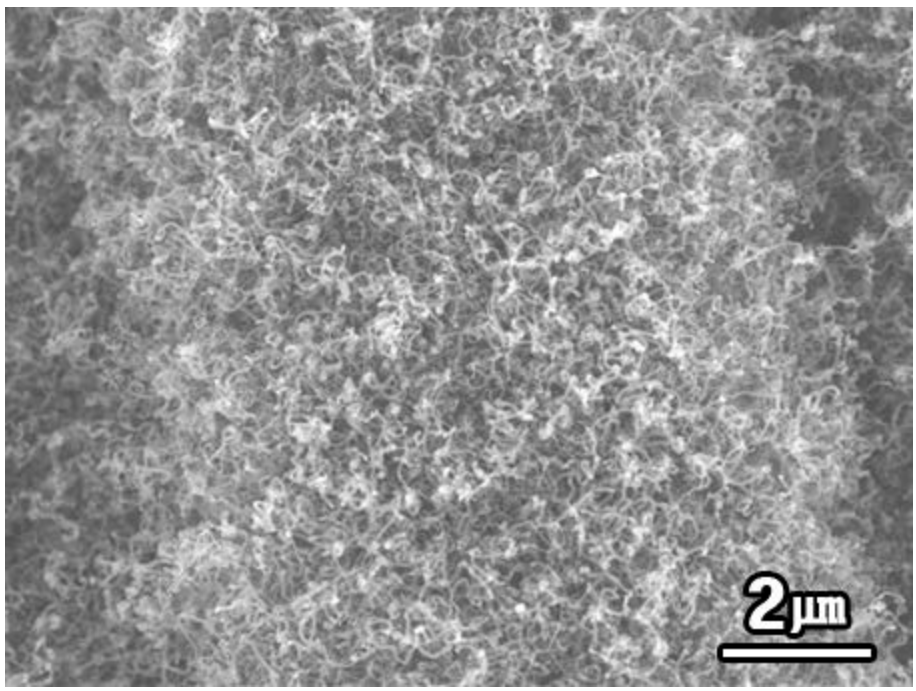

(d)

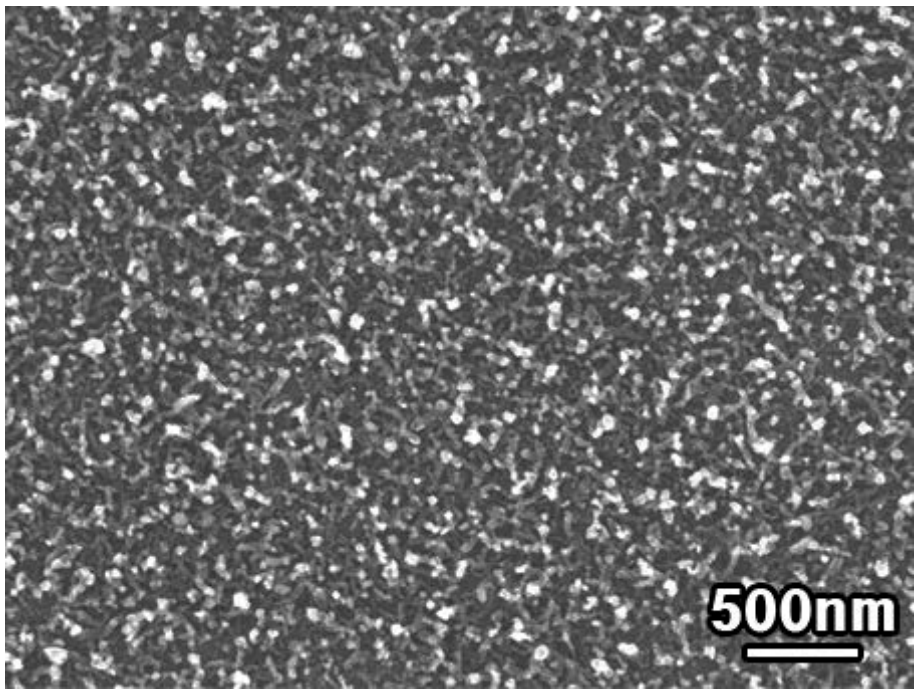

(e)

Figure 4.3 The morphology of the surface of the ground wires following FCVD growth. (a) Copper, (b) steel, (c) and aluminium wires and the (d) CF and (e) GF bundles

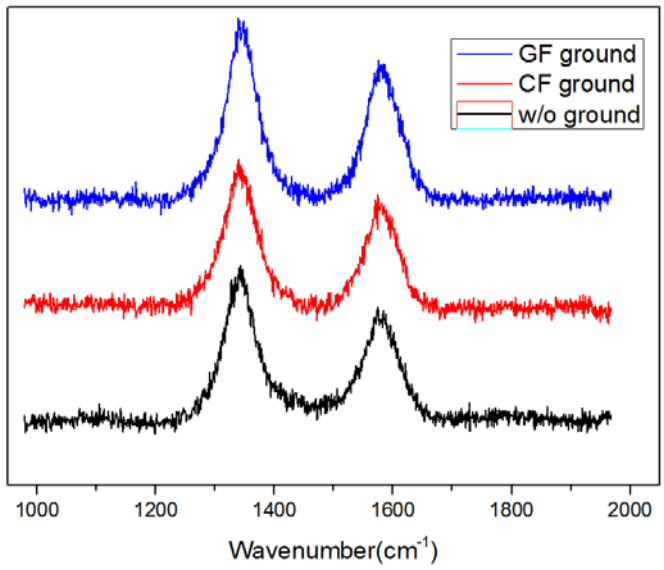

(a)

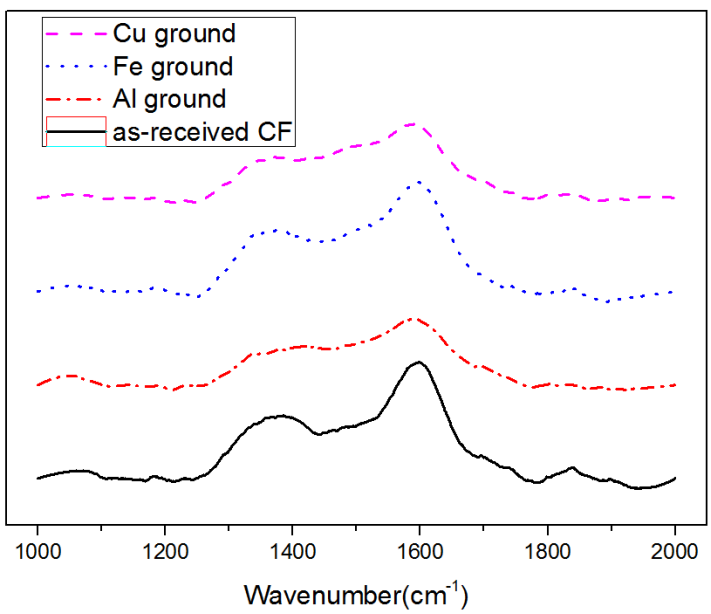

(b)

Figure 4.4 Raman spectra of the CF substrates after the FCVD growth process. (a) The CF substrates without grounding (bottom) and with non-metal (CF: middle GF: top) grounding, (b) the as-received CF and CF substrates with metal ground wires

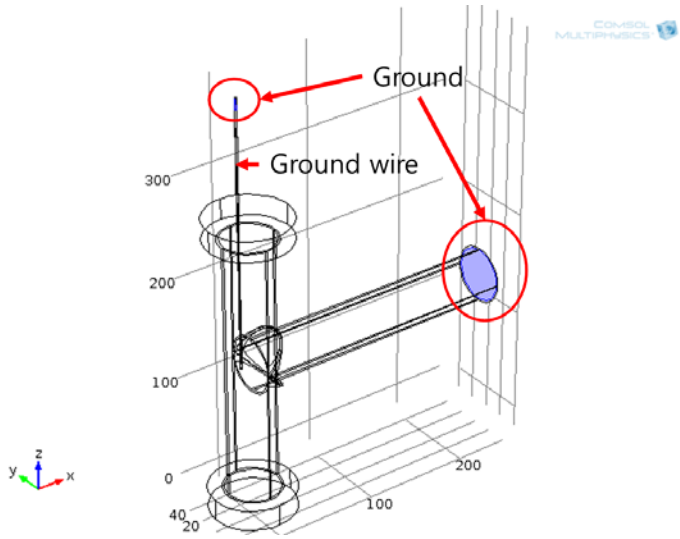
Ground
Ground wire
300
200
100
0
40
20
0
100
200
z
y
x

(a)

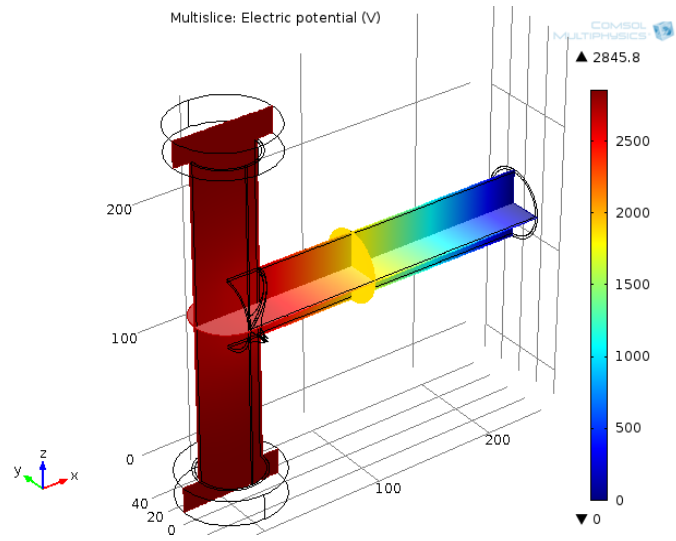
Multislice: Electric potential (V)
▲ 2845.8
2500
2000
1500
1000
500
0
▼ 0
200
100
0
40
20
0
100
200
z
y
x

(b)

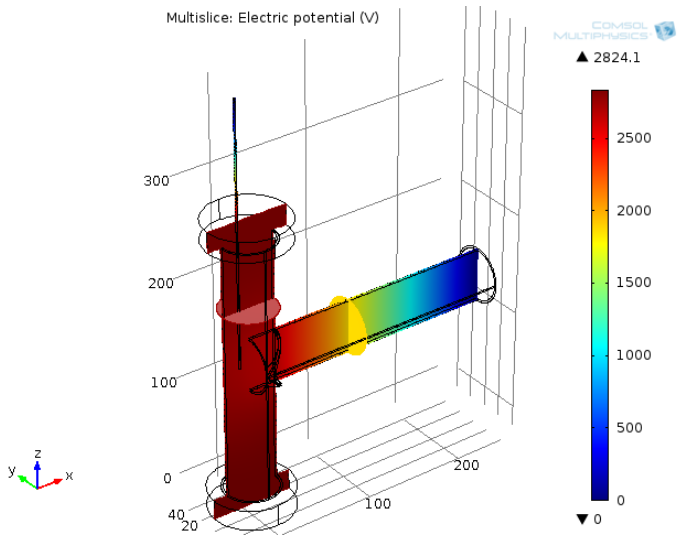
Multislice: Electric potential (V)
▲ 2824.1
2500
2000
1500
1000
500
0
▼ 0
300
200
100
0
40
20
100
200
z
y
x

(c)

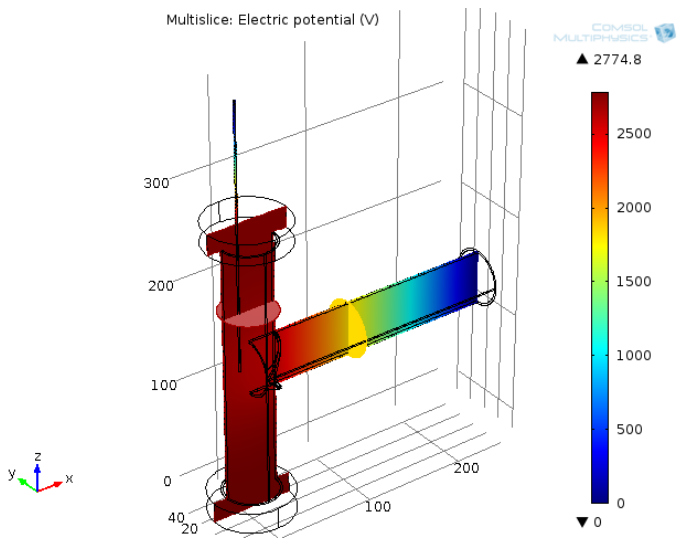
Multislice: Electric potential (V)
▲ 2774.8
2500
2000
1500
1000
500
0
▼ 0
300
200
100
0
40
20
100
200
z
y
x

(d)

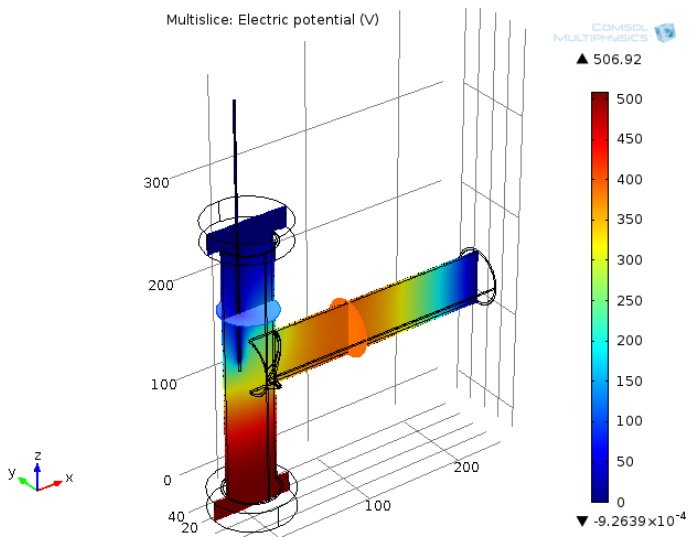

(e)

Figure 4.5 The electric potential distribution in the furnace with grounding wires with various relative permittivities, εr. (a) The geometry and location of the ground wires. (b) Without ground wires and with (c) silicon dioxide (εr = 3.9), (d) graphite (εr = 15), and (e) metal (εr = 100,000) ground wires

4.3.3 CNT-grafted CFs fabricated by continuous process

The compartments with slit were adopted on the jacket of the end of the T-shaped two-zone furnace for continuous supply of the CFs into the furnace and process speed was controlled by the take-up speed of the reel at the end of the process. Figure 4.6 and Figure 4.7 shows morphology and mechanical properties of the CNT-grafted CF after continuous process with each parameter. We could optimize the residence time of the CF in the CVD process and suitable CVD temperature by parametrical study. Finally, we concluded that 5 minutes of residence time in CVD atmosphere at 600^{o}C is suitable process parameter in our lab-scale T-shaped two zone furnace.

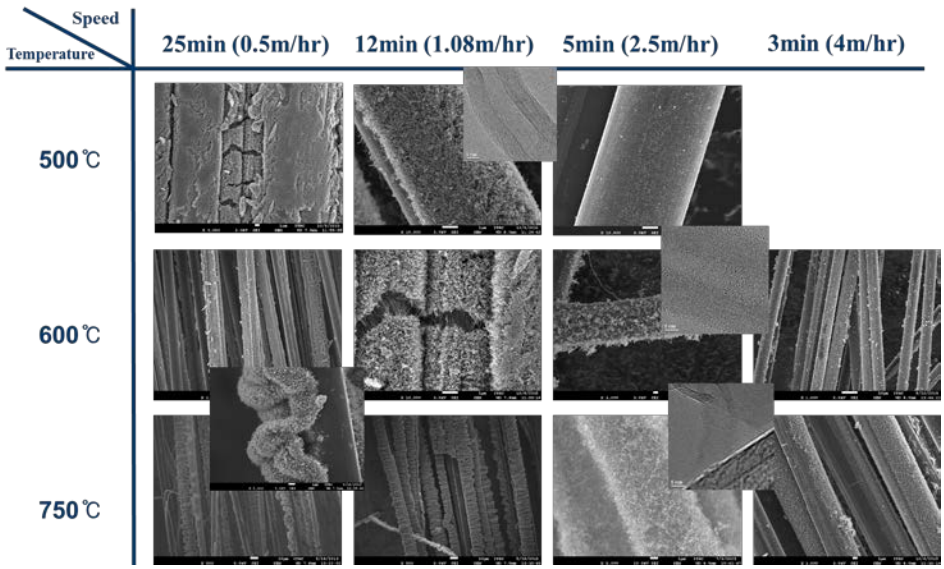

Figure 4.6. Variation of the morphology of the CNT-grafted CF on the condition of the continuous process

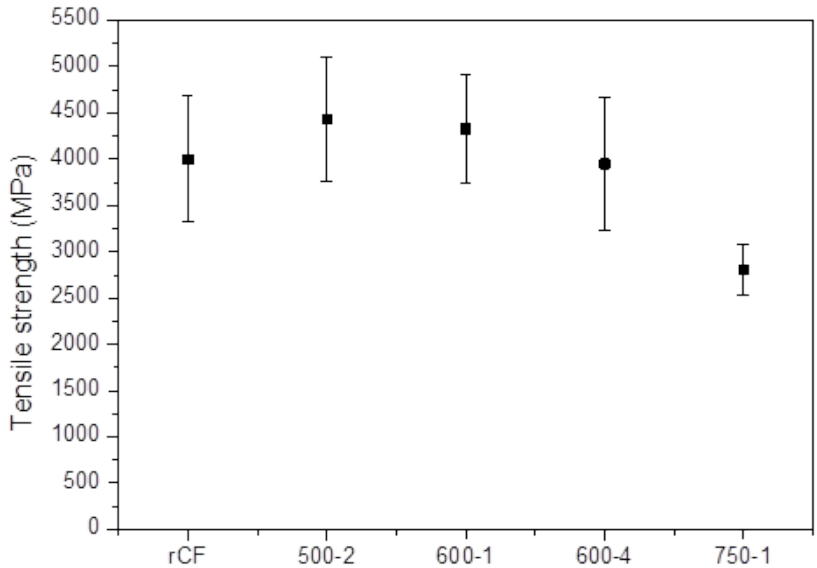

Figure 4. 7. Mechanical properties of the CNT-grafted CF with various condition

4.4. Summary

In this chapter, we demonstrated continuous process for the CNT-grafted CF and detailed parameter for process. Bimetallic catalysts and water-vapour assisted CVD were applied to prevent the mechanical degradation of the CNT-grafted CFs and boost speed of the process. We also investigated the effect of conductive pathways to ground on the growth of CNTs on CF substrates during FCVD. We found that CNTs did not grow when conducting pathways to ground existed. Finally, we optimized lab-scale continuous process by parametrical study.

5. Concluding remarks

It was the purpose of this study the fabrication of CNT-grafted CF without any damage on the tensile strength of CF itself with enhancement of IFSS, the investigation of their composite, and the development of the continuous process of CNT-grafted CFs in lab-scale.

We demonstrated that CNT-grafted CFs can be manufactured without mechanical degradation of the CFs. This was achieved using a bimetallic catalyst, which lowered the activation energy for CNT growth, thereby enabling a lower CVD temperature to be used. Inter-diffusion of CFs and catalysts, which is the main source of mechanical degradation and reduced CNT growth, was successfully avoided with the low-temperature CVD process

We fabricated CNT-grafted CFRP and CNT-grafted C/C composites without degradation of the mechanical properties of CFs by low temperature CVD process using Ni-Fe bimetallic catalysts. Unidirectional CNT-grafted CFRP showed 17% higher tensile strength and woven CNT-grafted CFRP showed 32% higher tensile strength. These improvements were come from increased interlaminar properrties and interfacial shear strength which helps load transfer in composites. In case of C/C composites, hierarchical structure of the CNT-grafted CF caused better wettability to the matrix material, liquid pitch. Thus, defects of the composites were decreased and thermal/mechanical properties of the composite were increased

We demonstrated continuous process for the CNT-grafted CF and detailed parame-

ter for process. Bimetallic catalysts and water-vapour assisted CVD were applied to prevent the mechanical degradation of the CNT-grafted CFs and boost speed of the process. We also investigated the effect of conductive pathways to ground on the growth of CNTs on CF substrates during FCVD. We found that CNTs did not grow when conducting pathways to ground existed. Finally, we optimized lab-scale continuous process by parametrical study.

References

[1] Nessim GD, Properties, synthesis, and growth mechanisms of carbon nanotubes with special focus on thermal chemical vapor deposition. Nanoscale 2010;2(8):1306-23

[2] Smith, Brian W., Marc Monthioux, and David E. Luzzi. "Carbon nanotube encapsulated fullerenes: a unique class of hybrid materials." Chemical Physics Letters 315.1 (1999): 31-36.

[3] Kreupl, Franz, et al. "Carbon nanotubes in interconnect applications." Microelectronic Engineering 64.1 (2002): 399-408

[4] Graham, A. P., et al. "Towards the integration of carbon nanotubes in microelectronics." Diamond and related materials 13.4 (2004): 1296-1300.

[5] Gojny, Florian H., et al. "Surface modified multi-walled carbon nanotubes in CNT/epoxy-composites." Chemical physics letters 370.5 (2003): 820-824.

[6] Kim, Jin Ah, et al. "Effects of surface modification on rheological and mechanical properties of CNT/epoxy composites." Carbon 44.10 (2006): 1898-1905.

[7] Allaoui, Aïssa, et al. "Mechanical and electrical properties of a MWNT/epoxy composite." Composites science and technology 62.15 (2002): 1993-1998.

[8] Kim, M. T., et al. "Property enhancement of a carbon fiber/epoxy composite by using carbon nanotubes." Composites Part B: Engineering 42.5 (2011): 1257-1261.

[9] Gojny, F. H., et al. "Carbon nanotube-reinforced epoxy-composites: enhanced stiffness and fracture toughness at low nanotube content." Composites science and technology 64.15 (2004): 2363-2371.

[10] Cheng, Q. F., et al. "Carbon nanotube/epoxy composites fabricated by

resin transfer molding." Carbon 48.1 (2010): 260-266.

[11] Chu, Ke, et al. "Fabrication and effective thermal conductivity of multi-walled carbon nanotubes reinforced Cu matrix composites for heat sink applications." Composites Science and Technology 70.2 (2010): 298-304.

[12] Fujii, Motoo, et al. "Measuring the thermal conductivity of a single carbon nanotube." Physical review letters 95.6 (2005): 065502.

[13] Kai, Zhang, et al. "Directly synthesizing CNT-TIM on aluminum alloy heat sink for HB-LED thermal management." Electronic Components and Technology Conference, 2008. ECTC 2008. 58th. IEEE, 2008.

[14] Salvetat, J-P., et al. "Mechanical properties of carbon nanotubes." Applied Physics A 69.3 (1999): 255-260.

[15] Dresselhaus, Mildred S., et al. "Carbon nanotubes." The Physics of Fullerene-Based and Fullerene-Related Materials. Springer Netherlands, 2000. 331-379.

[16] Dresselhaus, M. S., et al. "Electronic, thermal and mechanical properties of carbon nanotubes." Philosophical Transactions of the Royal Society of London A: Mathematical, Physical and Engineering Sciences 362.1823 (2004): 2065-2098.

[17] Miyagawa, Hiroaki, Manjusri Misra, and Amar K. Mohanty. "Mechanical properties of carbon nanotubes and their polymer nanocomposites." Journal of Nanoscience and Nanotechnology 5.10 (2005): 1593-1615.

[18] Ruoff, Rodney S., et al. "Radial deformation of carbon nanotubes by van der Waals forces." Nature 364.6437 (1993): 514-516.

[19] Yu, Min-Feng, et al. "Strength and breaking mechanism of multiwalled carbon nanotubes under tensile load." Science 287.5453 (2000): 637-640.

[20] Fujii, Motoo, et al. "Measuring the thermal conductivity of a single carbon nanotube." Physical review letters 95.6 (2005): 065502.

[21] Che, Jianwei, Tahir Cagin, and William A. Goddard III. "Thermal conductivity of carbon nanotubes." Nanotechnology 11.2 (2000): 65.

[22] Hone, James, et al. "Thermal conductivity of single-walled carbon nanotubes." Physical Review B 59.4 (1999): R2514.

[23] Chung, Deborah DL, and Deborah Chung. Carbon fiber composites. Butterworth-Heinemann, 2012.

[24] Buckley, John D., and Danny Dale Edie, eds. Carbon-carbon materials and composites. Vol. 1254. William Andrew, 1993.

[25] Donnet, Jean-Baptiste, and Roop Chand Bansal. Carbon fibers. CRC Press, 1998.

[26] Fitzer, E., W. Frohs, and M. Heine. "Optimization of stabilization and carbonization treatment of PAN fibres and structural characterization of the resulting carbon fibres." Carbon 24.4 (1986): 387-395.

[27] Edie, D. D. "The effect of processing on the structure and properties of carbon fibers." Carbon 36.4 (1998): 345-362.

[28] Chand, S. "Review carbon fibers for composites." Journal of Materials Science35.6 (2000): 1303-1313.

[29] Endo, Morinobu, Tsuneo Koyama, and Yoshihiro Hishiyama. "Structural improvement of carbon fibers prepared from benzene." Japanese Journal of Applied Physics 15.11 (1976): 2073

[30] Morgan, Peter. Carbon fibers and their composites. CRC press, 2005.

[31] Burchell, Timothy D., ed. Carbon materials for advanced technologies. Elsevier, 1999.

[32] E. Thostenson, W. Li, D. Wang, Z. Ren, T. Chou, Carbon nanotube/carbon fiber hybrid multiscale composites, Journal of Applied

Physics, 91 (2002) 6034-6037

[33] K. Kepple, G. Sanborn, P. Lacasse, K. Gruenberg, W. Ready, Improved fracture toughness of carbon fiber composite functionalized with multi walled carbon nanotubes, Carbon, 46 (2008) 2026-2033

[34] Lee, Geunsung, et al. "The effect of the surface roughness of carbon fibres on CNT growth by floating-catalyst chemical vapour deposition." International Journal of Nanotechnology 10.8/9 (2013): 800-810.

[35] Kim, Kyoung Ju, et al. "Improved tensile strength of carbon fibers undergoing catalytic growth of carbon nanotubes on their surface." Carbon 54 (2013): 258-267.

[36] Lee, Geunsung, et al. "Low-temperature grafting of carbon nanotubes on carbon fibers using a bimetallic floating catalyst." Diamond and Related Materials 68 (2016): 118-126.

[37] Bekyarova, Elena, et al. "Multiscale carbon nanotube− carbon fiber reinforcement for advanced epoxy composites." Langmuir 23.7 (2007): 3970-3974.

[38] He, Xiaodong, et al. "Preparation of a carbon nanotube/carbon fiber multi-scale reinforcement by grafting multi-walled carbon nanotubes onto the fibers." Carbon 45.13 (2007): 2559-2563.

[39] Lee, Geunsung, et al. "A method for preparing CNT-grafted carbon fibers and improved tensile strength of their composites." Composites Part A: Applied Science and Manufacturing 69 (2015): 132-138.

[40] Zhang, Han, et al. "Improved fracture toughness and integrated damage sensing capability by spray coated CNTs on carbon fibre prepreg." Composites Part A: Applied Science and Manufacturing 70 (2015): 102-110.

[41] Liu, Hao, et al. "Aligned multi-walled carbon nanotubes on different substrates by floating catalyst chemical vapor deposition: critical effects of buffer layer." Surface and Coatings Technology 202.17 (2008): 4114-

4120.

[42] Thostenson, E. T., et al. "Carbon nanotube/carbon fiber hybrid multiscale composites." Journal of Applied physics 91.9 (2002): 6034-6037.

[43] Zhang, Fu-Hua, et al. "Interfacial shearing strength and reinforcing mechanisms of an epoxy composite reinforced using a carbon nanotube/carbon fiber hybrid." Journal of materials science 44.13 (2009): 3574-3577.

[44] Qian, Hui, et al. "Carbon nanotube grafted carbon fibres: a study of wetting and fibre fragmentation." Composites Part A: Applied science and manufacturing 41.9 (2010): 1107-1114.

[45] Qian, Hui, et al. "Hierarchical composites reinforced with carbon nanotube grafted fibers: the potential assessed at the single fiber level." Chem. Mater 20.5 (2008): 1862-1869.

[46] Peng, Qingyu, et al. "Chemically and uniformly grafting carbon nanotubes onto carbon fibers by poly (amidoamine) for enhancing interfacial strength in carbon fiber composites." Journal of Materials Chemistry 22.13 (2012): 5928-5931.

[47] Thostenson, Erik T., and Tsu-Wei Chou. "Aligned multi-walled carbon nanotube-reinforced composites: processing and mechanical characterization." Journal of physics D: Applied physics 35.16 (2002): L77.

[48] Lv, Peng, et al. "Increasing the interfacial strength in carbon fiber/epoxy composites by controlling the orientation and length of carbon nanotubes grown on the fibers." Carbon 49.14 (2011): 4665-4673.

[49] Qian, Hui, et al. "Carbon nanotube-based hierarchical composites: a review." Journal of Materials Chemistry 20.23 (2010): 4751-4762.

[50] Bader, M.G., Tensile Strength of Uniaxial Composites, in Science and Engineering of Composite Materials. 1988. p. 1.

[51] Madhukar, M.S. and L.T. Drzal, Fiber-Matrix Adhesion and Its Effect

on Composite Mechanical Properties: II. Longitudinal (0°) and Transverse (90°) Tensile and Flexure Behavior of Graphite/Epoxy Composites. Journal of Composite Materials, 1991. 25(8): p. 958-991

[52] Hatta, H., K. Goto, and T. Aoki, Strengths of C/C composites under tensile, shear, and compressive loading: Role of interfacial shear strength. Composites Science and Technology, 2005. 65(15–16): p. 2550-2562

[53] Hatta, H., et al., Damage detection of C/C composites using ESPI and SQUID techniques. Composites Science and Technology, 2005. 65(7–8): p. 1098-1106

[54] Kim, B.W. and J.A. Nairn, Observations of Fiber Fracture and Interfacial Debonding Phenomena Using the Fragmentation Test in Single Fiber Composites. Journal of Composite Materials, 2002. 36(15): p. 1825-1858

[55] Zhou, X.F., J.A. Nairn, and H.D. Wagner, Fiber–matrix adhesion from the single-fiber composite test: nucleation of interfacial debonding. Composites Part A: Applied Science and Manufacturing, 1999. 30(12): p. 1387-1400

[56] Drzal, L.T., et al., Adhesion of Graphite Fibers to Epoxy Matrices: II. The Effect of Fiber Finish. The Journal of Adhesion, 1983. 16(2): p. 133-152.

[57] Zhao, F.M. and N. Takeda, Effect of interfacial adhesion and statistical fiber strength on tensile strength of unidirectional glass fiber/epoxy composites. Part I: experiment results. Composites Part A: Applied Science and Manufacturing, 2000. 31(1): p. 1203-1214

[58] Y.S. Song, J.R. Youn, Influence of dispersion states of carbon nanotubes on physical properties of epoxy nanocomposites, Carbon, 43 (2005) 1378-1385

[59] C. Singh, M.S. Shaffer, A.H. Windle, Production of controlled architectures of aligned carbon nanotubes by an injection chemical vapour dep-

osition method, Carbon, 41 (2003) 359-368

[60] S. Talapatra, S. Kar, S. Pal, R. Vajtai, L. Ci, P. Victor, M. Shaijumon, S. Kaur, O. Nalamasu, P. Ajayan, Direct growth of aligned carbon nanotubes on bulk metals, Nature nanotechnology, 1 (2006) 112-116

[61] R.G. de Villoria, S. Figueredo, A. Hart, S. Steiner Iii, A. Slocum, B. Wardle, High-yield growth of vertically aligned carbon nanotubes on a continuously moving substrate, Nanotechnology, 20 (2009) 405611

[62] K. Kuwana, H. Endo, K. Saito, D. Qian, R. Andrews, E.A. Grulke, Catalyst deactivation in CVD synthesis of carbon nanotubes, Carbon, 43 (2005) 253-260

[63] K.J. Kim, W.-R. Yu, J.H. Youk, J. Lee, Degradation and Healing Mechanisms of Carbon Fibers during the Catalytic Growth of Carbon Nanotubes on Their Surfaces, ACS Applied Materials & Interfaces, 4 (2012) 2250-2258

[64] A.A. Puretzky, D.B. Geohegan, S. Jesse, I.N. Ivanov, G. Eres, In situ measurements and modeling of carbon nanotube array growth kinetics during chemical vapor deposition, Applied Physics A, 81 (2005) 223-240

[65] W. Hu, D. Gong, Z. Chen, L. Yuan, K. Saito, C.A. Grimes, P. Kichambare, Growth of well-aligned carbon nanotube arrays on silicon substrates using porous alumina film as a nanotemplate, Applied Physics Letters, 79 (2001) 3083-3085

[66] J.S. Lee, T.J. Kang, Changes in physico-chemical and morphological properties of carbon fiber by surface treatment, Carbon, 35 (1997) 209-216

[67] C. Masarapu, B. Wei, Direct Growth of Aligned Multiwalled Carbon Nanotubes on Treated Stainless Steel Substrates, Langmuir, 23 (2007) 9046-9049

[68] D.C. Davis, J.W. Wilkerson, J. Zhu, V.G. Hadjiev, A strategy for im-

proving mechanical properties of a fiber reinforced epoxy composite using functionalized carbon nanotubes, Composites Science and Technology, 71 (2011) 1089-1097

[69] L. Brissonneau, R. Sahnoun, C. Mijoule, C. Vahlas, Investigation of nickelocene decomposition during chemical vapor deposition of nickel, Journal of The Electrochemical Society, 147 (2000) 1443-1448

[70] M. Bernhauer, M. Braun, K.J. Hüttinger, Kinetics of mesophase formation in a stirred tank reactor and properties of the products—V. Catalysis by ferrocene, Carbon, 32 (1994) 1073-1085

[71] K.-E. Kim, K.-J. Kim, W.S. Jung, S.Y. Bae, J. Park, J. Choi, J. Choo, Investigation on the temperature-dependent growth rate of carbon nanotubes using chemical vapor deposition of ferrocene and acetylene, Chemical Physics Letters, 401 (2005) 459-464

[72] W.D. Callister, D.G. Rethwisch, Materials science and engineering: an introduction, Wiley New York2007.

[73] Y. Guo, J. Liu, J. Liang, Surface state of carbon fibers modified by electrochemical oxidation, Journal of Materials Science and Technology, 21 (2005) 371-375

[74] F. Huang, K.T. Yue, P. Tan, S.-L. Zhang, Z. Shi, X. Zhou, Z. Gu, Temperature dependence of the Raman spectra of carbon nanotubes, Journal of Applied Physics, 84 (1998) 4022-4024

[75] F. Tuinstra, J.L. Koenig, Raman spectrum of graphite, The Journal of Chemical Physics, 53 (1970) 1126-1130

[76] F. Tuinstra, J. Koenig, Characterization of graphite fiber surfaces with Raman spectroscopy, Journal of Composite Materials, 4 (1970) 492-499.

[77] B.R. Pauw, M.E. Vigild, K. Mortensen, J.W. Andreasen, E.A. Klop, D.W. Breiby, O. Bunk, Strain-induced internal fibrillation in looped aramid filaments, Polymer, 51 (2010) 4589-4598.

[78] T. Kobayashi, K. Sumiya, Y. Fukuba, M. Fujie, T. Takahagi, K. Tashiro, Structural heterogeneity and stress distribution in carbon fiber monofilament as revealed by synchrotron micro-beam X-ray scattering and micro-Raman spectral measurements, Carbon, 49 (2011) 1646-1652

[79] A.F. Thünemann, W. Ruland, Microvoids in Polyacrylonitrile Fibers: A Small-Angle X-ray Scattering Study, Macromolecules, 33 (2000) 1848-1852

[80] W. Ruland, Carbon Fibers, Advanced Materials, 2 (1990) 528-536.

[81] Z. Hua, Y.J. Zhong, D.F. Li, Pores in PAN-based carbon fiber and effects of pore defects on mechanical properties, Materials science forum, Trans Tech Publ, 2007, pp. 1665-1668

[82] C. Zhu, X. Liu, X. Yu, N. Zhao, J. Liu, J. Xu, A small-angle X-ray scattering study and molecular dynamics simulation of microvoid evolution during the tensile deformation of carbon fibers, Carbon, 50 (2012) 235-243

[83] Tohgo, Keiichiro, Albert SD Wang, and Tsu-Wei Chou. "A criterion for split-ting crack initiation in unidirectional fiber-reinforced composites." Journal of composite materials 27.11 (1993): 1054-1076.

Korean abstract

본 논문은 탄소나노튜브의 탄소섬유 상의 직접적인 성장을 통해 탄소섬유의 표면적을 늘려 복합재료의 기저와의 계면전단강력을 증가시키는 나노-마이크로 계층구조의 탄소나노튜브 그라프트 탄소섬유를 탄소섬유의 기계적 물성의 손상 없이 제조하고, 그러한 강화재가 혼입된 복합재를 만들어 해당 복합재료의 향상된 성능을 평가하였다. 또한 해당 공정의 대량화를 위해 탄소나노튜브 그라프트 탄소섬유의 연속제조공정에 대해 연구하였다.

먼저 탄소섬유의 기계적 물성의 저하가 없는 탄소나노튜브 성장 공정을 위해 이중금속촉매를 이용하여 탄소나노튜브를 성장시키는 화학기상증착 공정의 온도를 낮추는데 성공하였으며 저온 공정이 탄소나노튜브 그라프트 탄소섬유의 기계적 물성에 끼치는 효과를 고온 공정에 의해 제조된 탄소나노튜브 그라프트 탄소섬유와 저온 공정에 의해 제조된 탄소나노튜브 그라프트 탄소섬유의 기계적 물성, 내부구조 등의 비교를 통해 확인하였다.

이후 탄소섬유 직물을 이용해 탄소나노튜브 그라프트 탄소섬유 에폭시 복합재료를 제조, 평가하였다. 이를 통해 일반 탄소섬유에폭시 복합재료의 기계적 물성과 비교하여 증가한 계면물성 및 층간물성의 효과를 확인하고, 평가된 시편의 파단면 비교, 인장시험 중 표면 크랙의

전파 관찰 등의 방법을 통하여 복합재료의 강화 메커니즘을 확인하였다. 제조된 탄소나노튜브 그라프트 탄소섬유 에폭시 복합재료는 일반 탄소섬유 복합재료에 비해 일축 복합재료의 경우 17%, 교차직물 복합재료의 경우 32%의 향상된 기계적 물성을 보였다.

탄소섬유 직물을 이용해 탄소나노튜브 그라프트 탄소섬유 강화 탄소/탄소 복합재료를 제조, 평가하였다. 제조된 탄소나노튜브 그라프트 탄소섬유 강화 탄소/탄소 복합재료는 탄소나노튜브 그라프트 탄소섬유의 나노-마이크로 계층구조로 인해 섬유와 기저 사이의 젖음성이 증가함으로써 일반 탄소섬유 강화 탄소/탄소 복합재료에 비해 더 긴밀한 내부구조를 구축하였다. 이로 인해 섬유분율 대비 기계적 강도가 58%, 열전도도가 온도범위에 따라 두께방향으로는 70~80%, 면 방향으로는 15~20% 향상되는 것을 확인할 수 있었다.

탄소나노튜브 그라프트 탄소섬유의 대량 제조 공정 개발을 위해 기존의 배치 방식의 탄소나노튜브 그라프트 탄소섬유 제조 공정을 연속공정화 하였다. 앞서 개발한 이중금속촉매 화학기상증착법을 이용한 저온 공정에 더해 수증기 보조 화학기상증착법을 도입하여 공정의 속도를 가속하였다. 기존 탄소나노튜브 그라프트 탄소섬유 제조 공정에서 문제가 되었던 음영효과는 스프레드 탄소섬유 다발을 이용하고 기존의 일자 형태의 전기로를 T자형으로 변형함으로써 해결하였다. 또한 전기로의 입구 부분에 격실을 도입함으로써 전기로 외부로부터

탄소섬유가 지속적으로 공급될 수 있도록 하였다.

핵심어: 계층구조의 강화제, 탄소나노튜브, 탄소섬유 복합재료, 일축 섬유강화 복합재료, 계면전단강력, 이중금속촉매

학번: 2014-30234